SPATIOTEMPORAL REGULATION OF CDC42 ACTIVITY DIRECTS SPECIFIC MEMBRANE TRAFFICKING EVENTS AT DISTINCT CELL SITES

Bethany F. Campbell

A dissertation

submitted to the Faculty of

the department of Biology

in partial fulfillment

of the requirements for the degree of

Doctor of Philosophy

Boston College
Morrissey College of Arts and Sciences
Graduate School

October 2024

SPATIOTEMPORAL REGULATION OF CDC42 ACTIVITY DIRECTS SPECIFIC MEMBRANE TRAFFICKING EVENTS AT DISTINCT CELL SITES

Bethany F. Campbell

Advisor: Maitreyi E. Das, Ph.D.

ABSTRACT

Polarization allows cells to form and maintain morphologies necessary for their diverse functions during processes such as growth, division, differentiation, and migration. Signaling proteins such as the family of small Rho GTPases promote polarization by spatiotemporally regulating cytoskeleton dynamics and coordinating membrane trafficking. Here, we investigate and define roles of the Rho GTPase Cdc42 in promoting polarization in *S. pombe.* As fission yeast, *S. pombe* cells grow from their cell ends during interphase and divide by medial fission to produce two new daughter cells. As cell-walled organisms, growth and division require intricate remodeling and expansion of the cell wall via incorporation of new membrane and proteins at these polarized sites. Thus, growth and division require specific sequences of membrane trafficking events to deliver and remove cargo at appropriate times and locations. During cytokinesis, fission yeast cells divide by synthesizing new cell wall called the septum to medially bisect the cell. The septum is synthesized behind the actomyosin ring to aid its constriction. Once ring constriction completes and the septum matures, the septum is partially digested to physically separate

the daughter cells. Previous work has shown that Cdc42 promotes the delivery of specific but not all septum-synthesizing enzymes as well as septum-digesting enzymes, but it was not known how Cdc42 activation is regulated at the division site to temporally coordinate these processes. Here, we show that the Cdc42 GAPs Rga4 and Rga6 promote proper septum synthesis and timely cell separation by locally decreasing Cdc42 activation during late cytokinesis. This work also reveals a role for Cdc42 in regulating clathrin-mediated endocytosis, both at the division site as well as at growing cell ends. To further explore this role, we systematically examined the behaviors of endocytic actin patches in mutants of Cdc42 regulators and compared these dynamics to wild-type controls. This characterization led to the observation that endocytic patches are best formed to induce successful patch internalization at sites of polarization where Cdc42 is active. In this work, we show that Cdc42 activation promotes proper endocytic patch behavior in a dose-dependent manner and that Cdc42 regulates endocytosis via its downstream effector, the Pak1 kinase. We also demonstrate that Cdc42 and Pak1 activity promote endocytosis through at least two pathways which regulate branched actin formation. First, we show that Cdc42 and Pak1 promote proper endocytic actin patch formation. Secondly, we show that Pak1-mediated phosphorylation of the endocytic Type I myosin promotes timely internalization of endocytic actin patches.

ACKNOWLEDGMENTS

This dissertation is a labor of persistence made possible by the support, love, patience, and encouragement of many people who I am blessed to have as mentors, friends, and family.

To begin, I extend special gratitude to my advisor, Dr. Maitreyi Das, who has supported me from my very first semester of grad school when I rotated in her lab at The University of Tennessee. Over the past six years, your mentorship has helped me develop confidence in my abilities as a cell biologist and as a woman in science. I truly would not have completed this Ph.D. without your unwavering support as I encountered challenges in the lab and beyond. Thank you for always having your door open to me for impromptu conversations about science and life.

Thank you to my past and present committee members: Dr. Andreas Nebenführ, Dr. Rachel McCord, Dr. Tian Hong, and Dr. Todd Reynolds at The University of Tennessee and Dr. David Burgess, Dr. Vicki Losick, Dr. Eric Folker, and Dr. Zoë Hilbert at Boston College. I especially thank Dr. Nebenführ for always giving detailed feedback on my committee reports and for teaching me many tips and tricks for light microscopy.

Thank you to all the members of the Das Lab, both past and present. I am thankful to have each of you as a friend. To Dr. Brian Hercyk, thank you for patiently teaching me all the basics about working with *S. pombe* and for answering my many questions. To Dr. Julie Rich-Robinson, thank you for always bringing cheer to the lab, especially during holidays,

and most especially at Halloween. To Dr. Udo Onwubiko, thank you for showing me how to be a thorough and dedicated researcher. To Dr. Samridhi Pathak, thank you for being my roommate when we first moved to Boston and for helping me adjust to life's changing seasons. To Dr. Dhanya Kalathil, thank you for always lending a listening ear and for noticing when I need one. To (soon-to-be-Dr.) Marcus Harrell, thank you for being my roommate as we complete our Ph.D.s and for treating my dog Sadie as your own. To Justin McDuffie, thank you for bringing laughter and fun to the lab. To Walker Vickers, thank you for coordinating with me to troubleshoot our CRISPR woes. To Carmen Rivera, thank you for baking and bringing so many delicious desserts to share and for organizing our lab and helping us all to stick to the system. To Ashlei Williams, thank you for always being dependable and for taking initiative in research. To Uma Patel, thank you for your eagerness to learn many different and challenging techniques and for helping me keep my research moving even while I am away from the lab.

To my parents Karen and Charles Campbell, thank you for encouraging me at every step of this journey. Thank you for perfectly timed phone calls and texts when I am missing home. To my sisters, Lauren and Addie, thank you for being the best ready-made friends I could ever ask for. To my aunt Deborah Thompson, thank you for giving the best advice and perspective on life. To my dog Sadie, thank you for being my constant companion and for bringing joy to each day. To all my family, thank you for loving me unconditionally. I dedicate this dissertation to my beloved late grandparents, Carl W. Campbell (1921–2000), Lila R. Campbell (1928 –2022), Emmett W. Jones (1927–2020), and Sylvia F. Jones (1945–2022), whom I know would be proud to see me reach this achievement.

TABLE OF CONTENTS

LIST OF ABBREVIATIONS

OE	old cell end
NE	new cell end
OETO	old end take off
NETO	new end take off
GTP	guanosine triphosphate
GDP	guanosine diphosphate
GEF	guanine nucleotide exchange factors
GAP	GTPase activating proteins
CRIB	Cdc42/Rac Interactive Binding domain
PAK	p21-activated kinase
WASP	Wiskott-Aldrich syndrome protein
t-SNARE	target SNARE (soluble N-ethylmaleimide-sensitive factor attachment protein receptor)
v-SNARE	vesicle SNARE (soluble N-ethylmaleimide-sensitive factor attachment protein receptor)
TRAPP	TRAnsport Protein Particle complex
PS	primary septum
SS	secondary septum
Bgs	β-glucan synthase
TEM	Transmission Electron Microscopy
F-BAR	Formin-Binding Protein 1 Homology-Bin-Amphiphysin-Rvs domain
TEDS site	Threonine (T) Glutamic Acid (E) Aspartic Acid (D) Serine (S) phosphorylation site

LIST OF TABLES

LIST OF FIGURES

1.0 CHAPTER 1 - INTRODUCTION

POLARIZATION AND MEMBRANE TRAFFICKING IN *S. POMBE*: DIFFERENTIAL REQUIREMENTS FOR CDC42

Bethany F. Campbell and Maitreyi E. Das

ABSTRACT

Many cell types must establish and maintain specific shapes to properly perform their functions. Changes in cell shape are achieved via polarization, which requires both cytoskeletal reorganization and membrane trafficking to direct proteins and lipids towards specific cell sites. In addition to exocytosis, which targets secretion to specific sites, polarization also requires endocytosis to promote recycling of proteins and membrane. Classically, the small Rho GTPase has been considered a central regulator of polarized growth in most eukaryotes. Recent works additionally demonstrate that Cdc42 promotes proper polarization at the division plane as cells divide. Here, we describe how *S. pombe* fission yeast cells grow, maintain their cell shape, and undergo cytokinesis via polarization, whilst highlighting the functions of Cdc42 in these processes.

1.1 POLARIZATION ESTABLISHES THE MORPHOLOGY OF *S. POMBE* FISSION YEAST

Polarization allows cells to form and maintain morphologies necessary for their diverse functions during growth, division, differentiation, migration, and maintenance of cell position and identity in tissues (Vicente-Manzanares and Sánchez-Madrid, 2000; Wodarz and Näthke, 2007). Signaling proteins promote polarization by spatiotemporally regulating cytoskeleton dynamics and coordinating membrane trafficking events (Etienne-Manneville, 2004; Nance and Zallen, 2011; Ridley, 2006). Unlike many cells which show diverse morphologies within the same cell type, *Schizosaccharomyces pombe* fission yeast maintain a strict rod-shaped morphology by directing polarized growth only at their cell ends. Indeed, mutations of polarity-regulating genes can disrupt this rod-shaped morphology and can induce rounding and branching of cells (Bähler and Pringle, 1998; Verde et al., 1995). To maintain their rod-shape, fission yeast cells grow in a highly regulated and predictable pattern. After medial cell division, a newly formed daughter cell initiates growth at its preexisting old end (OE), establishing the first site of polarized growth after division (Mitchison and Nurse, 1985) (Figure 1.1). After growing to a length of ~9 microns, *S. pombe* cells establish a second site of polarized growth at the new end (NE) to transition from monopolar to bipolar growth during new end take off (NETO) (Mitchison and Nurse, 1985) (Figure 1.1). This bipolar growth pattern allows fission yeast to grow in length until cells are ~14 microns long, after which they stop growing and prepare for medial division (Mitchison and Nurse, 1985). *S. pombe* divide by redirecting polarity machinery away from the cell ends and towards the cell middle to establish a medial division site (Arellano et al., 1999; Hachet et al., 2012). At this site, *S. pombe* cells

form a contractile actomyosin ring surrounded by a plasma membrane interface that is flanked by a septum composed of newly synthesized cell wall (Cheffings et al., 2016; Pollard, 2010; Pollard, 2014). In tight coordination, the actomyosin ring constricts as the septum forms until ring constriction completes and a medial septum spans the width of the mother cell (Hercyk et al., 2019a). After the septum matures, the innermost layer of the septum is digested (Cortés et al., 2016; Sipiczki, 2007), allowing the daughter cells to separate and initiate a new cycle of growth at the OE (Figure 1.1)

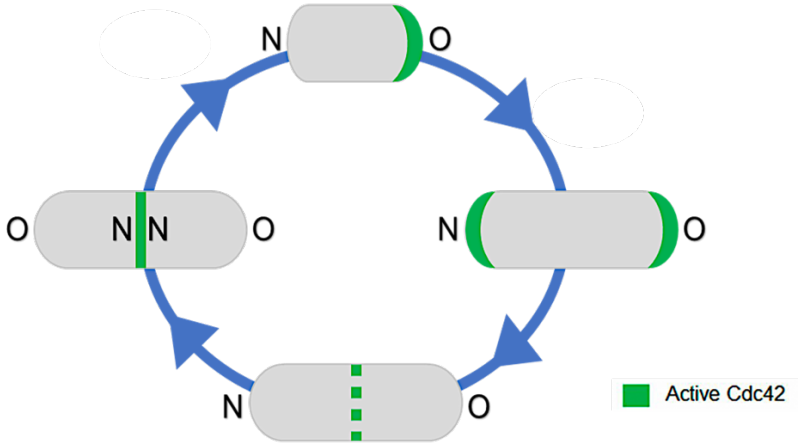

Figure 1.1 Fission yeast growth cycle and Cdc42 activation pattern. Top: Following old end take off (OETO), growth occurs first at the old cell end (O). The cell then transitions to bipolar growth when the new cell end (N) initiates growth at new end take off (NETO). After completion of cell growth, a septum forms and is remodeled to create cell walls for the new ends of both daughter cells upon cell separation. Sites of Cdc42 activation are depicted in green.

1.2 CDC42 ACTIVATION IS SPATIOTEMPORALLY REGULATED TO DIRECT POLARIZATION

In many eukaryotes, the family of small Rho GTPases (Cdc42, Rac, and Rho) are central regulators of polarization. Cdc42 in particular regulates polarization in many cell types by remodeling the actin cytoskeleton to direct transport of cell-building materials to sites of growth and cytokinesis (Etienne-Manneville, 2004; Hachet et al., 2012; Martin and Arkowitz, 2014; Melendez et al., 2011). From yeast to humans, Cdc42 is highly conserved in both structure and function across eukaryotic life (Johnson, 1999). In fact, fission yeast Cdc42 shares 83% sequence homology with human Cdc42 and both human and fission yeast Cdc42 fully complement growth in budding yeast (Miller and Johnson, 1994). As a GTPase, Cdc42 is active in its GTP-bound state and inactive when bound to GDP, and Cdc42 activity is required to promote cell growth (Hachet et al., 2012; Rincón et al., 2014). In *S. pombe* fission yeast, Cdc42 specifically promotes polarized growth via the activity of its known direct downstream effectors: For3, a formin that polymerizes actin cables (Faix and Grosse, 2006; Martin et al., 2007; Nakano et al., 2002), the p21-activated kinases (PAKs), Pak1 and Pak2, that organize actin to regulate polarized growth and the timing of mitosis and cytokinesis (Chang et al., 1999; Sells et al., 1998), Pob1, which promotes polarized growth in cooperation with For3 (Rincón et al., 2009; Toya et al., 1999), and two subunits of the octameric exocyst complex (Sec3 and Exo70), which aids exocytic vesicle tethering (Boyd et al., 2004; Finger et al., 1998; He et al., 2007; Zhang et al., 2000). Another known set of Cdc42 effectors are members of the Wiskott-Aldrich syndrome (WASP) family which activate the Arp2/3 complex to stimulate branched actin formation necessary for endocytosis (Higgs and Pollard, 2000; Miki et al., 1998; Rohatgi et al., 1999;

Takenawa and Suetsugu, 2007). However, the *S. pombe* WASP Wsp1 lacks the Cdc42/Rac Interactive Binding (CRIB) domain found in mammalian WASP; thus, a direct interaction between Cdc42 and Wsp1 is not thought to occur.

Like other GTPases, fission yeast Cdc42 is regulated by activators called guanine nucleotide exchange factors (GEFs) and inhibitors called GTPase activating proteins (GAPs). The GEFs induce conformational change in Cdc42 to allow GTP to bind and activate the GTPase, while the GAPs promote GTP hydrolysis to deactivate the GTPase (Bishop and Hall, 2000). In *S. pombe*, Cdc42 is regulated by two GEFs (Scd1 and Gef1) and three known GAPs (Rga4, Rga6, and Rga3) (Coll et al., 2003; Das et al., 2015; Das et al., 2007; Fukui and Yamamoto, 1988; Gallo Castro and Martin, 2018; Revilla-Guarinos et al., 2016) (Figure 1.2). Although Cdc42 is present throughout the endomembrane system, during interphase, the GEFs and GAPs spatially restrict Cdc42 activation to the plasma membrane of the cell ends to direct polarized growth (Hachet et al., 2012). Namely, the GEFs localize to the cell ends to activate Cdc42 at these sites (Hercyk et al., 2019b), while the GAPs primarily localize to the cell sides to keep Cdc42 inactive at these regions (Das et al., 2007; Revilla-Guarinos et al., 2016). In this manner, the GEFs and the GAPs regulate the activity of Cdc42 to spatially determine sites of polarized growth (Hachet et al., 2012). In *S. pombe*, Cdc42 is active at both growing cell ends and these ends compete with each other to activate Cdc42, resulting in oscillations of active Cdc42 between the ends (Das et al., 2012). Initially, the old end (OE) is dominant in this competition for active Cdc42 and thus grows first in a process termed old end take off (OETO) (Das et al., 2012) (Figure 1.1). After some time, Gef1 triggers Scd1-mediated Cdc42 activation at the new

end (NE) to promote bipolar growth via new end take off (NETO) (Hercyk et al., 2019b) (Figure 1.1). After the new end initiates growth during NETO, Cdc42 oscillations are most distinct as the two cell ends compete for Cdc42 (Das et al., 2012). During division, Cdc42 activation shifts to the medial division site, where it promotes formation of the primary (innermost) septum layer during cytokinesis as well as primary septum digestion following septum maturation (Campbell et al., 2022; Onwubiko et al., 2019; Onwubiko et al., 2021; Wei et al., 2016) (Figure 1.1). As at the cell ends, the GEFs and GAPs spatiotemporally restrict Cdc42 activation at the division site to direct polarization. During division, Cdc42 is first activated by Gef1 immediately after actomyosin ring assembly, while Scd1 activates Cdc42 along the ingressing membrane furrow at the onset of ring constriction (Hercyk and Das, 2019; Wei et al., 2016). The GAPs Rga4 and Rga6 then localize behind the constricting ring to deactivate Cdc42 during late cytokinesis (Campbell et al., 2022 – this dissertation).

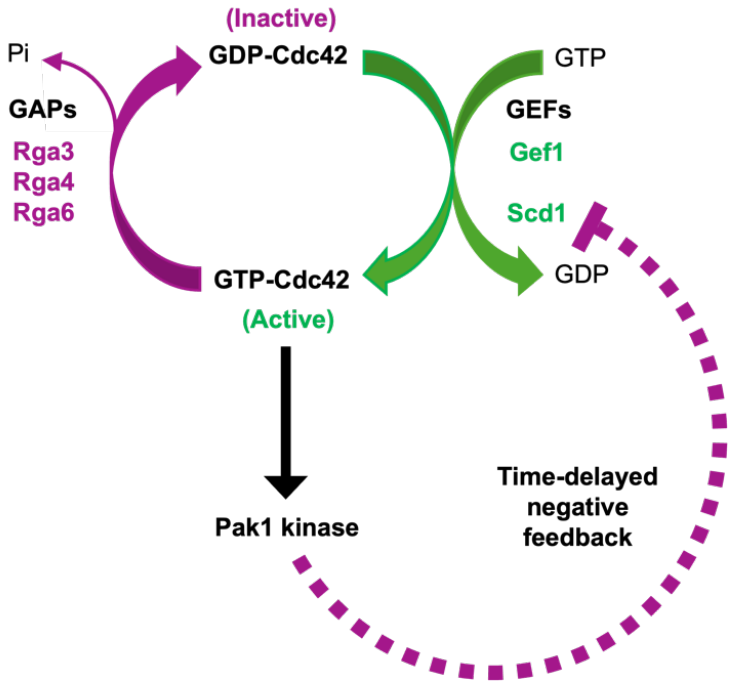

Figure 1.2 Positive and negative regulation of Cdc42 activity. GEFs activate Cdc42, while GAPs deactivate Cdc42. The GEF Scd1 and its scaffold Scd2 amplify Cdc42 activation via positive feedback where active Cdc42 recruits additional Scd1 for further Cdc42 activation. Cdc42 activated by Scd1-Scd2 activates downstream Pak1. The Pak1 kinase then inhibits Scd1-Scd2 mediated Cdc42 activation in a time-delayed negative feedback loop.

In addition to its GEFs and GAPs, Cdc42 is also regulated by its direct downstream effector, the Pak1 kinase (Fukui and Yamamoto, 1988; Lamas et al., 2020). Pak1 functions as a time-delayed negative regulator by breaking a positive feedback loop that amplifies Cdc42 activation (Das et al., 2012; Lamas et al., 2020) (Figure 1.2). In this feedback loop, the GEF Scd1 and its scaffold Scd2 recruit Cdc42 to the cell ends to promote polarization, while active Cdc42 itself recruits more Scd1 (Wheatley et al., 2005; Lamas et al., 2020). Pak1 then triggers Cdc42 deactivation at the cell ends by associating with Scd2, which serves as a scaffold to facilitate the interaction between Pak1 and Cdc42 (Chang et al., 1999). In *S. cerevisiae* budding yeast, the Pak1 ortholog (Cla4) mediates Cdc42 deactivation by phosphorylating the Cdc42 GEF that is also associated with the scaffold (Bose et al., 2001; Gulli et al., 2000). A similar mechanism of Cdc42 deactivation may also exist in fission yeast since Scd2 serves as a scaffold for both Scd1 and Pak1, in addition to Cdc42 itself (Chang et al., 1999). This Pak1-mediated time-delayed negative feedback loop gives rise to the anti-correlated oscillations of active Cdc42 between the cell ends as the ends compete to amplify Cdc42 activation (Das et al., 2012; Lamas et al., 2020). Notably, this positive feedback loop does not seem to be adequately established at the division site, since Scd1 and Scd2 appearance at the division site is much weaker than their presence at the cell ends (Hercyk et al., 2019b).

As peripheral membrane proteins, Cdc42 and all of its GEFs and GAPs contain membrane binding domains (Das et al., 2015; Das et al., 2007; Hirota et al., 2003; Revilla-Guarinos et al., 2016; Saito et al., 2007) (Figure 1.3). This is not surprising since cell polarization occurs through membrane trafficking events that deliver materials to expand the cell at

particular sites. While the functions of the Cdc42 GEFs and GAPs on Cdc42 activity are well-established in fission yeast, the influence of their membrane-binding abilities on Cdc42 dynamics remain incompletely characterized.

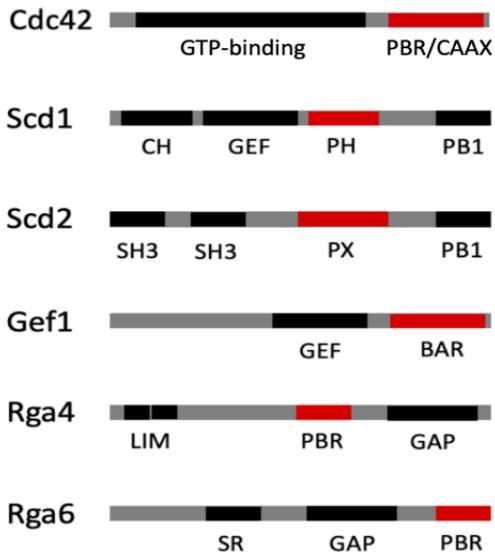

Figure 1.3. Membrane binding domains present in Cdc42 and its GEFs and GAPs. PBR: polybasic region; CAAX: CAAX domain, where C is a cysteine residue, AA are two aliphatic residues, and X is any C-terminal amino acid; PH: pleckstrin homology domain; PX: phox homology domain; and BAR: Bin/Amphiphysin/Rvs domain

1.3 MEMBRANE TRAFFICKING IS REQUIRED FOR POLARIZATION

Membrane trafficking events, which deliver and recycle proteins and membrane at target sites, are essential for polarization at sites of growth and division. Indeed, if exocytic trafficking is blocked at the Golgi with Brefeldin A, membrane furrowing and actomyosin ring constriction fail (Wang et al., 2016). Similarly, if the Arp2/3 complex is inhibited with CK-666 to block endocytosis, the primary septum synthase Bgs1 is not recruited to the division site and actomyosin ring constriction fails (Onwubiko et al., 2019). Exocytosis in *S. pombe* occurs in a manner common to eukaryotes in general. First, most post-Golgi secretory vesicles are transported via the Type V myosin along actin cables to sites where polarization will occur (Motegi et al., 2001), although some vesicles arrive by random walk

(Wang et al., 2016). As the vesicle approaches its destination, the t-SNARE Psy1 on the plasma membrane then captures the vesicle via its v-SNARE Syb1 to promote fusion of the vesicle with the plasma membrane (Jena, 2011; Wang et al., 2016). In *S. pombe*, tethering complexes include the octameric exocyst, which is essential for cell separation and promotes vesicle tethering at the rim of the division plane (Martín-Cuadrado et al., 2005; Wang et al., 2002; Wang et al., 2016) and the TRAPP-II complex, which promotes secretory vesicle tethering more interiorly within the cleavage furrow close to the actomyosin ring (Wang et. al, 2016). Prior work has proposed that TRAPP complexes function as GEFs for Rab GTPases to regulate vesicle trafficking, and this has been demonstrated for the Rab11 homolog in *Aspergillus nidulans* (Pinar et al., 2015). Similarly, the *S. pombe* TRAPP-II complex works preferentially with the Rab11 homolog Ypt3 at both the cell ends and the division site, but not with the Rab8 homolog Ypt2 (Wang et al., 2016). In *S. pombe,* many of these exocytic proteins have been implicated in the transport of integral membrane β-glucan synthases, which build new cell wall at growing cell ends and within the septum during division. In particular, the Type V myosin Myo52 transports the linear β-glucan synthase Bgs1, which synthesizes the primary (innermost) septum layer at the division site and promotes cell wall formation at growing cell ends (Cortés et al., 2002; Cortés et al., 2007; Estravis et al., 2012; Mulvihill et al., 2006). Additionally, the exocyst and TRAPP-II complex appear to promote Bgs1 recruitment to the division site since this is impaired in exocyst *sec8* mutants and in mutants of the TRAPP-II component *trs120* (Wang et al., 2016). Trs120 and Ypt3 also seem to facilitate transport of the branched β-glucan synthase Bgs4, since these proteins colocalize to the same puncta at polarized cell ends and at the division site (Wang et al., 2016). While Bgs1 plays a limited

role in cell wall formation at the cell ends, Bgs4 is the main glucan synthase required at the cell ends (Cortés et al., 2005). Bgs4 also synthesizes the secondary septa layers that flank the primary septum at the division site (Cortés et al., 2005). Given that Bgs1 and Bgs4 appear to be trafficked by the same exocytic machinery, it is of great interest to determine how they are directed to their proper locales, especially during septum synthesis when they must synthesize distinct layers of the septum in coordination.

1.4 CD42 PROMOTES CERTAIN MEMBRANE TRAFFICKING EVENTS REQUIRED FOR POLARIZATION

To facilitate the growth of *S. pombe* cells, polarization machinery must be directed towards the cell ends during interphase and then be shifted to the division site once cells enter mitosis. The signals that promote these localization changes, however, remain poorly understood. As both exocytosis and endocytosis are required for polarization, both of these membrane trafficking processes occur concomitantly at the cell ends during interphase and then shift to the division plane to promote cytokinesis.

In *S. pombe,* Cdc42 activity promotes several membrane trafficking events required for polarized growth and division. In *S. pombe,* actin cables are synthesized by the formin, For3, which is a known Cdc42 effector (Nakano et al., 2002). While actin cable formation is lost in *for3Δ* mutants, these cells do not exhibit major defects in polarized secretion (Bendezú and Martin, 2011; Estravís et al., 2011). However, *for3Δ* in combination with mutation of the *sec8* exocyst subunit results in depolarized cells (Bendezú & Martin, 2011).

As Sec8 is also a Cdc42 effector (Boyd et al., 2004; Finger et al., 1998), these results indicate that Cdc42 activation promotes polarization via cooperative function of actin cables and the exocyst complex (Bendezú & Martin, 2011). Initial studies reported that Cdc42 promotes the activity but not the localization of the exocyst (Roumanie et al., 2005), however more recent work demonstrates that Cdc42 also regulates exocyst localization. Specifically, hypomorphic *cdc42L160S* mutants exhibit numerous membrane trafficking defects including loss of exocyst localization to the cell ends, excessive accumulation of undocked vesicles, and impaired endosomal to vacuole fusion (Estravís et al., 2011). Results in budding yeast also demonstrate that overexpression of either constitutively active or dominant-negative Cdc42 results in vacuole fragmentation (Jones et al., 2010).

Cdc42 activation also promotes specific trafficking of the linear β-glucan synthase Bgs1 to polarized sites both at the cell ends and the division site (Estravís et al., 2012; Onwubiko et al., 2021; Campbell et al., 2022 – this dissertation). In hypomorphic *cdc42* mutants, Bgs1 trafficking to the cell ends and division site is greatly impaired, while trafficking of the branched β-glucan synthase Bgs4 appears normal (Estravís et al., 2012; Onwubiko et al., 2021). Specifically, GFP-Bgs1 seems to be trapped within large vesicle-like structures throughout the cytoplasm rather than concentrating at polarized regions (Estravís et al., 2012). Furthermore, *cdc42L160S* mutants exhibit impaired cell wall formation and mild cell lysis (Estravís et al., 2012), which additionally suggests that Cdc42 activity is required for proper polarized secretion of Bgs1 to synthesize cell wall. Together, these results show that Cdc42 promotes trafficking of the primary septum synthase Bgs1 to polarized sites but does not impact the delivery of the secondary septum synthase Bgs4. In accordance, these

two trafficking pathways are differentially regulated but still require proper coordination to build a structurally sound septum (Figure 1.4). Lastly, Cdc42 activity also facilitates the delivery of the primary septum digesting glucanases needed to physically separate daughter cells after septum maturation (Onwubiko et al., 2021). In hypomorphic *cdc42-1625* mutants, these glucanases are not properly targeted to the outer rim of the division plane to digest the primary septum (Onwubiko et al., 2021). Thus, Cdc42 activity promotes specific membrane trafficking events to facilitate polarization at distinct regions within the division plane and at the cell ends.

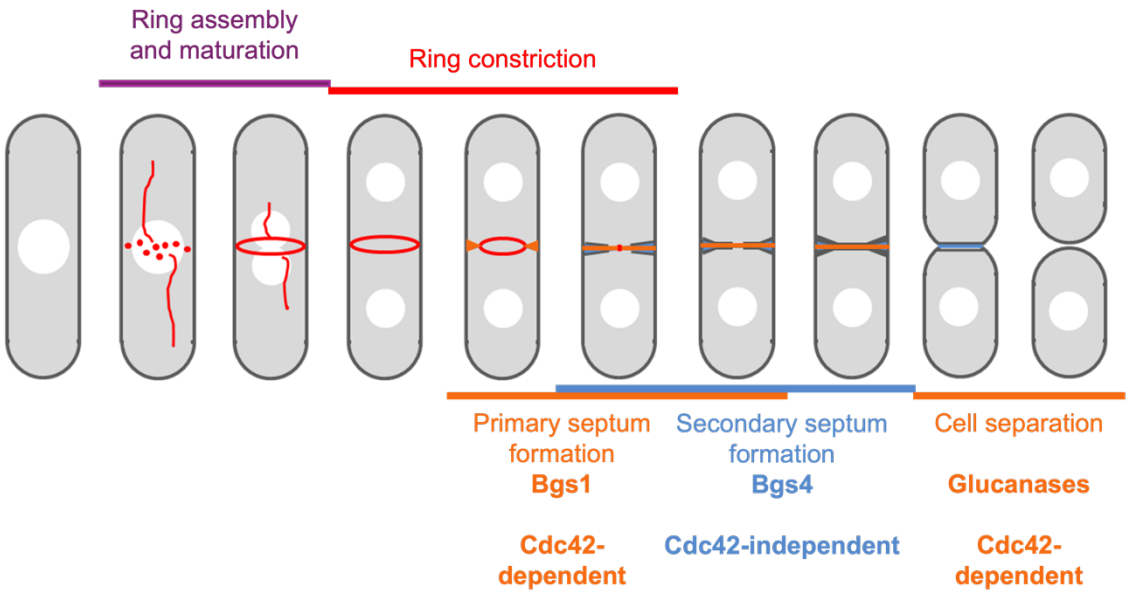

Figure 1.4. Sequence of membrane trafficking events during fission yeast cytokinesis. Early in cytokinesis, Cdc42 promotes primary septum formation via delivery of the linear β-glucan synthase Bgs1. After septum maturation, Cdc42 promotes separation of the daughter cells via delivery of the primary septum glucanases.

1.5 RESEARCH QUESTIONS & DIRECTIONS

While the septum synthases Bgs1 and Bgs4 are trafficked to the division site via shared exocytic machinery, it is interesting that Cdc42 only promotes delivery of Bgs1. Given that the primary septum serves as the template for secondary septum synthesis, it appears that Cdc42-dependent trafficking of Bgs1 may play a crucial role in proper septum formation. Additionally, it is not known how Cdc42 activation is spatiotemporally regulated at the division site to recruit Bgs1 during early cytokinesis and then later recruit the glucanases after completion of cytokinesis and septum maturation. Finally, it is also striking that Arp2/3-dependent endocytosis is required for Bgs1 recruitment to the division site, given that it is a cargo of exocytic machinery. While extensive research has demonstrated how actin patches assemble to enable endocytosis in yeast, several questions still remain. Previous reports have raised doubts about a role for Cdc42 in regulating clathrin-mediated endocytosis in fission yeast. Recent research from our lab has suggested that Cdc42 activation regulates endocytic patch dynamics (Onwubiko et al., 2019; Campbell et al., 2022; Campbell et al., 2024 – this dissertation). However, the molecular details of such a regulation are not known. These observations raise many questions that will be explored in this dissertation. First, how is Cdc42 activation spatiotemporally regulated at the division site to promote specific membrane trafficking events? Secondly, what is the significance of having separate trafficking pathways for Bgs1 and Bgs4? Why is endocytosis essential for polarization? Lastly, how does Cdc42 regulate endocytosis?

2.0 CHAPTER 2

Cdc42 GTPase activating proteins Rga4 and Rga6 coordinate septum synthesis and membrane trafficking at the division plane during cytokinesis

Cdc42 regulates furrow and septum ingression

Bethany F. Campbell, Brian S. Hercyk, Ashlei R. Williams, Ema San Miguel, Haylee G. Young, and Maitreyi E. Das

SYNOPSIS

The GTPase Cdc42 regulates cytokinesis in cell-walled fission yeast. Active Cdc42 promotes the initiation of septum (cell wall) synthesis to physically divide daughter cells. Here we show that Cdc42 activity must be decreased at the later stages of cytokinesis to enable proper septum formation. Mutants lacking Cdc42 inactivators, Rga4 and Rga6, lead to membrane trafficking defects and malformed septa consequently delaying cell separation.

2.1 ABSTRACT

Fission yeast cytokinesis is driven by simultaneous septum synthesis, membrane furrowing and actomyosin ring constriction. The septum consists of a primary septum flanked by secondary septa. First, delivery of the glucan synthase Bgs1 and membrane vesicles initiate primary septum synthesis and furrowing. Next, Bgs4 is delivered for secondary septum formation. It is unclear how septum synthesis is coordinated with membrane furrowing. Cdc42 promotes delivery of Bgs1 but not Bgs4. We find that after primary septum initiation, Cdc42 inactivators Rga4 and Rga6 localize to the division site. In *rga4Δrga6Δ* mutants Cdc42 activity is enhanced during late cytokinesis and cells take longer to separate. Electron micrographs of the division site in these mutants exhibit malformed septum with irregular membrane structures. These mutants have a larger division plane with enhanced Bgs1 delivery but fail to enhance accumulation of Bgs4 and several exocytic proteins. Additionally, these mutants show endocytic defects at the division site. This suggests that Cdc42 regulates primary septum formation and only certain membrane trafficking events. As cytokinesis progresses Rga4 and Rga6 localize to the division site to decrease Cdc42 activity to allow coupling of Cdc42-independent membrane trafficking events with septum formation for proper septum morphology.

2.2 GRAPHICAL ABSTRACT

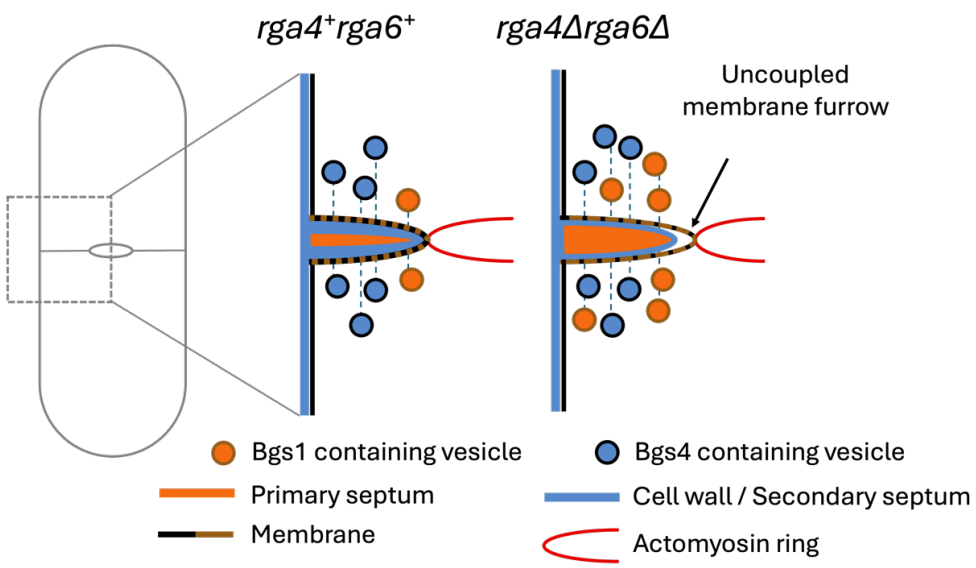

KEYWORDS

Cytokinesis, Cdc42 GTP-Binding Protein, GTPase-Activating Proteins, Endocytosis, Exocytosis, Membrane Furrow, Septum, Transport Vesicles, *Schizosaccharomyces pombe*

AUTHOR CONTRIBUTIONS

M.E.D., B.F.C. and B.S.H conceived the project. M.E.D. obtained funding for the project. B.F.C., B.S.H., and A.R.W. performed experiments and analyzed data. E.S.M. analyzed data. H.G.Y. performed experiments. B.F.C. and M.E.D. wrote the manuscript.

ACKNOWLEDGMENTS

We thank Dr. Andreas Nebenführ for discussions; Dr. Fred Chang, Dr. Pilar Perez, Dr. Sophie Martin, Dr. Mohan Balasubramanian, Dr. Fulvia Verde, and Dr. Jian-Qiu Wu for strains; and Dr. Jaydeep Kolape, Dr. John Dunlap, Dr. Tessa Burch-Smith, and Dr. Kirk Czymmek for electron microscopy. This research was funded by the National Science Foundation CAREER award #1941367 to M.E.D.

2.3 INTRODUCTION

2.3.1 Timeline of membrane trafficking events in *S. pombe* cytokinesis

Cytokinesis, the final step in cell division is a complex process involving multiple events. In fission yeast *Schizosaccharomyces pombe*, cytokinesis involves the assembly of an actomyosin ring which constricts along with membrane furrow formation and septum (cell wall) synthesis. It is unclear how ring constriction is tightly coupled to membrane furrowing and septum formation. Cdc42 is a central regulator of cell polarity and cell growth in most eukaryotes (Johnson, 1999). Recent work, however, has demonstrated that Cdc42 is also required for certain steps of cytokinesis in *S. pombe* (Onwubiko et al., 2021; Wei et al., 2016). During cytokinesis, numerous proteins are delivered in a sequential manner via distinct membrane trafficking events to ensure the fidelity of division. First, proteins necessary to form the contractile actomyosin ring are recruited to cortical nodes in the cell middle where division will occur (Wu et al., 2003). After the actomyosin ring assembles and matures, septum-synthesizing enzymes are delivered to build the tri-layer division septum that consists of a primary septum flanked by two secondary septa (Cortés et al., 2016). In addition, membrane is also delivered to the division site for furrow formation (Wang et al., 2016). Once the septum matures, the primary septum is digested to separate the daughter cells, while the secondary septa remain as daughter cell wall. In *S. pombe*, the primary septum is mostly synthesized by the linear-β-glucan synthase Bgs1 (Cortés et al., 2007), while the secondary septa are primarily synthesized by the branched β-glucan synthase Bgs4 (Cortés et al., 2007; Muñoz et al., 2013). Once Bgs1 arrives at the membrane adjacent to the actomyosin ring, primary septum synthesis initiates to drive ring

constriction (Cortés et al., 2016; Liu et al., 1999; Proctor et al., 2012; Wei et al., 2016). Shortly after septum synthesis initiation, Bgs4 is delivered to the division site to synthesize the secondary septa which further promotes and stabilizes ring constriction (Muñoz et al., 2013). Finally, after completion of ring constriction and septum maturation, the primary layer of the septum is digested by the glucanases Eng1 and Agn1 to physically separate the daughter cells, completing division (Dekker et al., 2004; Martín-Cuadrado et al., 2003; Martín-Cuadrado et al., 2005; Pérez et al., 2015; Santos et al., 2005; Wang et al., 2015). Cdc42 activity is necessary for the delivery of the primary septum synthase Bgs1 as well as the septum digesting glucanases Eng1 and Agn1 (Onwubiko et al., 2021; Wei et al., 2016).

2.3.2 Spatial coordination of membrane trafficking events during cytokinesis

In addition to temporally ordering the events of cytokinesis to ensure proper ring formation, ring constriction, membrane furrowing, and septum synthesis, membrane trafficking events are also spatially regulated to ensure that cargo is properly delivered to and removed from specific sites along the division plane (Hercyk et al., 2019a). In *S. pombe*, endocytosis occurs primarily at the outer rim of the membrane furrow, while exocytosis occurs all along the division plane to deliver protein cargo and new membrane to the division site (Wang et al., 2016). Specifically, the exocyst complex tethers exocytic vesicles at the outer edge of the membrane furrow, while the TRAPP-II complex regulates exocytosis throughout the whole membrane furrow to promote the tethering of vesicles containing the Rab11 GTPase Ypt3 and to a lesser extent the Rab8 GTPase Ypt2 (Wang et al., 2016). Notably, the TRAPP-II complex promotes the delivery of both the primary septum synthase Bgs1 as

well as the secondary septum synthase Bgs4 to the division site (Wang et al., 2016). To ensure efficient delivery of exocytic vesicles carrying cargo necessary for cytokinesis, a type V myosin motor Myo52 physically transports many of these vesicles along actin cables to the division site, although they can also arrive via random walk (Bendezú et al., 2012; Wang et al., 2016). Thus, cytokinetic membrane trafficking events are spatiotemporally regulated to control the delivery and removal of cargo and thereby coordinate ring constriction, membrane ingression, and septum synthesis.

2.3.3 Spatiotemporal regulation of Cdc42 activity during cytokinesis

Notably, Cdc42 activity is itself spatiotemporally regulated at the division plane via Guanine nucleotide Exchange Factors (GEFs) Gef1 and Scd1 which differentially regulate its activity (Hercyk et al., 2019b; Wei et al., 2016). During cytokinesis, Gef1 localizes to the cytokinetic ring and activates Cdc42 immediately after ring assembly, while Scd1 localizes behind the already constricting ring and activates Cdc42 along the ingressing membrane furrow (Wei et al., 2016). Cdc42 is inactivated by the GTPase activating proteins (GAPs) Rga4, Rga6, and Rga3 (Das et al., 2007; Gallo Castro and Martin, 2018; Revilla-Guarinos et al., 2016; Tatebe et al., 2008). These GAPs have been shown to localize to the division site, but their role in cytokinesis is unknown (Das et al., 2007; Gallo Castro and Martin, 2018; Revilla-Guarinos et al., 2016; Tatebe et al., 2008). Rga4 and Rga6 are the primary and secondary Cdc42 GAPs, respectively, since *rga4Δ* cells are wider than *rga6Δ* cells, while *rga3Δ* cells exhibit no morphology changes (Das et al., 2007; Gallo Castro and Martin, 2018; Revilla-Guarinos et al., 2016; Tatebe et al., 2008). The primary Cdc42 GAP Rga4 localizes to the division site after the initiation of septum synthesis (Das

et al., 2007). Similarly, the secondary Cdc42 GAP Rga6 localizes to the division site long after Cdc42 is activated at the division plane (Revilla-Guarinos et al., 2016). The third Cdc42 GAP Rga3 appears to function redundantly with the other two GAPs during vegetative growth, however, it is also present at the division site where it localizes in a manner similar to Cdc42 (Gallo Castro and Martin, 2018). Thus, it seems that Cdc42 is activated at the division site to initiate primary septum synthesis and drive cytokinetic ring constriction, however, it is unclear what role the GAPs play at the division site during cytokinesis.

2.3.4 Research summary

Here we show that the GAPs Rga4 and Rga6 decrease Cdc42 activity after septum formation initiates to coordinate septum synthesis and membrane trafficking within the division plane. In the absence of these GAPs, the balance between different membrane trafficking events is perturbed, the septum and membrane furrow exhibit morphological defects, and cell separation is delayed. These findings indicate that the spatiotemporal Cdc42 activation pattern is required to couple membrane furrowing with septum synthesis during cytokinesis.

2.4 RESULTS

2.4.1 The GAPs Rga4 and Rga6 localize to the membrane furrow to decrease Cdc42 activity during actomyosin ring constriction

Cdc42 is activated at the division site during actomyosin ring assembly (Hercyk and Das, 2019; Hercyk et al., 2019b; Wei et al., 2016). While each Cdc42 GAP also localizes to the division site, their localization patterns throughout cytokinesis have not been examined in detail. We observed the localizations of the GAPs relative to the actomyosin ring throughout each stage of cytokinesis. We find that Rga4-GFP and Rga6-GFP do not localize to the assembled actomyosin ring as marked by Rlc1-tdTomato before the onset of constriction, since there is a gap between each signal (Figure 1A and B, arrowheads). In contrast, Rga3-GFP localizes to the assembled ring before constriction initiates (Figure 2.1 C, asterisk). Rga4-GFP and Rga6-GFP instead localize to the ingressing membrane after the ring initiates constriction (Figure 2.1 A and B, arrowheads). Additionally, Rga4-GFP and Rga6-GFP remain at the division site following completion of ring constriction and loss of Rlc1-tdTom signal (Figure 2.1 A and B, arrowheads). Rga3-GFP signal is lost from the division site following ring constriction unlike that of Rga4-GFP and Rga6-GFP (Figure 2.1 C). Previous reports do not show an important role for Rga3 in regulating Cdc42 during vegetative growth (Gallo Castro and Martin, 2018). In addition, we find that Rga3-GFP localizes to the division site during early cytokinesis, when Cdc42 activity at this site is high, and is lost from the division site once ring constriction ends. In contrast, Rga4 and Rga6 localize to the division site only after ring constriction and septum synthesis

initiate and remain at this site throughout cytokinesis. Therefore, we investigated the role of Rga4 and Rga6 in late cytokinesis.

Since Cdc42 is first activated at the division site during ring assembly (Hercyk and Das, 2019; Hercyk et al., 2019b; Wei et al., 2016) while the GAPs Rga4 and Rga6 localize to the division site during ring constriction, we reasoned that these GAPs locally decrease Cdc42 activity at the division site during late cytokinesis. To test this, we deleted the GAP genes *rga4* and *rga6* and measured Cdc42 activation levels during late ring constriction in *rga4Δrga6Δ* cells compared to *rga4*$^{+}$*rga6*$^{+}$. Using a bio-probe that specifically binds active Cdc42 (CRIB-3xGFP) (Tatebe et al., 2008), we observed that Cdc42 activation at the division site is increased in the absence of *rga4* and *rga6* (Figure 2.2 A-C). During late ring constriction, the sum CRIB-3xGFP intensity is increased in cells lacking *rga4* and *rga6* (Figure 2.2 A and B). However, *rga4Δrga6Δ* mutant cells are wider than *rga4*$^{+}$*rga6*$^{+}$ cells (Supplemental Figure 2.1 A). Thus, it is possible that the increased sum intensity is simply attributable to the wider cell division site. To rule out this possibility, we measured the mean intensity of CRIB-3xGFP at the division site of *rga4Δrga6Δ* mutants and *rga4*$^{+}$*rga6*$^{+}$ cells. We find that the mean intensity of CRIB-3xGFP at the division site is also higher in *rga4Δrga6Δ* mutant cells as compared to *rga4*$^{+}$*rga6*$^{+}$ cells (Figure 2.2 C). These findings indicate that both the total amount of active Cdc42 and the average Cdc42 signal are increased at the division site in the absence of these GAPs.

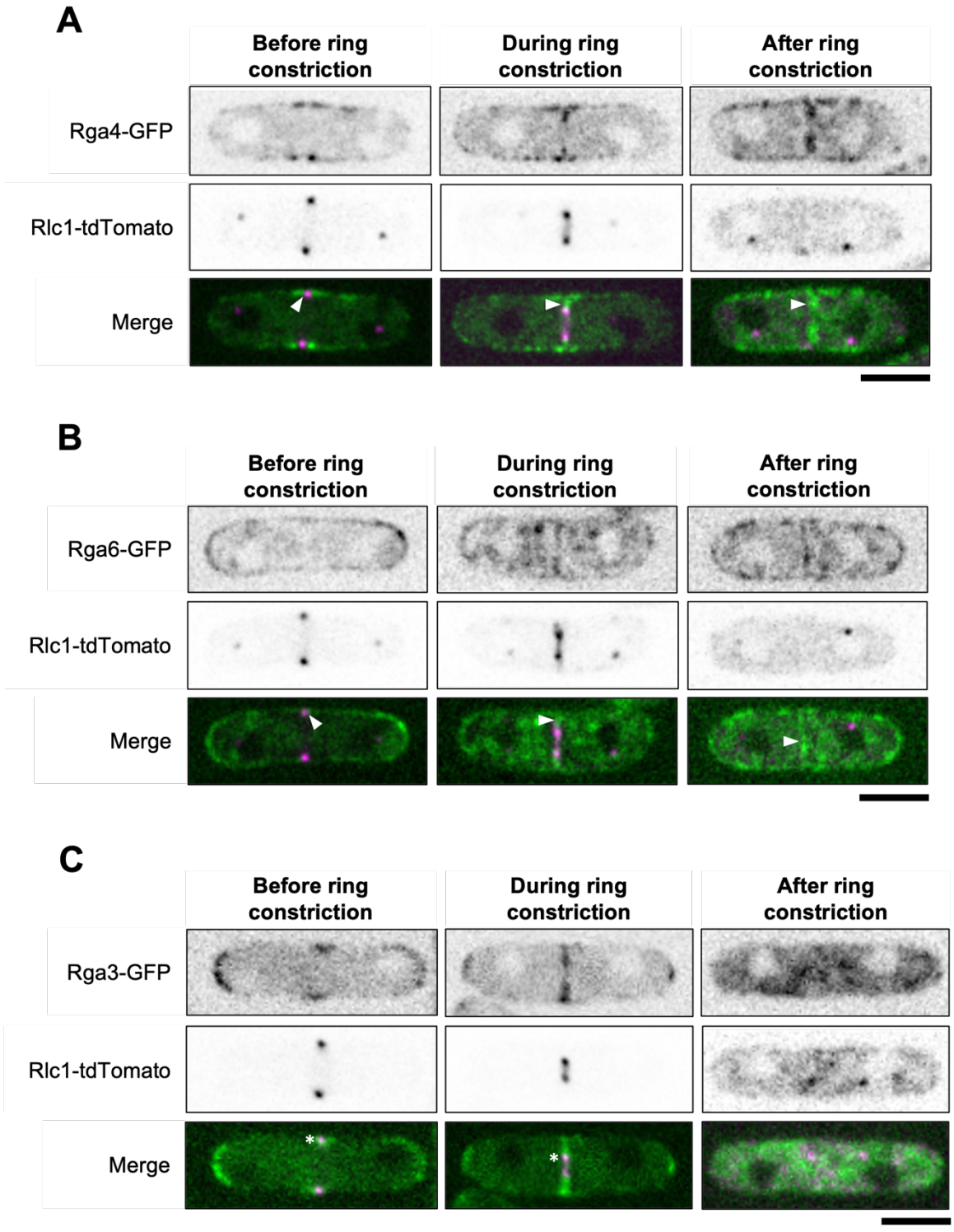

Figure 2.1. The GAPs Rga4 and Rga6 localize to the ingressing membrane furrow during cytokinesis. Before the onset of ring constriction, Rga4-GFP (A) and Rga6-GFP (B) do not co-localize with the ring marker Rlc1-tdTom (white arrowheads). During ring constriction, Rga4-GFP (A) and Rga6-GFP (B) localize

to the membrane furrow just behind the actomyosin ring where they spread through the membrane furrow. After completion of ring constriction, both Rga4-GFP (A) and Rga6-GFP (B) remain at the division site (white arrowheads). (C) Rga3 co-localizes with the actomyosin ring both before and during ring constriction (white asterisks). After ring constriction, Rga3-GFP is lost from the division site (scale bar = 5⌈m).

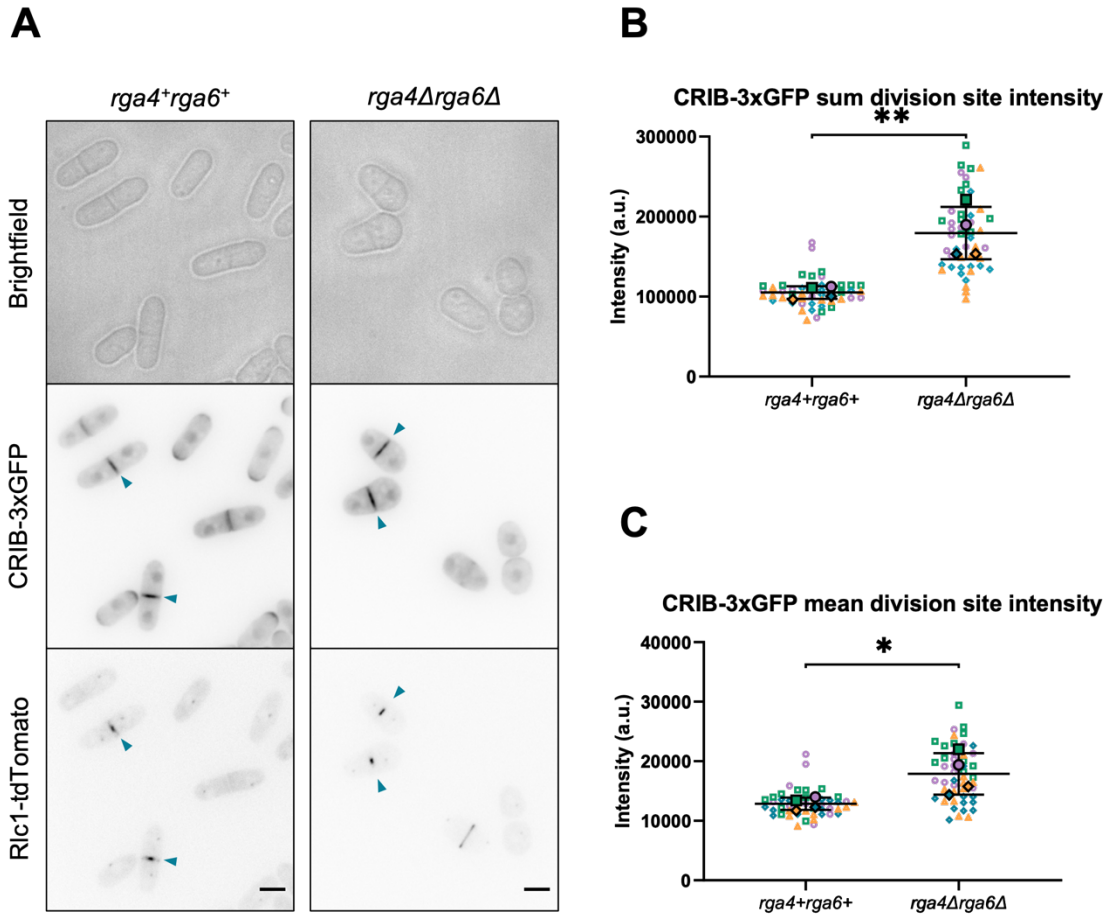

Figure 2.2 Cdc42 activation at the division site is increased during ring constriction in the absence of *rga4* and *rga6*. (A) Cdc42 activity marked with the bio-probe CRIB-3xGFP is enhanced at the division site (arrowheads) in *rga4Δrga6Δ* cells compared to *rga4*$^{+}$*rga6*$^{+}$ cells (inverted sum projections; scale bars = 5 μm). (B) Total CRIB-3xGFP intensity at the division site during ring constriction is increased in the absence of *rga4* and *rga6*. (C) Mean CRIB-3xGFP intensity at the division site during ring constriction is increased in the absence of *rga4* and *rga6*. Colors = distinct experiment. Open symbols = individual cells. Solid symbols = means of each experiment. n≥12 cells per genotype per experiment. Unpaired Student's *t*-test was used to calculate the statistical significance using the means of each experiment. *, $p<0.05$; **, $p<0.01$.

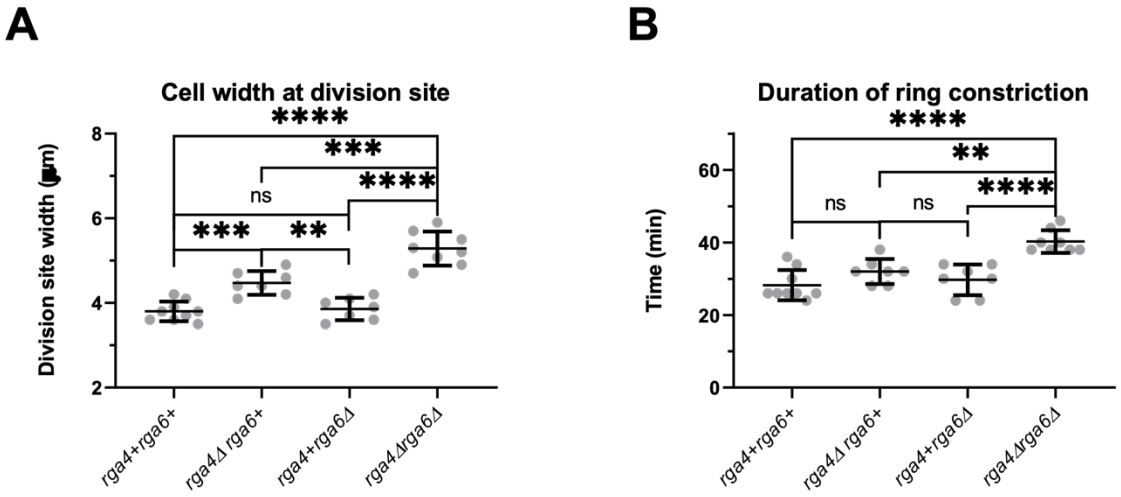

Supplemental Figure 2.1. Loss of *rga4* and *rga6* results in wider cells. (A) Loss of *rga4* and *rga6* additively increases cell width compared to *rga4*$^{+}$*rga6*$^{+}$ cells. (B) Duration of ring constriction is longer in *rga4Δrga6Δ* mutants compared to *rga4*$^{+}$*rga6*$^{+}$*, rga4Δ*, and *rga6Δ* cells. Statistical test used is Ordinary one-way ANOVA with Tukey's multiple comparisons. n.s., not significant; *, $p< 0.05$; **, $p< 0.01$; ***, $p<0.001$; ****, $p< 0.0001$.

2.4.2 The GAPs Rga4 and Rga6 ensure timely cell separation following actomyosin ring constriction

Mutant cells lacking *rga4* and *rga6* show altered cell polarity, resulting in shorter, wider cells (Supplemental Figure 2.1 A (Gallo Castro and Martin, 2018; Revilla-Guarinos et al., 2016)). We wondered if in addition to cell polarization, these GAPs also play a role in cytokinesis. We find that in *rga4Δrga6Δ* cells, the onset of ring constriction following spindle pole body (SPB) separation is not delayed with respect to *rga4*$^{+}$*rga6*$^{+}$, *rga4Δ,* and *rga6Δ* cells (Figure 2.3 A). Next, we analyzed ring constriction in these cells. As wider cells with larger actomyosin rings, *rga4Δrga6Δ* cells take longer to constrict their rings relative to *rga4*$^{+}$*rga6*$^{+}$ cells and the single GAP mutants (Figure S1B). Since *rga4Δrga6Δ* cells are wider than *rga4*$^{+}$*rga6*$^{+}$ cells, it is not surprising that the ring takes longer to constrict as this has been observed in other wide mutants such as *scd1Δ* (Wei et al., 2016). However, the rate of ring constriction remains the same in the double GAP mutant compared to the controls, suggesting that there is no defect in constriction (Figure 2.3 B). In contrast, we find that *rga4Δrga6Δ* cells take nearly twice as long to undergo cell separation following completion of ring constriction compared to *rga4*$^{+}$*rga6*$^{+}$ cells (Figure 2.3 C-E). For example, a *rga4*$^{+}$*rga6*$^{+}$ cell separates into two daughter cells (red box) 12 minutes after completion of ring constriction (red arrowhead) (Figure 2.3 C), while an example *rga4Δrga6Δ* cell takes 24 minutes to separate into daughter cells (red box) following completion of ring constriction (red arrowhead) (Figure 2.3 D). While the single GAP mutants (*rga4Δ* and *rga6Δ*) also exhibit delayed cell separation following ring constriction, the cell separation delay is most pronounced in the *rga4Δrga6Δ* mutant, where 50% of cells have not separated at 30 minutes post ring constriction, while all *rga4*$^{+}$*rga6*$^{+}$

cells have successfully separated (Figure 2.3 E). These findings suggest that Rga4 and Rga6 function additively to regulate timing of cell separation following completion of ring constriction.

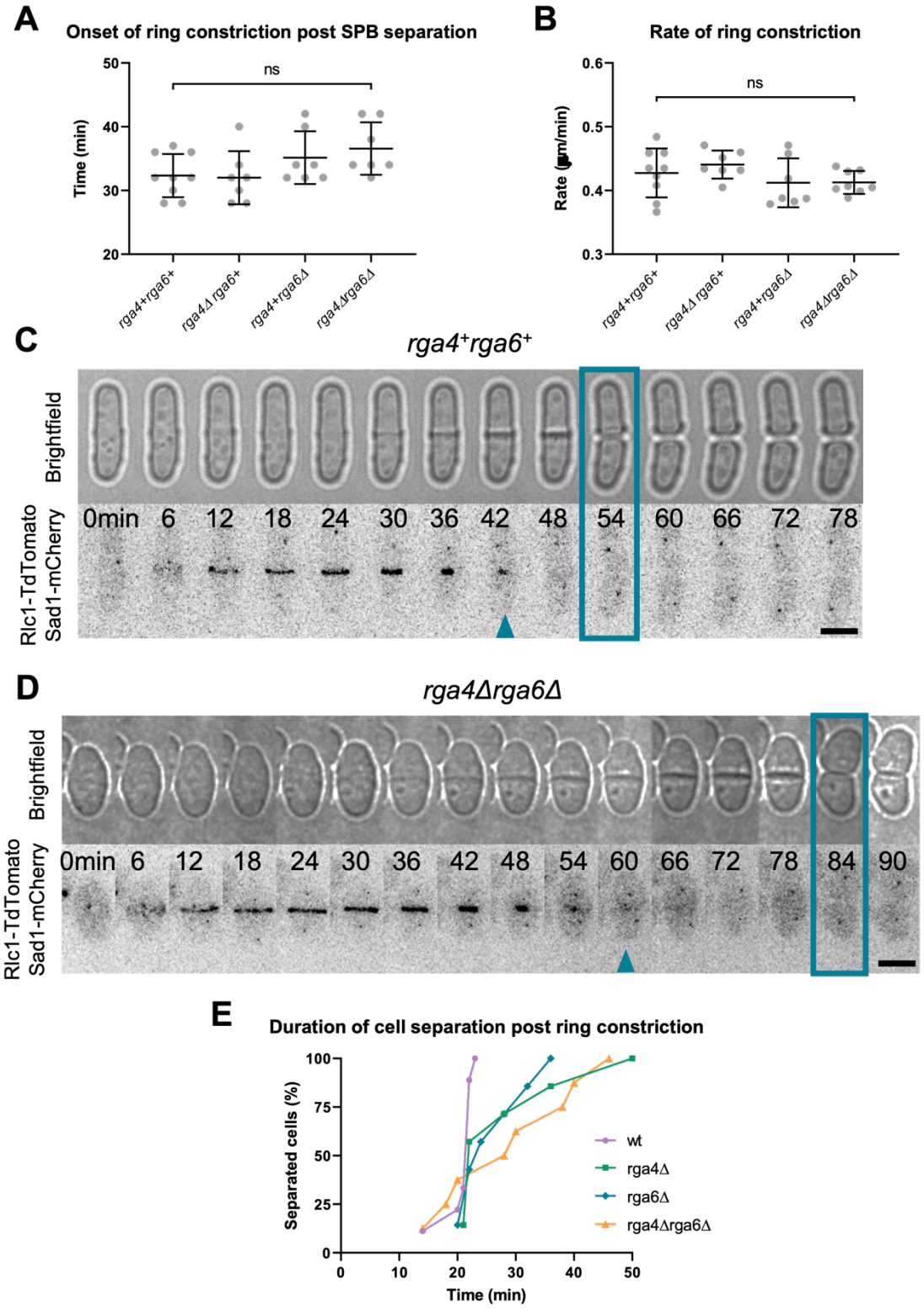

Figure 2.3. Loss of *rga4* and *rga6* results in delayed cell separation. (A) Onset of ring constriction measured from spindle pole body (SPB) separation is not delayed in the absence of *rga4* and *rga6* (n≥7 cells).

(B) Rate of ring constriction remains constant in the absence of *rga4* and *rga6* (n≥7 cells). (C) Example *rga4*$^{+}$*rga6*$^{+}$ cell separating into two daughter cells (yellow box) after completion of ring constriction (yellow arrowhead) where Rlc1-tdTom marks the actomyosin ring (scale bar = 5μm). (D) Example *rga4Δrga6Δ* cell separating into two daughter cells (yellow box) following completion of ring constriction (yellow arrowhead; scale bar = 5μm). (E) The single GAP mutants also exhibit a delay in cell separation, but the delay is longer in the double mutant (n≥7 cells). Statistical test used is Ordinary one-way ANOVA with Tukey's multiple comparisons. n.s., not significant.

2.4.3 Rga4 and Rga6 are required for proper septum morphology

In fission yeast, cell separation delays are often caused by improper localization of the primary septum digesting glucanases Eng1 and Agn1 (Martín-Cuadrado et al., 2005; Santos et al., 2005; Wang et al., 2015). To probe the cause of delayed cell separation, we examined the localization patterns of Eng1-GFP and Agn1-GFP (Liu et al., 1999; Martín-Cuadrado et al., 2003) at the division site of *rga4Δrga6Δ* mutants compared to *rga4*$^{+}$*rga6*$^{+}$ cells. Eng1-GFP and Agn1-GFP appear to properly localize to the outer rim of the membrane furrow and to the center of the division plane as a dot in a manner similar to *rga4*$^{+}$*rga6*$^{+}$ cells (Supplemental Figure 2.2 A-C (Wang et al., 2015)). Since Eng1 and Agn1 are properly delivered to the division site in the absence of *rga4* and *rga6*, the delay in cell separation does not seem to result from the inability of the glucanases to digest the primary septum to physically separate the daughter cells.

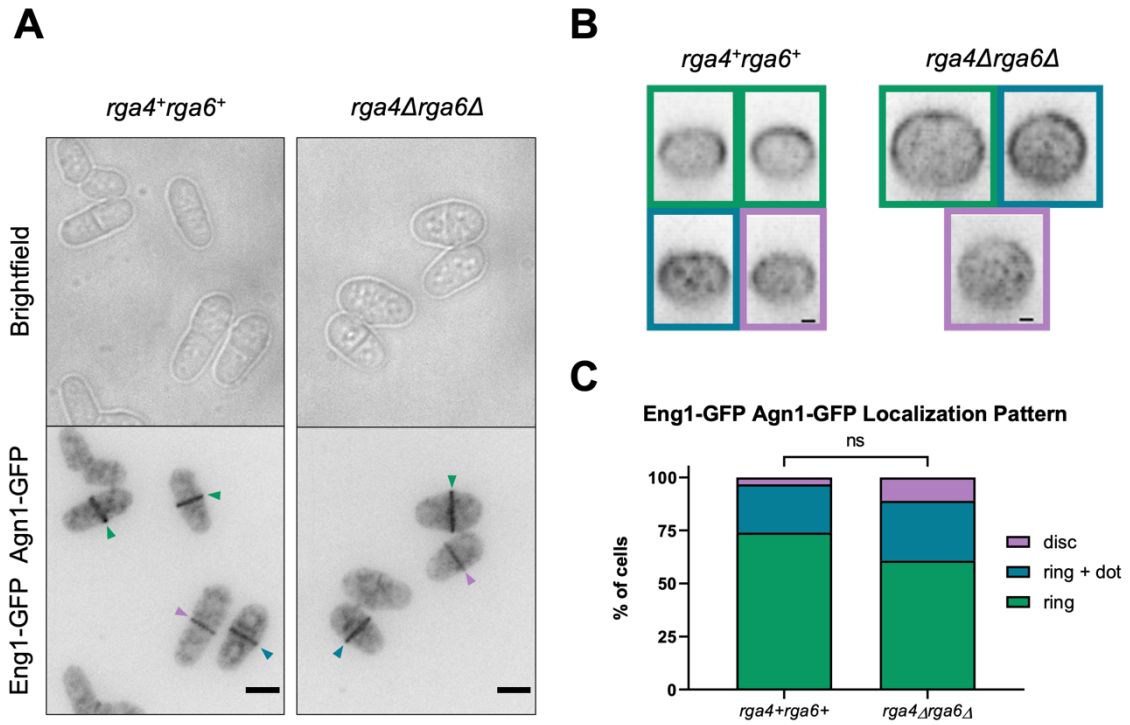

Supplemental Figure 2.2. The primary septum digesting glucanases Eng1 and Agn1 localize properly in the absence of *rga4* and *rga6*. (A) Eng1-GFP and Agn1-GFP localize to the division site in the absence of *rga4* and *rga6* in a manner similar to *rga4⁺rga6⁺* cells (blue, green, and purple arrows; scale bars = 5µm). (B) 3D-reconstructions of the division sites of *rga4⁺rga6⁺* and *rga4Δrga6Δ* cells illustrate that Eng1-GFP and Agn1-GFP properly localize to both the outer rim of the membrane furrow as a ring (green panels corresponding to cells marked with green arrowheads) and to the center of the division plane as a dot in addition to the membrane rim (blue panels corresponding to cells marked with blue arrowheads). Few cells in either genotype exhibited mislocalization of Eng1-GFP and Agn1-GFP as a disk (purple panels corresponding to cells marked with purple arrowheads; scale bar = 1µm). (C) Quantification of Eng1-GFP and Agn1-GFP localization patterns at the division site in *rga4⁺rga6⁺* and *rga4Δrga6Δ* cells, where N = 3 replicate experiments, n≥29 cells for each genotype. Statistical test used was unpaired Student's *t*-test, n.s., not significant.

Cell separation delays can also occur if the primary septum does not form properly (Cortés et al., 2007). Thus, we assessed the structural integrity of the septum in the *rga4Δrga6Δ* mutant cells. To test this, we used transmission electron microscopy (TEM) to image the division sites of *rga4*$^{+}$*rga6*$^{+}$ and *rga4Δrga6Δ* cells. Wild-type *rga4*$^{+}$*rga6*$^{+}$ cells typically build straight septa tightly coupled to the membrane furrow (Figure 2.4 A). In contrast, in *rga4Δrga6Δ* cells, we observed several morphological defects in the septa and the plasma membrane flanking the septa (Figure 2.4 B). The septa of *rga4Δrga6Δ* cells are spatially disorganized. The leading edge of the ingressing septum does not clearly show the plasma membrane in the mutant cells (Figure 2.4 B, *i* and *ii*, arrowheads). We often observed a gap in the membrane at the leading edge of the membrane furrow in *rga4Δrga6Δ* cells (Figure 2.4 B, C). Additionally, some *rga4Δrga6Δ* septa appear to have plasma membrane trapped within it (Figure 2.4 B, *iii* and *iv*). As expected, the primary and secondary septa is clearly distinguishable in *rga4*$^{+}$*rga6*$^{+}$ cells (Figure 2.4 A, arrows). However, in *rga4Δrga6Δ* cells we noticed that the secondary septum was not easily distinguishable from the primary septum (Figure 2.4 B, *i* and *ii*, arrows). Moreover, the primary septum was wider than normal in *rga4Δrga6Δ* mutants (Figure 2.4 D). Upon quantification of these aberrant morphological defects, we conclude that in *rga4Δrga6Δ* cells, a greater proportion of cells do not clearly show the leading edge of the ingressing membrane furrow (Figure 4C), show increased primary septa (Figure 2.4 D), and exhibit membrane trapped within the completed septum (Figure 2.4 E). Overall, the division planes of *rga4Δrga6Δ* mutants display morphological defects, particularly with respect to membrane organization, that are not frequently observed in *rga4*$^{+}$*rga6*$^{+}$ cells.

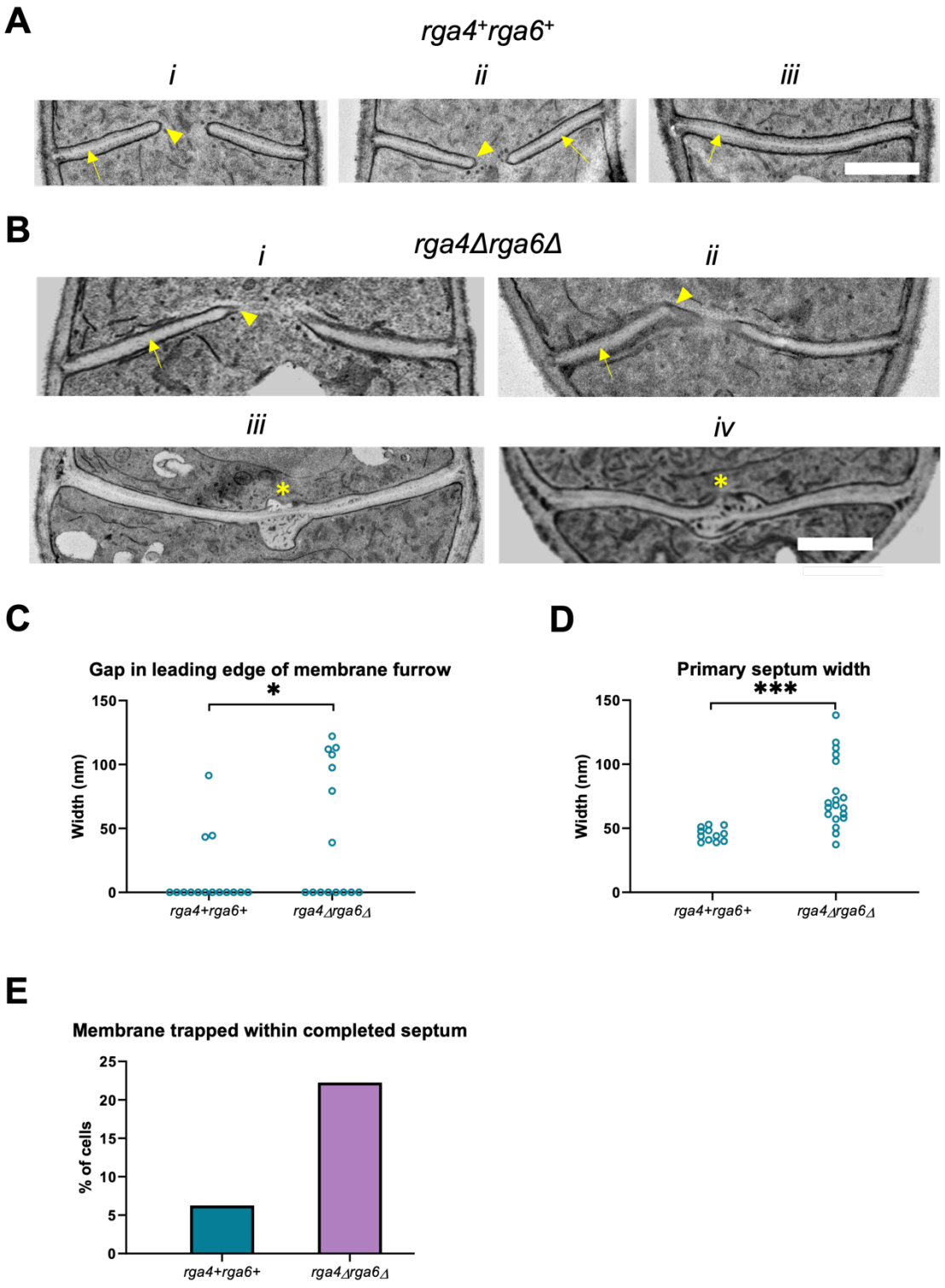

Figure 2.4. Loss of *rga4* and *rga6* results in malformed division septa. (A) In *rga4*⁺*rga6*⁺ cells, the plasma membrane (black) flanking the septum (gray) is tightly coupled with the synthesizing septum (*i* and *ii*, arrowheads) as well as the completed septum (*iii*). Additionally, the white primary septum (arrows) is

readily distinguishable from the gray flanking secondary septa (scale bar = 1μm). (B) In *rga4Δrga6Δ* cells, several septum morphology defects are evident, ranging from plasma membrane that is discontinuously visible at the membrane furrow (*i* and *ii*, arrowheads), to primary septum that is not visually distinct from the secondary septa (*i* and *ii*, arrows), to plasma membrane trapped within the completed septum (*iii* and *iv*, asterisks; scale bar = 1μm). (C) Quantification of the distance of the gap that is sometimes observed between the leading edges of the membrane furrow in *rga4*$^{+}$*rga6*$^{+}$ cells and *rga4Δrga6Δ* cells (n=15 cells per genotype). (D) Quantification of the thickness of the primary septum in *rga4*$^{+}$*rga6*$^{+}$ cells and *rga4Δrga6Δ* cells (n≥12 cells per genotype). (E) Quantification of the mean percentage of cells that show membrane trapped within the completed septum (n≥6 cells per genotype for two independent experiments). Unpaired Student's *t*-test was used to calculate statistical significance using the means of each experiment. *, $p< 0.05$; ***, $p<0.001$; n.s., not significant

2.4.4 Rga4 and Rga6 help to maintain the balance of different septum synthesizing enzymes recruited to the division site

Next, we asked if the septum morphology defects observed by TEM were due to the uncoupling or imbalance of septum synthesis and membrane furrowing in these mutants. To test this, we investigated the localization of the septum synthases Bgs1 and Bgs4, which are mainly required for the primary and secondary septa, respectively. Previous reports have shown that Cdc42 is required for the recruitment of Bgs1 to the division site but not that of Bgs4 (Estravis et al., 2012; Onwubiko et al., 2021; Wei et al., 2016). We measured the sum intensities of GFP-Bgs1 and GFP-Bgs4 at the division sites of cells during late ring constriction, since this is the stage at which both the primary and the secondary septum are simultaneously synthesized behind the constricting ring. Overall, both synthases localize properly to the division site during late ring constriction in the absence of *rga4* and *rga6* (Figure 2.5 A and D, arrowheads). 3D-reconstructions of division sites in *rga4*$^{+}$*rga6*$^{+}$

and *rga4Δrga6Δ* cells show that GFP-Bgs1 (Figure 2.5 B) and GFP-Bgs4 (Figure 2.5 E) properly flank constricting and constricted rings marked with Rlc1-tdTom.

As shown previously, *rga4Δrga6Δ* cells are wider than *rga4*$^{+}$*rga6*$^{+}$ cells and therefore have a larger division site. This suggests that these mutants should have an increased need for the septum synthesizing enzymes due to the enlarged division site. To test this, we measured the sum intensity of GFP-Bgs1 and GFP-Bgs4 normalized to the area of the division site in cells during late ring constriction, where the ring is more than 50% constricted. We calculated the area of the division site in individual cells and divided the measured sum intensity for each cell by its calculated area. After normalizing the sum intensity to division site area in individual cells, we found that GFP-Bgs1 signal scales with increasing cell width since the overall GFP-Bgs1 sum intensity over area is not altered in the absence of *rga4* and *rga6* (Figure 2.5 C). In contrast, GFP-Bgs4 signal does not scale with increasing cell width since *rga4Δrga6Δ* cells have less GFP-Bgs4 sum intensity over area than *rga4*$^{+}$*rga6*$^{+}$ cells (Figure 2.5 F). These findings indicate that loss of *rga4* and *rga6* differentially impacts delivery of the septum synthases Bgs1 and Bgs4. While Cdc42-dependent delivery of Bgs1 scales with increased division site area in the wider *rga4Δrga6Δ* mutant, the amount of Cdc42-independent delivery of Bgs4 to the division site in these cells does not scale. Thus, loss of *rga4* and *rga6* and the resulting increase in Cdc42 activity lead to an enhancement of Cdc42-mediated delivery of Bgs1, while Cdc42-independent delivery of Bgs4 is unaltered.

After finding that Cdc42-dependent trafficking of Bgs1 is enhanced in the absence of *rga4* and *rga6*, we wondered whether Sbg1, a protein that physically interacts with Bgs1 and stabilizes it at the division site, is also delivered in a manner that scales to the larger division site of *rga4Δrga6Δ* mutants (Davidson et al., 2016; Sethi et al., 2016). Following the same approach, we measured the sum intensity of eGFP-Sbg1 at the division site normalized to division site area in both *rga4*$^{+}$*rga6*$^{+}$ and *rga4Δrga6Δ* cells during late ring constriction. This analysis reveals that Sbg1 accumulation indeed scales to the increased division site area in the absence of *rga4* and *rga6* (Figure 2.6 A and C). As with Bgs1, Sbg1 properly flanks constricting and constricted rings at the membrane furrow as visualized with 3D-reconstructions of division sites in *rga4*$^{+}$*rga6*$^{+}$ and *rga4Δrga6Δ* cells (Figure 2.6 B).

To further investigate the specificity of the membrane trafficking pathways altered in the absence of *rga4* and *rga6*, we also examined the accumulation of Smi1, an intrinsically disordered protein which physically interacts with Bgs4 and promotes the localization of both Bgs1 and Bgs4 to the division site, albeit with greater preference for Bgs4 (Longo et al., 2022). Unlike with Sbg1, Smi1-mEGFP sum intensity at the division site is reduced in the absence of *rga4* and *rga6* during late ring constriction, especially upon normalization to division site area, thus indicating that Smi1 delivery does not scale with the enlarged division site in *rga4Δrga6Δ* mutants (Figure 2.6 D, E and F). Together, these results suggest that loss of *rga4* and *rga6* leads to an imbalance in the recruitment of Bgs1 and its specific binding partner Sbg1 compared to the recruitment of Bgs4 and its binding partner Smi1 at the division site.

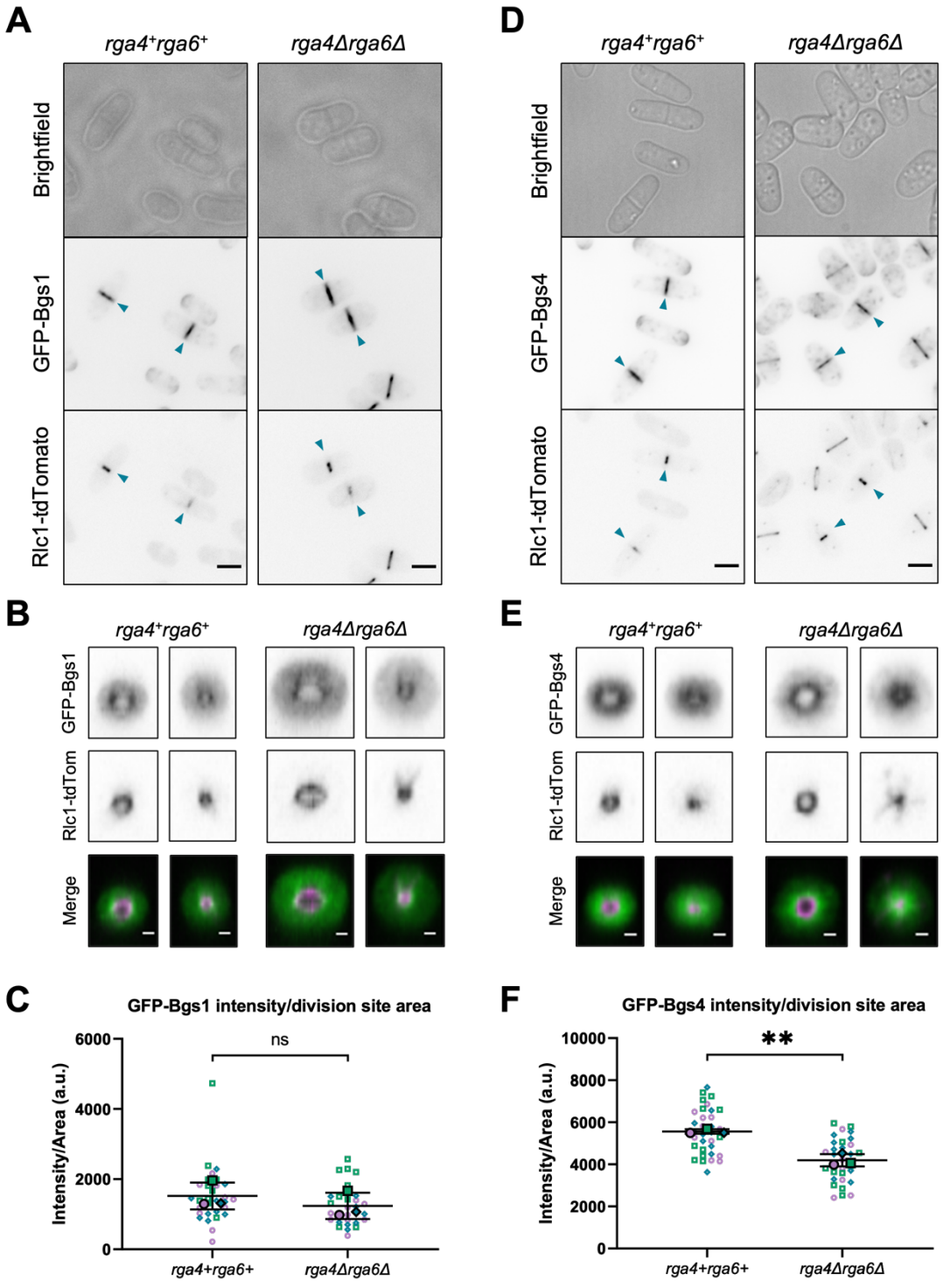

Figure 2.5. Cdc42-dependent Bgs1 delivery to the division site is enhanced in the absence of *rga4* and *rga6*, while Cdc42-independent Bgs4 delivery is not. (A) GFP-Bgs1 sum intensity at the division site in *rga4Δrga6Δ* cells is increased (arrowheads) compared to *rga4⁺rga6⁺* cells (arrowheads) during late ring

constriction (inverted sum projections; scale bars = 5 μm). (B) 3D-reconstructions of the division planes of cells with constricting and constricted rings (marked by Rlc1-tdTom) do not show any defect in the spatial organization of GFP-Bgs1 at the membrane furrow in *rga4Δrga6Δ* cells (scale bars = 1 μm). (C) GFP-Bgs1 sum intensity normalized to division site area is not different between *rga4*$^{+}$*rga6*$^{+}$ and *rga4Δrga6Δ* cells during late ring constriction. (D) GFP-Bgs4 sum intensity at the division site in *rga4Δrga6Δ* cells (arrowheads) is diminished compared to *rga4*$^{+}$*rga6*$^{+}$ cells (arrowheads) during late ring constriction (inverted sum projections; scale bars = 5 μm). (E) 3D-reconstructions of the division plane during ring constriction (Rlc1-tdTomato) show decreased intensity of GFP-Bgs4 at the membrane furrow in *rga4Δrga6Δ* cells (scale bars = 1 μm). (F) GFP-Bgs4 sum intensity normalized to division site area is less in *rga4Δrga6Δ* cells compared to *rga4*$^{+}$*rga6*$^{+}$ cells during late ring constriction. Colors = distinct experiment. Open symbols = individual cells. Solid symbols = means of each experiment. n≥10 cells per genotype per experiment. Unpaired Student's *t*-test, was used to calculate statistical significance using the means of each experiment. n.s., not significant; **, $p<0.01$.

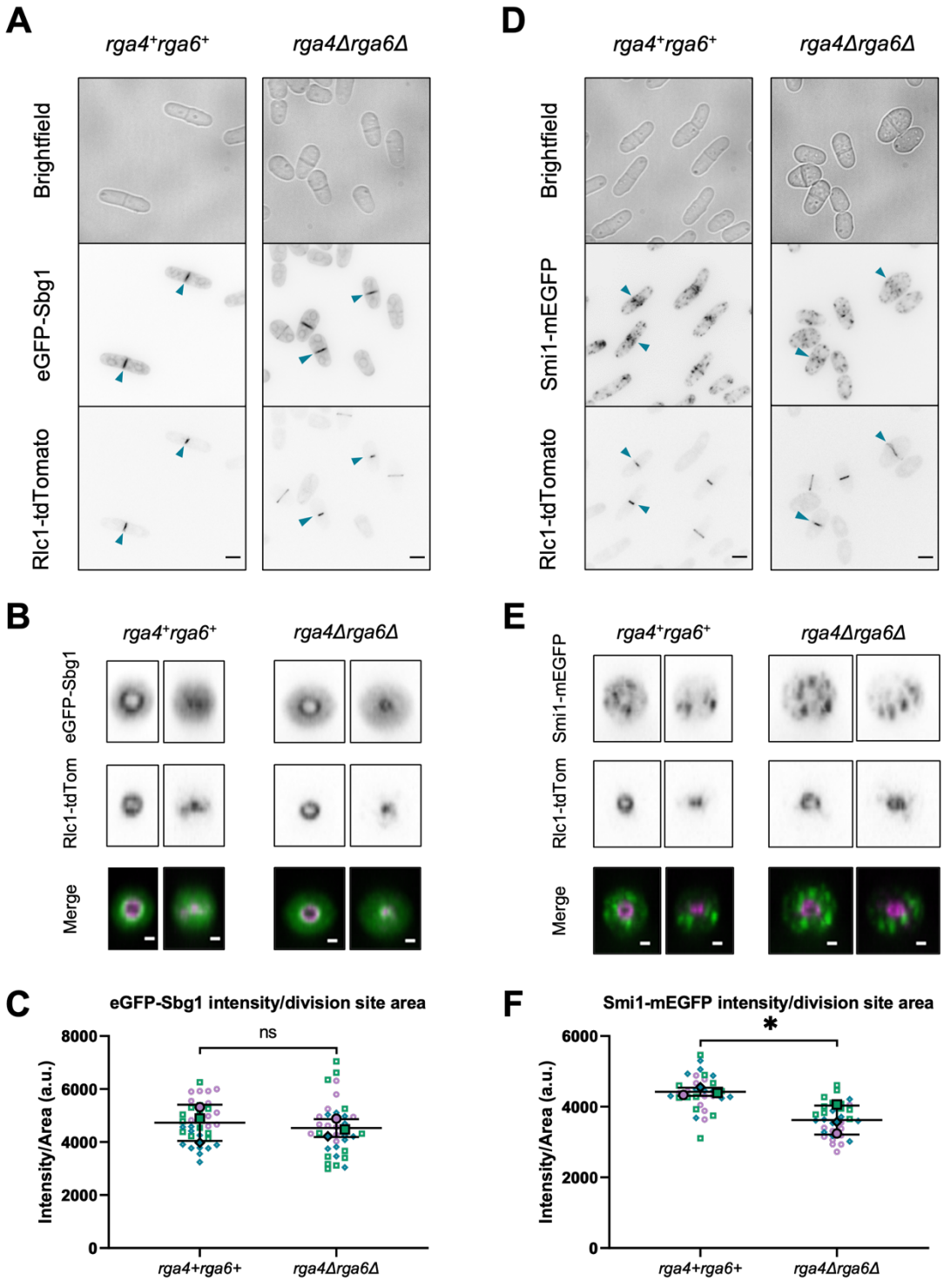

Figure 2.6. Accumulation of Bgs1-associated Sbg1 is enhanced at the division site in the absence of *rga4* and *rga6*, while accumulation of Bgs4-associated Smi1 does not increase. (A) eGFP-Sbg1 sum intensity at the division site in *rga4⁺rga6⁺* and *rga4Δrga6Δ* cells (arrowheads) during late ring constriction (inverted

sum projections; scale bars = 5 μm). (B) 3D-reconstructions of the division plane during late ring constriction (Rlc1-tdTomato) show proper spatial organization of eGFP-Sbg1 at the membrane furrow in *rga4Δrga6Δ* cells (scale bars = 1 μm). (C) eGFP-Sbg1 sum intensity normalized to division site area is the same between *rga4*$^{+}$*rga6*$^{+}$ and *rga4Δrga6Δ* cells during late ring constriction (Rlc1-tdTom). (D) Smi1-mEGFP sum intensity at the division site (arrowheads) is decreased in the absence of *rga4* and *rga6* during late ring constriction (inverted sum projections; scale bars = 5 μm). (E) 3D-reconstructions of the division plane during ring constriction (Rlc1-tdTomato) show proper localization of Smi1-mEGFP at the membrane furrow in *rga4Δrga6Δ* cells (scale bars = 1 μm). (F) Smi1-mEGFP sum intensity normalized to division site area is decreased in *rga4Δrga6Δ* cells compared to *rga4*$^{+}$*rga6*$^{+}$ cells during late ring constriction. Colors = distinct experiment. Open symbols = individual cells. Solid symbols = means of each experiment. n≥10 cells per genotype per experiment. Unpaired Student's *t*-test, was used to calculate statistical significance using the means of each experiment. n.s., not significant; *, $p < 0.05$.

2.4.5 Accumulation of exocytic proteins does not scale with enlarged division site in the absence of *rga4* and *rga6*

The septum synthases are known to be delivered to the division site by membrane trafficking events (Arasada and Pollard, 2014; Arasada and Pollard, 2015; Mulvihill et al., 2006; Wang et al., 2016). Given the differential recruitment of the septum synthases at the division site in *rga4Δrga6Δ* mutants we asked if membrane trafficking was correspondingly altered in these mutants. Previous reports suggest that both Bgs1 and Bgs4 are delivered via vesicle trafficking pathways that include Ypt3 (a Rab11 GTPase), Trs120 (a component of the TRAPP-II complex), Syb1 (a v-SNARE), and Myo52 (a Type V myosin motor) (Mulvihill et al., 2006; Wang et al., 2016). Thus, we measured the levels of these vesicular trafficking markers at the division site. Following the same paradigm used with the septum synthases and their binding partners, we measured the sum intensities

normalized to the division site area for mEGFP-Ypt3, Trs120-3xGFP, GFP-Syb1, and Myo52-GFP during late ring constriction. We specifically chose to examine the localization of Ypt3 since it has been shown to be involved in TRAPP-II-mediated exocytosis throughout the membrane furrow and since its puncta largely co-localize with the septum synthase Bgs4, a vesicle cargo (Wang et al., 2016). When mEGFP-Ypt3 sum intensity is normalized to the area of the division site, there appears to be less Ypt3 accumulation in the absence of *rga4* and *rga6* (Figure 2.7 B). The overall distribution of Ypt3 within the division plane, however, is unperturbed in *rga4Δrga6Δ* cells compared to *rga4*$^{+}$*rga6*$^{+}$ cells, indicating that Ypt3 remains properly localized, albeit is less abundant relative to the size of the division site (Figure 2.7 A). Next, we examined the localization of Trs120, a subunit of the TRAPP-II complex which largely co-localizes with Ypt3 to promote exocytic vesicle tethering and which promotes delivery of Bgs4 puncta, both at the division site and the cell ends (Wang et al., 2016). After normalizing to the size of the division site, the sum intensity of Trs120-3xGFP does not scale to division site area in the absence of *rga4* and *rga6* (Figure 2.7 D). We did not see any change in the localization pattern of Trs120 at the division site (Figure 2.7 C).

We then investigated the localization of the post-Golgi v-SNARE Syb1 which physically tethers exocytic vesicles as a component of the SNARE complex. Similar to Bgs4, Ypt3, and Trs120 during late ring constriction, the sum intensity of GFP-Syb1 normalized to the area of the division site is decreased in the absence of *rga4* and *rga6* (Figure 2.7 F). Notably, the distribution pattern of Syb1 at the division site is slightly altered in *rga4Δrga6Δ* cells. In *rga4*$^{+}$*rga6*$^{+}$ cells, Syb1 is primarily localized to the outer rim of the

division plane. In *rga4Δrga6Δ* mutants, Syb1 at the outer edge of the division plane appears dampened and instead coalesces as large bright puncta throughout the division plane (Figure 2.7 E). Finally, we also examined the localization of the myosin-V motor Myo52, which physically transports exocytic vesicles along actin cables to be delivered throughout the membrane furrow (Wang et al., 2016). After normalizing for division site area, Myo52-GFP sum intensity is less in the absence of *rga4* and *rga6*, similar to the other exocytic proteins examined (Figure 2.7 H). Like the other exocytic proteins aside from Syb1, Myo52 also properly localizes throughout the division plane in the mutant (Figure 2.7 G). For a further analysis of membrane trafficking markers, we also examined the sum intensity of Ypt2 (a Rab8 GTPase) and Psy1 (t-SNARE) normalized to division site area in $rga4^{+}rga6^{+}$ and *rga4Δrga6Δ* cells. As with the other exocytic markers, neither Ypt2-mEGFP sum intensity nor GFP-Psy1 sum intensity at the division site scaled to the increased division site area of *rga4Δrga6Δ* mutants (Supplemental Figure 2.3 C-D). In fact, Ypt2-mEGFP sum intensity is markedly decreased at the membrane furrow in the absence of *rga4* and *rga6* as visualized with 3D-reconstructions of the division plane (Supplemental Figure 2.3 A). While GFP-Psy1 remains localized throughout the membrane furrow in the absence of *rga4* and *rga6*, 3D-reconstructions of the division plane reveal an increased incidence of bright puncta in the mid-region of the membrane furrow (Supplemental Figure 2.3 B, white arrowheads), which mimics the increase in Syb1 puncta likewise observed in *rga4Δrga6Δ* mutants (Figure 2.7 E). In summary, no striking defects in the localization patterns of the exocytic proteins examined were observed, aside from some altered localization of the SNARE components Syb1 and Psy1. Rather than being mislocalized, the examined exocytic markers appear to be less abundant relative to division site area in the absence of

rga4 and *rga6*. These findings indicate that, in *rga4Δrga6Δ* mutants, even though Bgs1 and Sbg1 recruitment is enhanced, several vesicular exocytic events do not scale proportionally to the enlarged division site.

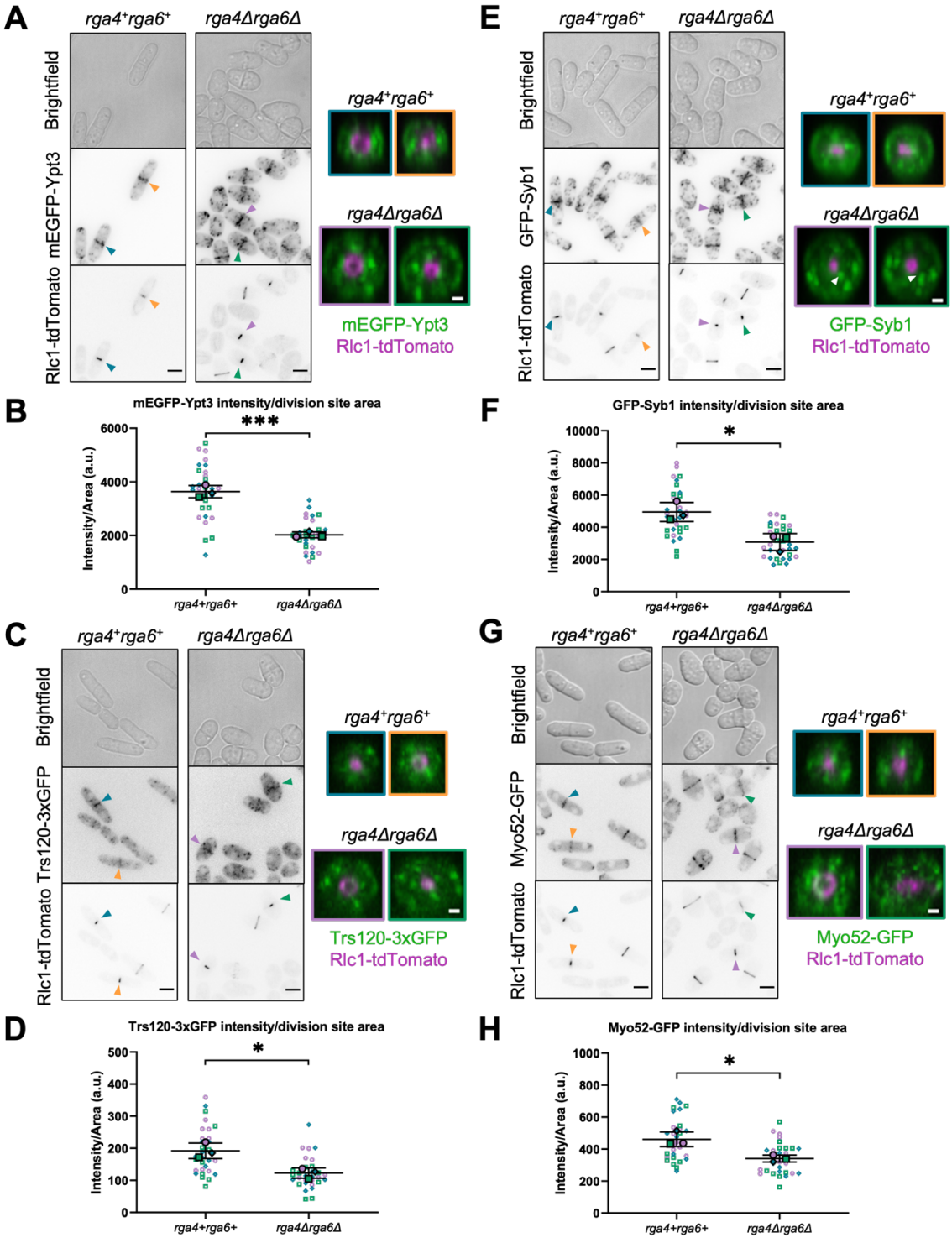

Figure 2.7. Exocytic markers Ypt3, Syb1, Trs120 and Myo52 do not scale with the enlarged division plane in *rga4Δrga6Δ* mutants. (A, C, E, and D) Sum intensity projections of exocytic proteins Rab11 GTPase mEGFP-Ypt3 (A), TRAPP-II subunit Trs120-3xGFP (C), v-SNARE GFP-Syb1 (E), and Type V

myosin motor Myo52-GFP (G) at the division site in *rga4*$^{+}$*rga6*$^{+}$ and *rga4Δrga6Δ* cells (arrowheads) during late ring constriction (inverted sum projections; scale bars = 5 μm). 3D division site projections show that each protein besides GFP-Syb1 (E, white arrowheads) is properly localized in the absence of *rga4* and *rga6* (scale bars = 1 μm). 3D-reconstructions are color-coded to arrowheads to indicate cells depicted. (B, D, F, and H) Sum intensities of mEGFP-Ypt3 (B), Trs120-3xGFP (D), GFP-Syb1 (F), and Myo52-GFP (H) normalized to division site area are decreased in *rga4Δrga6Δ* cells compared to *rga4*$^{+}$*rga6*$^{+}$ cells during late ring constriction. Only cells in the late stages of ring constriction were used for this analysis (indicated by colored arrowheads). Symbol colors in graphs = distinct experiments. Open symbols = individual cells. Solid symbols = means of each experiment. n≥10 cells per genotype per experiment. Unpaired Student's *t*-test, was used to calculate statistical significance using the means of each experiment. *, $p< 0.05$; ***, $p<0.001$.

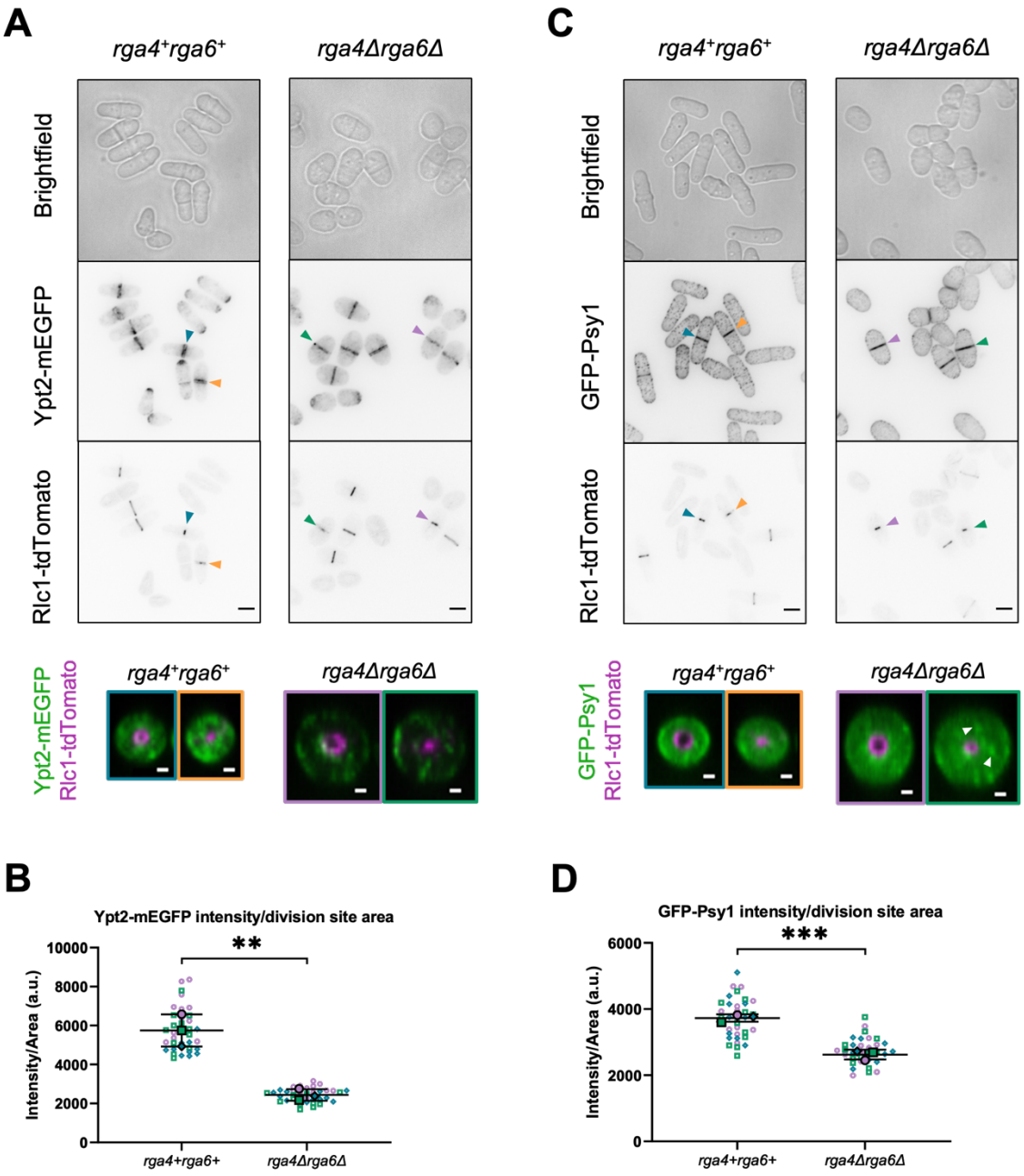

Supplemental Figure 2.3. Exocytic markers Ypt2 and Psy1 do not scale with the enlarged division plane in *rga4Δrga6Δ* mutants. (A and C) Sum intensity projections of exocytic proteins Rab8 GTPase Ypt2-mEGFP (A) and t-SNARE GFP-Psy1 (C) at the division site in *rga4⁺rga6⁺* and *rga4Δrga6Δ* cells (arrowheads) during late ring constriction (inverted sum projections; scale bars = 5 µm). 3D division site projections show that Ypt2-mEGFP signal is greatly decreased at the membrane furrow in the absence of *rga4* and *rga6* (A), while GFP-Psy1 exhibits a greater incidence of bright puncta in the mid-region of the

furrow (white arrowheads) in the absence of *rga4* and *rga6* (C). 3D-reconstructions are color-coded to arrowheads to indicate cells depicted. (B and D) Sum intensities of Ypt2-mEGFP (B) and GFP-Psy1 (D) normalized to division site area are decreased in *rga4Δrga6Δ* cells compared to *rga4*$^{+}$*rga6*$^{+}$ cells during late ring constriction. Only cells in the late stages of ring constriction were used for this analysis (indicated by colored arrowheads). Symbol colors in graphs = distinct experiments. Open symbols = individual cells. Solid symbols = means of each experiment. n≥10 cells per genotype per experiment. Unpaired Student's *t*-test, was used to calculate statistical significance using the means of each experiment. **, $p< 0.01$; ***, $p<0.001$.

2.4.6 Rga4 and Rga6 promote proper endocytosis

Membrane trafficking includes both delivery of materials via exocytosis as well as recycling of materials via endocytosis. We have previously shown that Cdc42 activity is required for proper endocytic dynamics at the division site (Onwubiko et al., 2019). Here we show that loss of *rga4* and *rga6* results in aberrant membrane organization at the division site. Hence, we asked if excessive Cdc42 activity as seen in *rga4Δrga6Δ* mutants leads to defects in membrane remodeling including endocytosis. To do this, we used the actin filament cross-linker fimbrin Fim1 to mark sites of endocytosis. In the absence of *rga4* and *rga6,* Fim1-mEGFP remains localized to the division site as observed in sum projections of both *rga4*$^{+}$*rga6*$^{+}$ and *rga4Δrga6Δ* cells (Figure 2.8 A). Next, as with the exocytic markers, we measured the sum intensity of Fim1-mEGFP in both genotypes and then normalized intensity to division site area. After normalization, Fim1-mEGFP sum intensity does not scale to the enlarged division site in the absence of *rga4* and *rga6* (Figure 2.8 B). This indicates that endocytosis is not enhanced in these mutants with respect to the enlarged division plane.

We then investigated the dynamics of endocytosis in *rga4Δrga6Δ* mutants compared to *rga4*$^{+}$*rga6*$^{+}$ cells. To do this, we again used Fim1-mEGFP to mark sites of endocytosis and generated time-lapse movies to track the dynamics of the endocytic patches. We find that at the division site the average lifetime of Fim1-mEGFP patches is reduced in *rga4Δrga6Δ* mutants compared to *rga4*$^{+}$*rga6*$^{+}$ cells (Figure 2.8 C). However, accurately tracking distinct endocytic patches at the division site is challenging due to their dense concentration at that site. Thus, we also measured the lifetime of Fim1-mEGFP labeled endocytic patches at the cell ends of interphase cells, using cell polarity to enhance our understanding of cytokinesis as we have used cytokinesis as a paradigm to understand cell polarity (Hercyk and Das, 2019; Hercyk et al., 2019b). Using this approach, we confirmed that the average endocytic patch lifetime is also decreased in the absence of *rga4* and *rga6* at the cell ends (Supplemental Figure 2.4 A).

To further investigate the dynamics of endocytic patches at the division site, we generated montages from Fim1-mEGFP timelapse movies to observe the internalization patterns in both *rga4*$^{+}$*rga6*$^{+}$ cells and *rga4Δrga6Δ* mutants. To capture these internalization events, we created montages formed from a selection line drawn a 45-degree angle between the division plane and the long axis of cells. These montages show that endocytic patches consistently undergo successful internalization in *rga4*$^{+}$*rga6*$^{+}$ cells (Figure 2.8 D). In contrast, in *rga4Δrga6Δ* mutants we observe an increased incidence of aberrant endocytic patch movements (Figure 2.8 D). These include stalled events in which a patch fails to complete internalization, retraction events in which a patch reverses its motion and moves back to the plasma membrane, and incomplete patch internalization (Figure 2.8 D).

Overall, we find that endocytic patches do not internalize as deeply into the interior of the cell from the plasma membrane in the absence of *rga4* and *rga6* (Figure 2.8 D and E). To clearly illustrate the observed endocytic defect in the absence of *rga4* and *rga6*, we then determined the percentages of endocytic patches which do not internalize beyond 350 nm, the distance from the plasma membrane at which vesicle scission is thought to occur (Basu et al., 2014). In *rga4*$^{+}$*rga6*$^{+}$ cells, approximately 11% of observed endocytic patches fail to internalize beyond 350 nm, while approximately 34% of observed endocytic patches in *rga4Δrga6Δ* cells do not internalize beyond 350 nm, suggesting these patches may fail scission (Figure 2.8 F). To determine whether these internalization defects are global in nature, we also investigated the internalization dynamics and distances of Fim1-mEGFP labeled endocytic patches at the cell ends of interphase cells. As at the division site, we found that endocytic patches at the cell ends display similar aberrant motions and do not internalize as deeply into the cell from the cortex in the absence of *rga4* and *rga6* (Supplemental Figure 2.4 B and C). We also observed an increase in the percentage of endocytic patches that fail to internalize beyond 350 nm (Supplemental Figure 2.4 D). Together, these observations indicate that loss of *rga4* and *rga6* results in global endocytic defects that decrease both the lifetime of endocytic patches as well their ability to internalize from the plasma membrane.

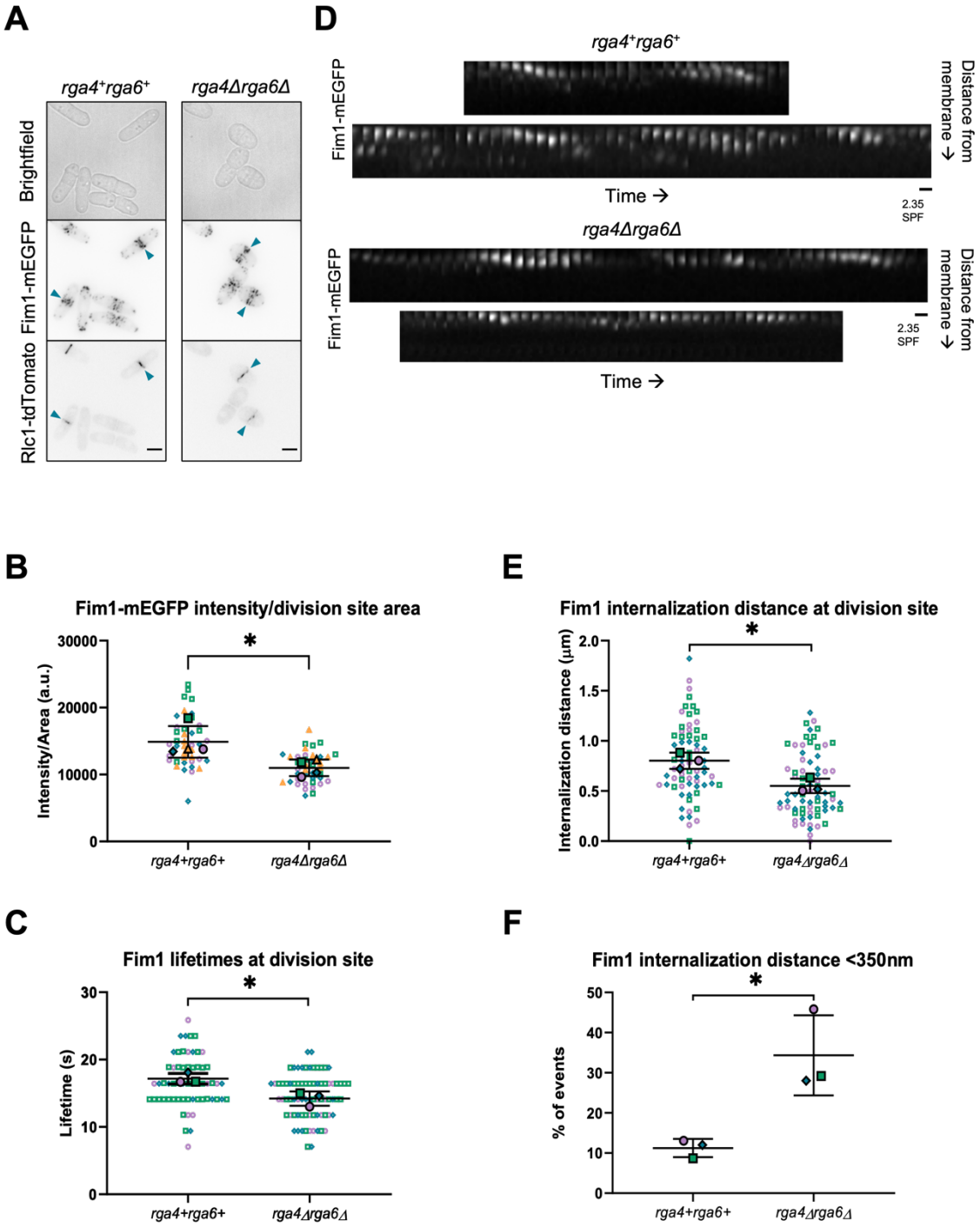

Figure 2.8. Endocytosis at the division site is impaired in the absence of *rga4* and *rga6*. (A) Fim1-mEGFP sum intensity at the division site in *rga4⁺rga6⁺* and *rga4Δrga6Δ* cells (arrowheads) during late ring constriction (inverted sum projections; scale bars = 5 µm). (B) Fim1-mEGFP sum intensity normalized to division site area is less in the absence of *rga4* and *rga6* (n≥10 cells). (C) At the division site, the lifetimes

of Fim1-labeled endocytic patches are shorter on average in the absence of *rga4* and *rga6* (n≥10 endocytic patches per experiment). (D) Montages generated at the division site illustrate that Fim1-mEGFP labeled endocytic patches do not internalize as far into the cell interior and exhibit aberrant motions in the absence of *rga4* and *rga6* (scale bars = 800nm; frame rates = 2.35 seconds per frame (SPF)). (E) Fim1-mEGFP labeled endocytic patches do not internalize as deeply into the cell interior from the plasma membrane in the absence of *rga4* and *rga6* (n≥23 endocytic patches per genotype per experiment). (F) At the division site, the proportion of endocytic patches that fail to internalize beyond 350 nm from the plasma membrane is increased in the absence of *rga4* and *rga6* (n≥23 endocytic patches per genotype per experiment). Symbol colors in graphs = distinct experiments. Open symbols = individual cells. Solid symbols = means of each experiment. Unpaired Student's *t*-test, was used to calculate statistical significance using the means of each experiment. *, $p<0.05$.

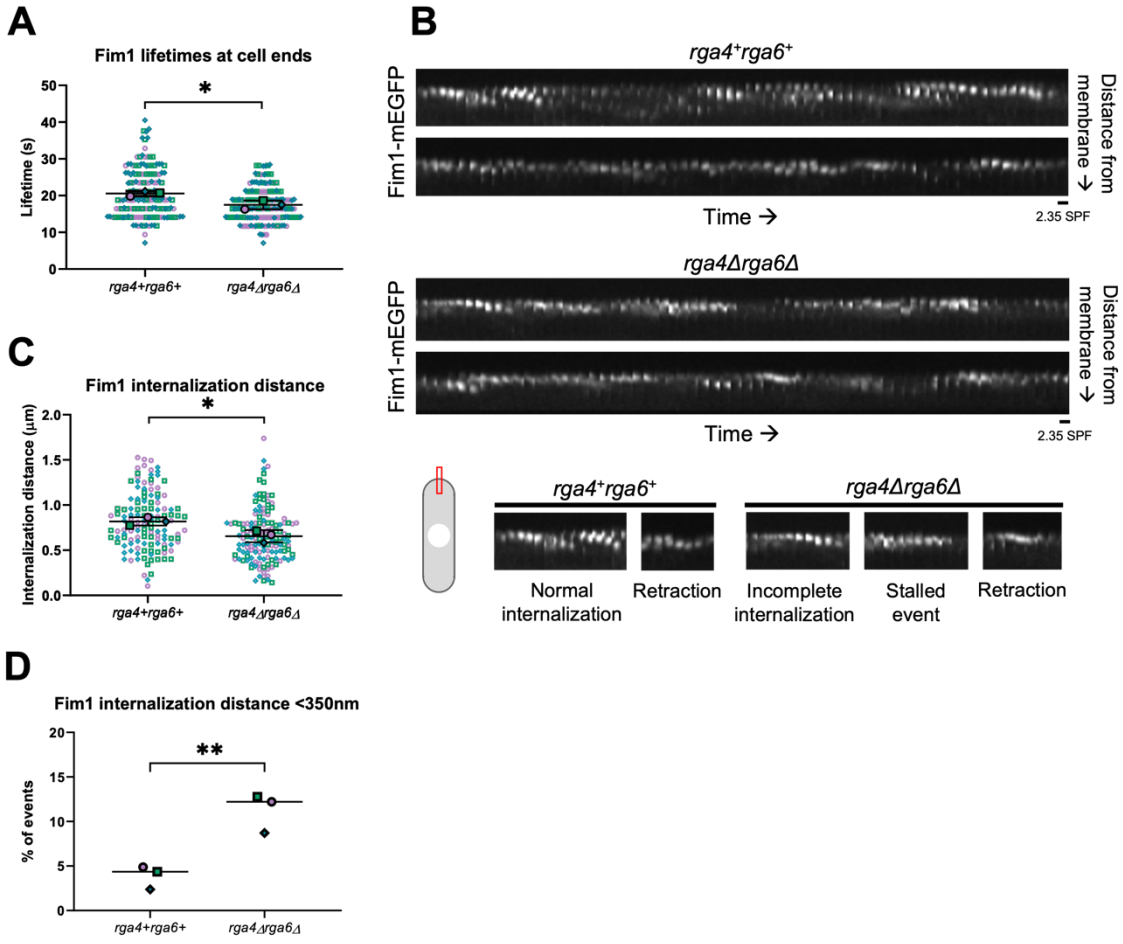

Supplemental Figure 2.4. Endocytosis at the cell ends is impaired in the absence of *rga4* and *rga6*. (A) The lifetimes of Fim1-labeled endocytic patches are decreased in the absence of *rga4* and *rga6* at the cell ends of interphase cells (n≥45 endocytic patches per experiment). (B) Montages generated at the ends of interphase cells illustrate that Fim1-mEGFP labeled endocytic patches do not internalize as far into the cell interior and exhibit aberrant motions in the absence of *rga4* and *rga6* (scale bars = 800nm; frame rates = 2.35 seconds per frame (SPF)). (C) Fim1-mEGFP labeled endocytic patches do not internalize as deeply into the cell interior from the plasma membrane in the absence of *rga4* and *rga6* (n≥41 endocytic patches per genotype per experiment). (D) At the cell ends, the proportion of endocytic patches that fail to internalize beyond 350 nm from the plasma membrane is increased in the absence of *rga4* and *rga6* (n≥41 endocytic patches per genotype per experiment). Symbol colors in graphs = distinct experiments. Open symbols = individual cells. Solid symbols = means of each experiment. Unpaired Student's *t*-test, was used to calculate statistical significance using the means of each experiment. *, $p<0.05$; **, $p<0.01$.

2.5 DISCUSSION

2.5.1 Cdc42 activity influences the spatiotemporal regulation of cytokinetic membrane trafficking

Previous reports have shown that membrane trafficking events are essential for successful cytokinesis (Arasada and Pollard, 2015; Onwubiko et al., 2021; Wang et al., 2016). Our findings illustrate the importance of spatiotemporally regulating membrane trafficking events during cytokinesis to properly coordinate actomyosin ring constriction, membrane furrow ingression, and septum synthesis. In early cytokinesis, Cdc42 promotes the recruitment of Bgs1 that is mainly required for primary septum formation (Wei et al., 2016). Next, Bgs4, that is mainly required for secondary septum formation, is recruited to the division site via a Cdc42-independent mechanism (Estravis et al., 2012; Wei et al., 2016). Delivery of these enzymes via membrane-bound vesicles is coupled to membrane remodeling events necessary for furrow formation (Wang et al., 2016). Here we show that spatiotemporal regulation of Cdc42 activity at the division site helps to maintain proper coupling of the delivery of different septum synthesizing enzymes and membrane remodeling via trafficking events.

The primary septum is built first and only comprises a small portion of the septum, while the secondary septum is formed next and is the major component. This highlights the importance of spatiotemporally regulating the delivery of Bgs1 and Bgs4, the enzymes that synthesize different components of the septum. First, Bgs1 needs to be delivered to the division site where it helps to anchor the actomyosin ring to the membrane and promote

primary septum synthesis, thus initiating ring constriction and furrow formation. This is followed by the delivery of Bgs4 at the ingressing membrane to enable secondary septum formation. It is unclear how the delivery of Bgs1 and Bgs4 are regulated to ensure this spatiotemporal distinction. We posit that this is mediated by spatiotemporal regulation of Cdc42 since it is required for the delivery of Bgs1 but not Bgs4. Decreasing Cdc42 activity after onset of septum ingression ensures proper delivery of Bgs4 and corresponding membrane trafficking events. In *rga4Δrga6Δ* mutants, Bgs4 levels do not scale with septum size, which may lead to a delay in septum maturation and a subsequent delay in cell separation. Interestingly, while enhanced Cdc42 activity leads to increased Bgs1 delivery, we did not see any increase in the levels of several exocytic proteins at the division site that are involved in cytokinesis. Similarly, enhanced Cdc42 activity also enhanced the localization of Sbg1 protein that binds to and promotes Bgs1 delivery but not of Bgs4 or its associating protein Smi1. This indicates that upon misregulation of Cdc42 activity, the balance of the delivery of septum synthesizing enzymes and Cdc42-independent membrane trafficking events is disrupted. Further research will mechanistically define these different cargo-specific Cdc42-dependent and -independent delivery events. Normally in fission yeast, during early septation, Bgs1-dependent primary septa form and this is followed by the Bgs4-dependent secondary septa flanking the primary septa. Our analysis of electron micrographs of the GAP mutants shows enhanced primary septa, while the secondary septa is not clearly visible. Conceivably the increased Bgs1 delivery leads to an increase in linear beta-glucan within the septum. It is possible that the balance between the different membrane trafficking events helps to maintain the spatial organization of the different septa.

2.5.2 Spatiotemporal regulation of Cdc42 activity promotes spatiotemporal control of endocytosis

Here we also show that misregulation of Cdc42 activity leads to endocytic defects at the division site. Without proper internalization of endocytic vesicles from the division site, the spatial organization of the membrane furrow is likely perturbed. Indeed, we find that *rga4Δrga6Δ* mutants exhibit aberrant septum morphology with membrane trapped within the closed septum. In the absence of *rga4* and *rga6*, endocytosis is globally misregulated during both cytokinesis and interphase, which suggests that Cdc42 activity must be properly regulated to ensure efficient endocytosis. Indeed, Cdc42 is already known to promote endocytosis when activated by one of its GEF activators, Gef1 (Onwubiko et al., 2021). Interestingly, when Cdc42 activity is impaired in *gef1Δ* cells, an endocytic protein Cdc15 over accumulates in endocytic patches and Cdc15-labeled endocytic patches display longer lifetimes (Onwubiko et al., 2021). Fittingly, these endocytic patch dynamics in *gef1Δ* cells are the exact opposite of those observed in *rga4Δrga6Δ* cells, which indicates that Cdc42 is an important regulator of endocytosis. As a molecular switch, Cdc42 is active when GTP-bound and inactive when bound to GDP. Thus, the molecular regulation of Cdc42 activity may be an efficient way to spatiotemporally control endocytosis to ensure that membrane and proteins are properly recycled from the plasma membrane.

During interphase, active Cdc42 and its GAPs Rga4 and Rga6 display little overlap in their localization since Cdc42 is active at the growing cell ends while these GAPs localize to the cell sides (Das et al., 2007; Revilla-Guarinos et al., 2016). The other GAP Rga3, conversely, co-localizes with active Cdc42 at growing cell ends as well as at polarity sites

in mating cells (Gallo Castro and Martin, 2018). During cytokinesis, however, both active Cdc42 and its GAPs are present at the division site. This observation suggests that some change occurs to minimize the boundary between active Cdc42 and its GAPs during cytokinesis. Recently, Rga4 localization patterns were found to change in a cell cycle-dependent manner . During interphase, Rga4 localizes to the cell sides in a punctate corset pattern (Das et al., 2007), but when cells enter mitosis, Rga4 spreads more homogeneously along the cortex and localizes even up to the cell ends (Rich-Robinson et al., 2021). Thus, it is possible that cell cycle-dependent regulation of Rga4 enables its localization to the division site to decrease Cdc42 activation after the onset of actomyosin ring constriction. Furthermore, Rga6 displays similar localization dynamics throughout the cell cycle, where it localizes as puncta along the cell sides during interphase, proceeds to the cell ends during early cytokinesis, and then localizes to the division site during ring constriction (Revilla-Guarinos et al., 2016). Taken together, here we show that the GAPs Rga4 and Rga6 spatiotemporally regulate Cdc42 activity at the division site to enable proper coupling of membrane furrow ingression and septum synthesis.

2.5.3 Cdc42 activity requires precise regulation during cytokinesis to enable proper septum synthesis and cell separation

In addition to *S. pombe*, previous studies have implicated a role for Cdc42 in cytokinesis in other eukaryotes. For example, in animal cells, injection of constitutively active Cdc42 impairs membrane furrowing in *Xenopus laevis* embryos, leading to cytokinesis failure (Drechsel et al., 1997). RNAi depletion of Cdc42 in asymmetrically dividing *C. elegans* embryos also results in cytokinetic failure when performed in formin mutants (Jordan et al., 2016). However, it should be noted that perturbed Cdc42 function does not cause cytokinetic failure in many metazoan cell types (Jordan et al., 2016), perhaps due to fundamental differences between animal and yeast cytokinesis, such as the lack of a cell wall in animal cells. Similar to our findings, previous study in *S. cerevisiae* budding yeast found that Cdc42 hyperactivation during mitotic exit results in delayed cell separation and aberrant septum morphology (Atkins et al., 2013). Additionally, another budding yeast study reported that Cdc42 works antagonistically with another Rho GTPase, Rho1, to regulate secondary septum (SS) formation (Onishi et al., 2013). While Rho1 activity is necessary to promote SS formation, Cdc42 hyperactivation impairs SS synthesis, (Onishi et al., 2013) which then prolongs cytokinesis as reported (Atkins et al., 2013). Previous research has shown a positive role for Cdc42 in early cytokinesis (Jordan et al., 2016; Wei et al., 2016), while this current work and others show a negative role for Cdc42 in late cytokinesis. Thus, together this suggests that Cdc42 needs to be tightly regulated during cytokinesis to allow membrane furrow ingression, septum formation and timely cell separation.

2.6 MATERIALS AND METHODS

2.6.1 Strains and cell culture

The *S. pombe* strains used in this study are listed in Table 1. All strains are isogenic to the original strain PN567. Cells were cultured in yeast extract (YE) medium and grown exponentially at 25°C for 3 rounds of 8 generations before imaging. Standard techniques were used for genetic manipulation and analysis (Moreno et al., 1991).

2.6.2 Microscopy

Imaging was performed at room temperature (23–25°C). We used an Olympus IX83 microscope equipped with a VTHawk two-dimensional array laser scanning confocal microscopy system (Visitech International, Sunderland, UK), a Hamamatsu electron-multiplying charge-coupled device digital camera (Hamamatsu EM-CCD Digital Camera ImageM Model: C9100-13 Serial No: 741262, Hamamatsu, Hamamatsu City, Japan) and a 100×/1.49 NA UAPO lens (Olympus, Tokyo, Japan). We also used a spinning disk confocal microscope system with a Nikon Eclipse inverted microscope with a 100×/1.49 NA lens, a CSU-22 spinning disk system (Yokogawa Electric Corporation) and a Photometrics EM-CCD camera (Photometrics Technology Evolve with excelon Serial No: A13B107000). Images were acquired with MetaMorph (Molecular Devices, Sunnyvale, CA) and analyzed with ImageJ (National Institutes of Health, Bethesda, MD (Schneider et al., 2012)). For still and *z*-series imaging, the cells were mounted directly on glass slides with a #1.5 coverslip (Thermo Fisher Scientific, Waltham, MA) and imaged immediately, and with fresh slides prepared every 10 min. *Z*-series images were acquired with a depth

interval of 0.4 μm. For time-lapse images, cells were placed in 3.5 mm glass-bottom culture dishes (MatTek, Ashland, MA) and overlaid with YE medium containing 0.6% agarose and 100 μM ascorbic acid as an antioxidant to minimize toxicity to the cell, as reported previously (Frigault et al., 2009; Wei et al., 2017).

2.6.3 Electron microscopy

Transmission electron microscopy was performed as described previously (Chappell and Warren, 1989). Cells were washed three times in sterile water, fixed for 1 h in 2% potassium permanganate at room temperature, and then harvested by centrifugation, washed three times in sterile water, resuspended in 70% ethanol, and incubated overnight at 4°C. Samples were then dehydrated by sequential washes in 90% ethanol (twice for 15 min) and washed in 100% ethanol (three times for 20 min). The pellet was resuspended in propylene oxide for 10 min, incubated in a 1:1 mixture of propylene oxide and Spurr's medium for 1 h, and incubated in neat Spurr's medium for 1 h. This was followed by another change of medium and incubation at 65°C for 1 h. Finally, samples were embedded in Spurr's medium in a capsule, and resin in the medium was allowed to polymerize at 60°C overnight. Blocks were sectioned with a diamond knife and stained with uranyl acetate and lead citrate. The cells were then examined in a Zeiss Libra 200MC electron microscope (Oberkochen, Germany) at the University of Tennessee Imaging Core facility or in a ThermoFisher Scientific Talos 120C G2 Transmission Electron Microscope at the Donald Danforth Plant Science Center Imaging Core facility.

2.6.4 Onset of ring constriction analysis

Onset of ring constriction in individual cells was measured as the time that elapsed from spindle pole body separation (marked with Sad1-mCherry) to the time point at which the ring (marked with Rlc1-tdTom) began to constrict, where the width of the ring is first measurably smaller than that of the previous time point.

2.6.5 Rate of ring constriction analysis

Rate of ring constriction was calculated by dividing the circumference of individual cells by the time each took to complete ring constriction in time lapse movies. The start of ring constriction was denoted as the first time point at which the breadth of the ring (marked with Rlc1-tdTom) was measurably smaller than that of the previous time point. The end of ring constriction was marked as the time point at which the ring had constricted into a dot that did not further condense in subsequent time points. The circumference of cells was calculated using the following formula: C = 3.14 x D, where D is the diameter of a cell measured across the division site.

2.6.6 Duration of cell separation post ring constriction analysis

The duration of cell separation in individual cells was measured as the time that elapsed following the completion of ring constriction (as previously described) and the time point at which daughter cells physically separated, as shown in the DIC channel.

2.6.7 Analysis of fluorescence intensity normalized to division site area

rga4^{+}*rga6*$^{+}$ and mutant cells expressing fluorescent proteins were grown to OD 0.2-0.5 and imaged on slides. Depending on the fluorophore, 21-24 *z*-planes were collected at a *z*-

interval of 0.4 µm for either or both the 488 nm and 561 nm channels. The same number of z-slices were collected for *rga4*$^{+}$*rga6*$^{+}$ and mutant cells expressing the same fluorophore using the same imaging settings. ImageJ was used to generate sum projections from the *z*-series and to measure the sum fluorescence intensity of each fluorophore at the division site. The background fluorescence in a cell-free region of the image was subtracted to generate the normalized intensity. Only cells found within the central 80% of the imaging field were used for analysis. This was done to account for uneven illumination of the imaging field. Additionally, only cells in late ring constriction (at least 50% constricted) were used for analysis in order to standardize our plasma membrane area measurements at the division site. Sum signal intensity was then measured and normalized to division site area on a cell-by-cell basis using the following approach**:** Sum intensity measurements at the division site were made by drawing a selection line across the division plane that was 10 pixels (1.6 microns) in breadth to capture all of the fluorescent signal at the division site. The length of the selection line was adjusted to match the width of each individual cell, in order to capture the signal from the first pixel showing signal at one side of the cell to the last pixel showing signal at the other cell side. The width of the cell was measured in microns using the DIC channel, in which a selection line was drawn to span across the division site from one cell side to the other. The measured sum intensities were then normalized to the division site area on a cell-by-cell basis. Division site area was calculated using the following formula: $A = (3.14 \times (D/2)^2) \times 2$, in which D = cell diameter (cell width) at the division site. The area was multiplied by 2 in the equation since the division site has two membrane planes, one on each side of the synthesizing septum. The sum fluorescence intensity of each individual cell measured was then divided by its calculated

division site area to determine the amount of fluorescent signal spread across the division site area. A Student's two-tailed *t*-test, assuming unequal variance, was used to determine significance through comparison of each strain's mean normalized intensities.

2.6.8 Analysis of vesicle tracking

The dynamics of endocytic patches marked with Fim1-mEGFP were imaged in a single medial plane with a frame rate of 2.35s for ~7 minutes. Cells were placed in glass-bottom culture dishes as previously described for time-lapse imaging. To determine endocytic patch lifetime at the division site, Fim1-mEGFP patches were tracked manually. To determine endocytic patch lifetime at the cell ends, Fim1-mEGFP patches were tracked using the FIJI plugin TrackMate where estimated blob diameter = 0.9 micron. Background fluorescence was subtracted from the imaging field away from cells to sharpen the signal of patches for ease of tracking. Lifetime was measured as the time from which a patch first displayed distinguishable fluorescence at the cell cortex to when the fluorescence was no longer detectable. To ensure that patches were tracked from the beginning of patch formation through patch disassembly, patches selected for tracking 1. gradually increased in intensity until a peak intensity was reached and 2. decreased in intensity following peak intensity (Berro and Pollard, 2014; Wang et al., 2016). Patches tracked with TrackMate were also manually reviewed to ensure tracking accuracy.

At the division site, internalization distances of endocytic patches marked with Fim1-mEGFP were measured from montages generated from 5 pixel-wide (800 nm-wide) selection lines drawn at a 45-degree angle between the division plane and the long axis of cells. At the cell ends of interphase cells, a similar approach was followed to create

montages using 5 pixel-wide (800 nm-wide) selection lines drawn perpendicularly across cell ends and parallel to the long axis of cells. To measure the distance of internalization at both the division site and the cell ends, the centroid position of the patch was manually tracked to calculate the displacement of the patch from the cortex as it internalized. The internalization distance was calculated as the distance between the farthest patch centroid position and that of the initial patch centroid position at the cell cortex.

2.6.9 Statistical tests

GraphPad Prism was used to determine significance. One-way ANOVA, followed by a Tukey's multiple comparisons post-hoc test, was used to determine individual *p*-values when comparing three or more samples. When comparing two samples, an unpaired Student's *t*-test (two-tailed, unequal variance) was used to determine significance.

Strain	Genotype	Source
PN567	*h+ ade6-704 leu1-32 ura4-d18*	Paul Nurse
FV513	*h- rga4Δ::ura4+ ade6-704 leu1-32 ura4-D18*	Das et al., 2007
PPG45.11	*h+ rga6Δ::kanMX ade- leu1-32 ura4-D18*	Revilla-Guarinos et al., 2016
YMD672	*h- rga4Δ::ura4+ rga6Δ::kanMX ade- leu1-32 ura4-D18*	This study
YMD314	*CRIB-3xGFP-ura4+ rlc1-tdTomato-NATr sad1-mCherry:kanMX ade6-M21X leu1-32 ura4-D18*	Lab stock
YMD746	*rga6Δ::kanMX CRIB-3xGFP-ura4+ rlc1-tdTomato-NATr sad1-mCherry:kanMX ade6-M21X leu1-32 ura4-D18*	This study
YMD754	*rga4Δ::kanMX CRIB-3xGFP-ura4+ rlc1-tdTomato-NATr sad1-mCherry:kanMX ade6-M21X leu1-32 ura4-D18*	This study
YMD787	*rga4Δ::ura4+ rga6Δ::kanMX CRIB-3xGFP-ura4+ rlc1-tdTomato-NATr sad1-mCherry:kanMX ade6-M21X leu1-32 ura4-D18 his7+*	This study
YMD771	*rga6-GFP-kanMX rlc1-tdTomato-NATr sad1- mCherry:kanMX ade6-M216 leu1-32 ura4-D18*	This study
YMD772	*rga4-GFP-kanMX rlc1-tdTomato-NATr sad1- mCherry:kanR ade6-M216 leu1-32 ura4-D18*	This study
YMD1865	*rga3-GFP-kanMX rlc1-tdTomato-NATr ade6-M216 leu1-32 ura4-D18*	This study
YMD1463	*eng1-GFP-kanMX agn1-GFP-kanMX rlc1-tdTomato-NATr ade6-M216 leu1-32 ura4-D18*	This study
YMD1465	*rga4Δ::ura4+ rga6Δ::kanMX eng1-GFP-KanMX agn1-GFP-KanMX rlc1-tdTomato-NATr ade6-M216leu1-32 ura4-D18*	This study
YMD1452	*Δbgs1::ura4 Pbgs1::GFP-bgs1:leu1+ rlc1-tdTomato-NATr leu1-32 ura4-D18*	Onwubiko et al., 2020
YMD1848	*rga4Δ::ura4+ rga6Δ::kanMX Δbgs1::ura4 Pbgs1::GFP-bgs1:leu1+ rlc1-tdTomato-NATr leu1-32 ura4-D18*	This study
YMD1447	*h- Δbgs4::ura4 Pbgs4::GFP-bgs4:leu1+ rlc1-tdTomato-NATr sad1-mCherry:kanMX leu1-32 ura4-D18*	This study
YMD1449	*rga4Δ::ura4+ rga6Δ::kanMX Δbgs4::ura4 Pbgs4::GFP-bgs4:leu1+ rlc1-tdTomato-NATr sad1-mCherry:kanMX leu1-32 ura4-D18*	This study
YMD1670	*kanMX6-Pypt3-mEGFP-ypt3 rlc1-tdTomato-NATr ade6-210 leu1-32 ura4-D18*	This study
YMD1711	*rga4Δ::ura4+ rga6Δ::kanMX kanMX6-Pypt3-mEGFP-ypt3 rlc1-tdTomato-NATr ade6-210 leu1-32 ura4-D18*	This study
JW6731-1	*h- trs120-3GFP-kanMX6 rlc1-tdTomato-natMX6 ade6-M210 leu1-32 ura4-D18*	Wang et al., 2016
YMD1679	*rga4Δ::ura4+ rga6Δ::kanMX trs120-3GFP-kanMX6 rlc1-tdTomato-natMX6 ade6-M210 leu1-32 ura4-D18*	This study
YMD1751	*kanMX-GFP-syb1 rlc1-tdTomato-natMX6 ade6-M216 leu1-32 ura4-D18*	This study
YMD1755	*rga4Δ::ura4+ rga6Δ::kanMX kanMX-GFP-syb1 rlc1-tdTomato-natMX6 ade6-M216 leu1-32 ura4-D18*	This study
YMD1756	*myo52-GFP::kanMX rlc1-tdTomato-natMX6 ade6-M216 leu1-32 ura4-D18*	This study
YMD1731	*rga4Δ::ura4+ rga6Δ::kanMX myo52-GFP::kanMX rlc1-tdTomato-natMX6 ade6-M216 leu1-32 ura4-D18*	This study
JW6771-1	*h+ fim1-mEGFP-kanMX6 rlc1-tdTomato-natMX6 ade6-M210 leu1-32 ura4-D18*	Wang et al., 2016
YMD1110	*rga4Δ::ura4+ rga6Δ::kanMX fim1-mEGFP-kanMX6 rlc1-tdTomato-natMX6 ade6-M210 leu1-32 ura4-D18*	This study
YMD1947	*h+ kanMX6-Pypt2-mEGFP-ypt2 rlc1-tdTomato-natMX6 ade6-M210 leu1-32 ura4-D18*	This study
YMD1969	*rga4Δ::ura4+ rga6Δ::kanMX kanMX6-Pypt2-mEGFP-ypt2 rlc1-tdTomato-natMX6 ade6-M210 leu1-32 ura4-D18*	This study
YMD719	*h- psy1Δ::kanMX6 leu1+::GFP-psy1 rlc1-tdTomato-natMX6 ade6-M210 ura4*	Wang et al., 2016
YMD1974	*rga4Δ::ura4+ rga6Δ::kanMX psy1Δ::kanMX6 leu1+::GFP-psy1 rlc1-tdTomato-natMX6 ade6-M210 leu1-32 ura4-D18*	This study
YMD2008	*h- Hygr:eGFP-sbg1+ rlc1-tdTomato-natMX6 ade6-M210 leu1-32 ura4-D18*	This study
YMD2010	*rga4Δ::ura4+ rga6Δ::kanMX Hygr:eGFP-sbg1+ rlc1-tdTomato-natMX6 ade6-M210 leu1-32 ura4-D18*	This study
YMD2013	*smi1-mEGFP-kanMX6 rlc1-tdTomato-natMX6 ade6-M210 leu1-32 ura4-D18*	This study
YMD2015	*rga4Δ::ura4+ rga6Δ::kanMX smi1-mEGFP-kanMX6 rlc1-tdTomato-natMX6 ade6-M210 leu1-32 ura4-D18*	This study

Table 2.1. List of strains used in Chapter 2.

3.0 CHAPTER 3

Cdc42 activity is differentially modulated via its regulators to spatiotemporally direct synthesis and dynamics of endocytic branched actin networks at distinct cell sites

Cdc42 regulates endocytosis at sites of polarity

Bethany F. Campbell, Ashlei R. Williams, Uma Patel, and Maitreyi E. Das

SYNOPSIS

Endocytosis in yeasts requires branched actin formation to provide sufficient force to overcome high internal turgor pressure. In the absence of proper actin formation, endocytic patches fail to internalize. Here, we show that Cdc42 activity regulates endocytosis in a dose-dependent manner, where both insufficient and excessive activation result in poor endocytic patch internalization. The Cdc42 effector Pak1 kinase promotes both proper formation of endocytic patches as well as proper patch internalization via its target, the endocytic Type I myosin.

3.1 ABSTRACT

Endocytosis is essential for cell growth, enabling nutrient uptake and membrane protein recycling. In fission yeast, endocytosis occurs at growing cell ends, at the division site, and along the cell sides. Endocytic vesicles internalize only once branched actin networks assemble. We find that endocytosis at these distinct sites is differentially regulated by the conserved GTPase Cdc42. In fission yeast, Cdc42 is active at growing cell ends and the medial division site, yet not at the cell sides. Branched actin-mediated endocytosis also occurs primarily at the cell ends and the division site, with few events at the cell sides. In wild-type cells, we find that endocytic events at the cell ends and the division site behave similarly during internalization, whereas events at the cell sides behave erratically and internalize poorly. We then asked if the polarization of active Cdc42 promotes differential endocytic dynamics at these distinct sites by examining endocytic behavior in polarity mutants. In *S. pombe*, Cdc42 is activated by a strong GEF, Scd1, and a transient GEF, Gef1. In *gef1* mutants, where Cdc42 activity is Scd1-dependent, endocytic lifetimes are prolonged and internalization is delayed at the cell ends, whereas dynamics at the cell sides do not change. In contrast, in *scd1* mutants where Cdc42 is activated transiently by Gef1 in a non-polarized manner, endocytic events behave similarly at all sites. Using cytokinesis as a paradigm for polarization, we show that active Cdc42 is necessary for endocytosis. During cytokinesis, Cdc42 is activated at the division site first by Gef1 followed by Scd1. Endocytosis at the division site initiates around the time of actomyosin ring formation when Gef1 activates Cdc42 at that site. In *gef1* mutants, Cdc42 activity and branched actin assembly are both delayed at the division site. These results indicate that the two GEFs differentially regulate Cdc42 and that Gef1 is the primary GEF required for endocytosis.

We also describe roles for the downstream Cdc42 effector Pak1 kinase and its putative Type I myosin target, Myo1. These results indicate that Cdc42 activity is precisely modulated at distinct cell sites to spatiotemporally direct branched actin-mediated endocytosis.

3.2 GRAPHICAL ABSTRACT

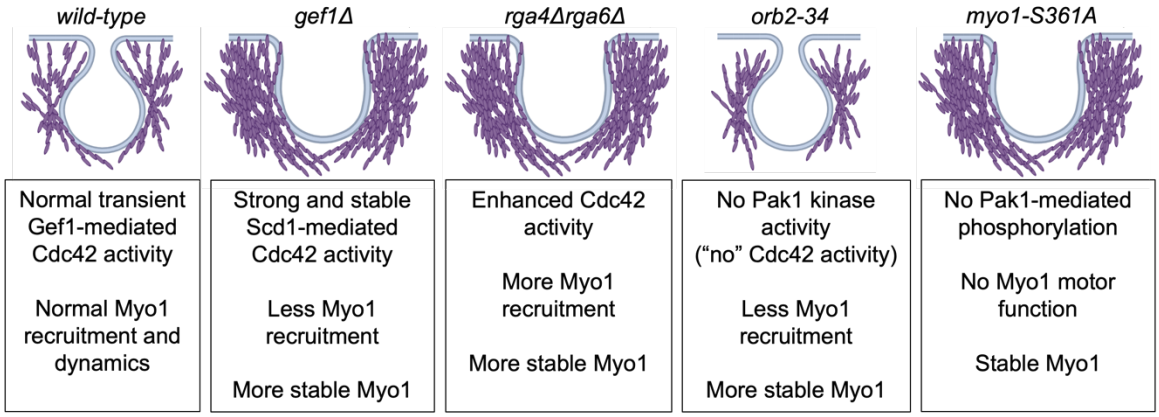

KEYWORDS

Polarization, Branched Actin Networks, Clathrin-mediated Endocytosis, Cdc42 GTPase, p21-Activated Kinase, Type I Myosin, Guanine Nucleotide Exchange Factors, GTPase-Activating Proteins, *Schizosaccharomyces pombe*

AUTHOR CONTRIBUTIONS

M.E.D. and B.F.C. conceived the project. M.E.D. obtained funding for the project. B.F.C., A.R.W., and U.P. performed experiments and analyzed data. B.F.C. and M.E.D. wrote the manuscript.

3.3 INTRODUCTION

3.3.1 Branched actin network assembly is required for clathrin-mediated endocytosis in *S. pombe*

Endocytosis is an essential process by which cells uptake nutrients and recycle proteins from the plasma membrane. In cell-walled organisms such as *S. pombe* fission yeast, internal turgor pressure is quite high at ~10 atm (Basu et al., 2014; Lacy et al., 2018), roughly equivalent to a racing bike tire. To overcome such high turgor pressure, successful clathrin-mediated endocytosis in yeasts requires synthesis of branched actin networks to produce enough counteractive force to invaginate the plasma membrane and subsequently internalize endocytic vesicles (Aghamohammadzadeh and Ayscough, 2009; Basu et al., 2014; Nickaeen et al., 2022). In *S. pombe*, branched actin is formed by the Arp2/3 complex with the help of nucleation promoting factors such as the Type I myosin Myo1 and the WASP Wsp1 (Sirotkin et al., 2005). Actin binding proteins such as fimbrin Fim1 also localize to endocytic patches to crosslink the branched actin and stimulate force production within the patch (Skau et al., 2011). Furthermore, if endocytosis is impaired, cells cannot grow or divide. Once treated with the Arp2/3 complex inhibitor, CK-666, *S. pombe* cells halt their growth during interphase and actomyosin rings fail to constrict during cytokinesis (Onwubiko et al., 2019). Thus, regulation of branched actin formation is an essential cellular process for *S. pombe* cell viability.

3.3.2 Sites of clathrin-mediated endocytosis mirror regions of polarization in *S. pombe*

In rod-shaped *S. pombe* cells, clathrin-mediated endocytic events primarily occur at sites of polarization, namely the cell ends during interphase and the division site during cytokinesis (Gachet and Hyams, 2005; Sirotkin et al., 2010). However, some endocytic actin patches also form at non-growing cell sides. Previous works have shown that sites of endocytosis coincide with regions of cell growth and cytokinesis (Gatchet & Hyams, 2005). The GTPase Cdc42 is the major regulator of polarity in *S. pombe* and is active only at polarized cell ends and the division site and not at the cell sides (Das et al., 2012). Additionally, Cdc42 is activated at the division site just before endocytosis initiates at the division plane, with Cdc42 activation occurring during actomyosin ring formation and endocytosis commencing during ring maturation after ring assembly (Hercyk and Das, 2019; Magliozzi et al., 2020; Wang et al., 2016; Wei et al., 2016). Further work has connected Cdc42 activation to Arp2/3-mediated endocytosis since both are required for septum formation and onset of actomyosin ring constriction in fission yeast (Wei et. al, 2016; Onwubiko et al., 2019). Studies in mammalian MDCK cells also indicate that Cdc42 regulates both endocytic trafficking and exocytic secretion (Kroschewski et al., 1999). Specifically, expression of dominant negative $Cdc42^{T17N}$ mislocalizes basolateral membrane proteins to the apical membrane, while expression of constitutively active $Cdc42^{Q61L}$ depolarizes actin from the apical membrane, causing actin to instead appear throughout the cell periphery (Kroschewski et al., 1999).

3.3.3 GEFs spatiotemporally regulate Cdc42 activation at sites of polarization and endocytosis

In *S. pombe*, Cdc42 is independently activated by two GEFs, a transient and mostly cytoplasmic GEF, Gef1, which localizes to cortical puncta at polarized regions (Das et al., 2015; Hercyk et al., 2019b), as well as a strong GEF, Scd1, which localizes throughout polarized regions and promotes sustained Cdc42 activation via a positive feedback loop (Das et al., 2012; Das and Verde, 2013; Lamas et al., 2020). Like Cdc42, both of these GEFs are present at polarized cell ends, but it remains unclear which one arrives first at this site to initiate Cdc42 activation, although Scd1 has been shown to prevent ectopic localization of Gef1 (Hercyk et al., 2019b). Previous research has shown that Gef1 is recruited to cortical patches via the F-BAR protein Cdc15 (Hercyk and Das, 2019), which promotes endocytosis and is itself recruited to endocytic actin patches via the endocytic Type I myosin, Myo1 (Arasada and Pollard, 2011; Carnahan and Gould, 2003). Conversely, Cdc15 does not recruit Scd1 to cortical patches (Hercyk and Das, 2019). Additionally, loss of *gef1* leads to excessive accumulation and prolonged lifetimes of Cdc15 within endocytic patches, which can intriguingly be rescued by expression of a constitutively active *cdc42G12V* allele (Onwubiko et al., 2019). Together, these reports suggest that Cdc15 recruits Gef1 to endocytic patches to promote Cdc42 activation and that this recruitment is important to regulate endocytic patch dynamics.

3.3.4 Cdc42-dependent activation of PAKs regulates function of the endocytic Type I myosin

Prior research has additionally linked Cdc42 activity to the regulation of endocytosis via its direct downstream effector, the p21-activated kinase (PAK) (Murray and Johnson, 2001; Ottilie et al., 1995; Wu et al., 1997), which is activated by binding GTP-bound Cdc42 to relieve its autoinhibition (Bokoch, 2003). Like Cdc42, PAK is conserved across eukaryotic life from yeast to humans, functioning as a serine/threonine kinase (Manser et al., 1994; Marcus et al., 1995). In unicellular eukaryotes, PAK is known to phosphorylate the endocytic Type I myosin in organisms such as slime molds, amoebas, and yeasts (Brzeska et al., 1997; Lechler et al., 2001; Lechler et al., 2000; Lee et al., 2000; Murray and Johnson, 2001; Wu et al., 1997), including *S. pombe* (Attanapola et al., 2009; Magliozzi et al., 2020). In these organisms, PAK promotes the ATPase activity and motor function of the Type I myosin by phosphorylating a conserved serine or threonine residue located in the motor domain known as the TEDS-site (Bement and Mooseker, 1995; Fujita-Becker et al., 2005; Pedersen et al., 2023). Specifically, TEDS-site phosphorylation facilitates association of the myosin with actin, stabilizing the complex (Fujita-Becker et al., 2005). In *S. pombe*, phospho-null mutation of the TEDS-site abrogates proper localization of Myo1 to endocytic actin patches, instead causing the myosin to localize uniformly along the plasma membrane (Attanapola et al., 2009). Additionally, we have recently shown that Pak1 promotes successful internalization of endocytic patches and even its own removal via endocytosis at growing cell ends of *S. pombe* (Harrell et al., 2024). These findings suggest that regulation of Cdc42 activation may be necessary to facilitate proper endocytic patch dynamics.

3.3.5 Research summary

Here we use genetic approaches and quantitative live cell imaging to better define the intricate connections between sites of polarization and endocytosis. We show that endocytic actin patches display disparate dynamics at distinct cell sites and that these behaviors are mediated by Cdc42 and Pak1 activation. While our recent work shows that endocytosis ensures proper spatiotemporal regulation of Cdc42 activation (Harrell et al., 2024), here we demonstrate that Cdc42 activation likewise spatiotemporally directs endocytosis.

3.4 RESULTS

3.4.1 Endocytic events at distinct regions in the cell show differential dynamics

To our knowledge, the dynamic behaviors of individual endocytic patches within each distinct region have not been characterized and reported. We were thus curious to determine how endocytic patches at polarized regions behave compared to those at non-growing regions. To do this, we performed 1-sec interval timelapse imaging of asynchronous cultures of wild-type cells expressing mEGFP-tagged fimbrin Fim1, a branched actin crosslinker (Nakano et al., 2001), which promotes actin bundling necessary for endocytic patch internalization (Skau et al., 2011). This approach allowed us to simultaneously capture the dynamics of individual endocytic patches at the cell ends, the cell sides, and the division site (Figure 3.1 A). We then used TrackMate to track the trajectories of individual Fim1-mEGFP patches. From this data, we found that Fim1-mEGFP-labeled endocytic patches have disparate lifetimes at each region, with patches at the cell sides exhibiting the shortest lifetimes, while patches at the division site show the longest lifetimes (Figure 3.1 B). While the lifetimes at polarized cell ends and the division site are statistically different in duration, the mean lifetimes for both regions (~16 sec at the cell ends and ~18 sec at the division site) fall within the reported average range for Fim1-mEGFP lifetimes (Sirotkin et al., 2010; Berro and Pollard, 2014).

Mean patch intensity was also measured frame-by-frame throughout each patch's lifetime. This analysis revealed that endocytic patches at the cell ends and the division site recruit Fim1-mEGFP at the same rate and to the same peak intensity (Figure 3.1 C). Conversely,

endocytic patches at the cell sides recruited ~50% less Fim1-mEGFP at peak intensity compared to the polarized sites (Figure 3.1 C). Using TrackMateR, we calculated the diffusive properties of tracked Fim1-mEGFP patches to characterize their respective dynamics. Calculations show that endocytic patches at the division site are the slowest moving (Figure 3.1 D) and most stable with the least diffusion of all sites (Figure 3.1 F). In contrast, endocytic patches at the cell sides move the fastest (Figure 3.1 D) and exhibit the highest diffusion rate (Figure 3.1 F). Patches at the cell ends display a comparatively intermediate speed and diffusion rate (Figure 3.1 D and F). However, mean squared displacement (MSD) analysis reveals that endocytic patches at the cell ends and the division site exhibit similar degrees of directed motion, while patches at the cell sides demonstrate more diffusive behavior overall (Figure 3.1 E). Together, these data indicate that endocytic patches at polarized regions recruit twice as much Fim1-mEGFP, are longer-lived, and exhibit more stable and directed dynamics compared to patches at the non-growing cell sides.

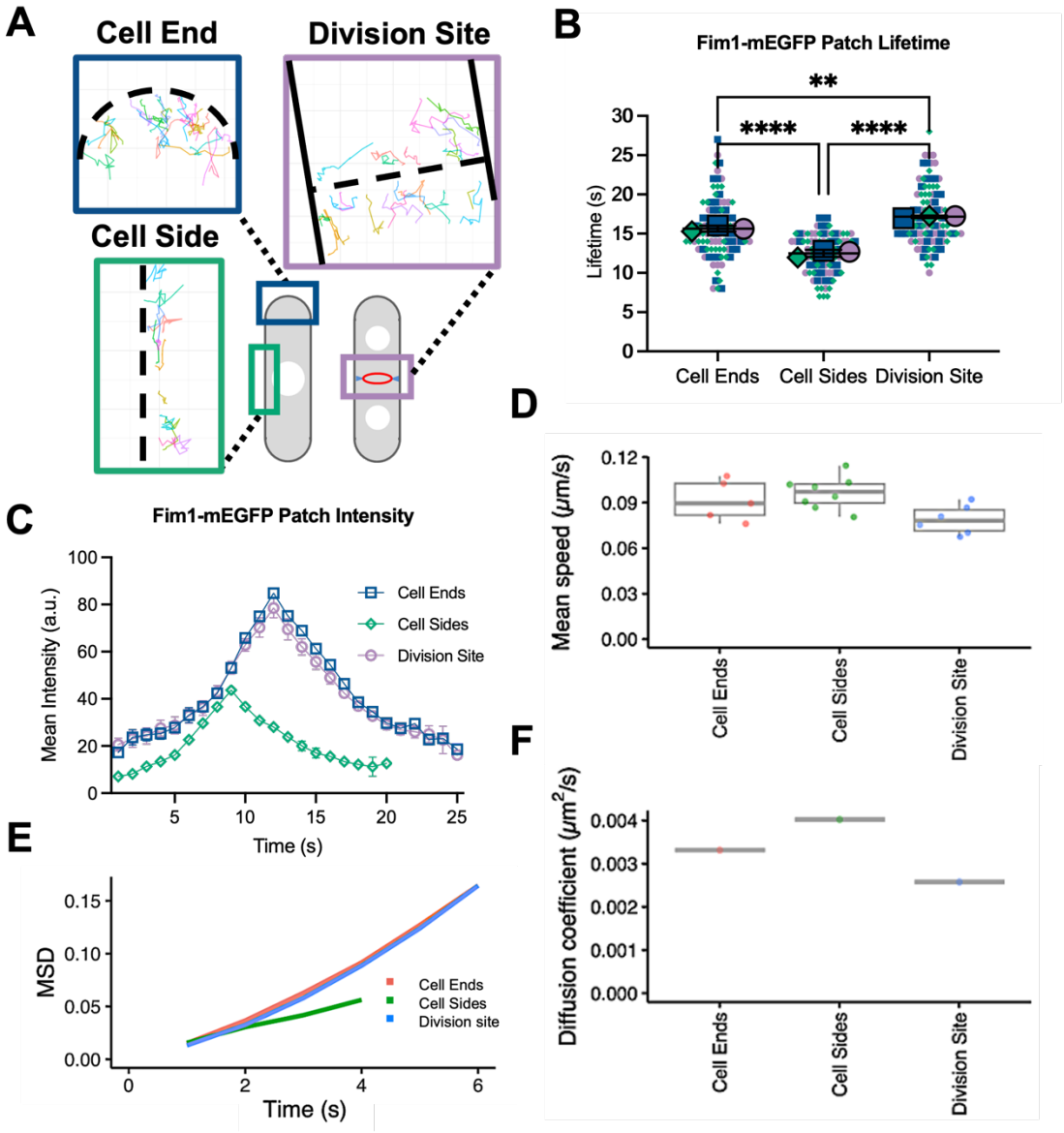

Figure 3.1. **Endocytic events at distinct regions in the cell show differential dynamics.** (A) Endocytic events occur at different regions of polarized *S. pombe* cells. Colored tracks indicate trajectories of individual Fim1-mEGFP patches. (B) Lifetimes of Fim1-mEGFP labeled endocytic patches at each region. (C) Mean Fim1-mEGFP peak intensity in endocytic patches at each region. (D) Mean speed of endocytic patches at each region averaged from individual cells. (E) MSD (mean square displacement) of Fim1-mEGFP patches calculated for each region. (F) Diffusion coefficient of Fim1-mEGFP patches at each region. ($n \geq 28$ patches per region per triplicate experiment; $n \geq 6$ cells analyzed per region). Ordinary one-way ANOVA with Tukey's multiple comparisons. ****, $p < 0.0001$; **, $p < 0.01$

3.4.2 Cdc42 activity promotes timely formation of endocytic branched actin networks at the division site

Our findings that endocytic events behave differently at polarized regions compared to non-growing cell sides suggest that polarity regulators may influence endocytic dynamics. Indeed, Cdc42 has been shown to promote uptake of Lucifer Yellow via endocytosis in *S. pombe* (Murray & Johnson, 2001). Connecting previous observations that sites of endocytosis mirror sites of Cdc42 activation, we asked if Cdc42 activation is necessary for endocytosis. To test this idea, we asked if a delay in Cdc42 activation at the division site would consequently delay onset of endocytic activity within the division plane. We selected the division site since the mechanism of Cdc42 activation is best understood at this site. The GEF Gef1 is the first GEF to appear and activate Cdc42 at the division site, and loss of Gef1 consequently leads to a delay in Cdc42 activity at this site (Wei et. al, 2016) since the other Cdc42 GEF, Scd1, depends on Gef1 for timely localization to the division site (Hercyk et al., 2019b). While decreased Cdc42 activation in *gef1Δ* mutants delays actomyosin ring constriction due to insufficient recruitment of Bgs1, the timing of mitotic events proceeds normally (Wei et. al, 2016). Thus, we measured the timing of Fim1-mEGFP appearance at the division site relative to onset of mitosis marked by spindle pole body (SPB) separation in *gef1Δ* cells compared to *gef1*$^{+}$ controls. These experiments show that Fim1-mEGFP first appears at the division site ~12 mins after SPB separation in *gef1*$^{+}$ cells (green dotted box, Figure 3.2 A and B), while Fim1-mEGFP appearance in *gef1Δ* cells is delayed to ~20 mins post-SPB separation (green dotted box, Figure 3.2 A and B). Intriguingly, Cdc42 is also first activated at the division site ~10-12 min post-SPB separation in wild-type cells (Hercyk and Das, 2019; Wei et al., 2016). Fim1-mEGFP

patches then appear uniformly throughout division site ~20 mins post-SPB separation in *gef1*$^{+}$ controls (solid green box, Figure 3.2 A and C) compared to ~28 mins post-SPB separation in *gef1Δ* mutants (solid green box, Figure 3.2 A and C). These findings suggest that Cdc42 activation is indeed required for endocytosis.

We were then curious to determine the timing of Cdc42 activation and appearance of Fim1 at the division site in *gef1*$^{+}$ as well as *gef1Δ* cells. In *gef1*$^{+}$ cells, Fim1-mCh appears throughout the division site (purple box) ~7-8 mins after Cdc42 is activated, as visualized by the CRIB-3xGFP bio-probe which binds active GTP-bound Cdc42 (green box and arrowheads, Figure 3.2 D and E). Comparatively, in *gef1Δ* cells, Fim1-mEGFP appears throughout the division site (purple box) ~4 mins after Cdc42 activation (green box and arrowheads, Figure 3.2 D and E). This suggests that endocytosis starts soon after Cdc42 activation in *gef1Δ* mutants since these cells have already progressed through mitosis and thus many cellular events are already complete. Our findings suggest that *gef1Δ* cells are simply waiting for Cdc42 to be activated to initiate endocytosis. Together, these data suggest that Cdc42 activation is required for the onset of endocytosis within the division site.

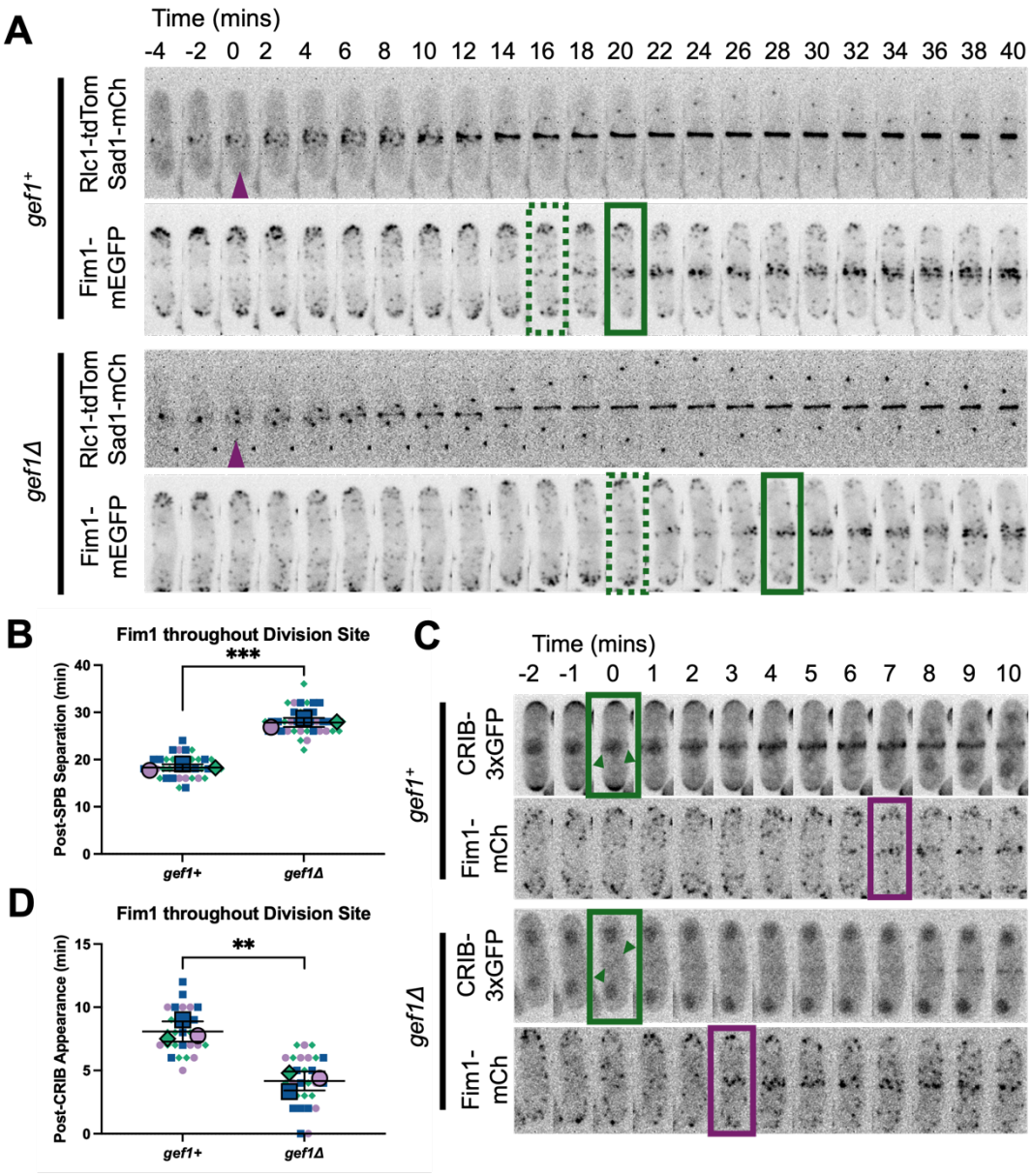

Figure 3.2. Timely initiation of endocytosis at the division site requires active Cdc42. (A) Representative cells showing initial (green dotted box) and uniform (solid green box) Fim1-mEGFP appearance at the division site relative to Sad1-mCh to mark spindle pole body (SPB) separation (purple arrowhead). (B) Quantification of A, where time 0 = SPB separation. (C) Representative cells showing CRIB-3xGFP appearance (green box) vs. Fim1-mCh appearance (purple box) at the division site. (D) Quantification of C, where time 0 marks CRIB-3xGFP appearance (green arrowheads) at the division site. (n ≥ 8 cells per genotype per experiment). Unpaired Student's *t*-test. ****, $p< 0.0001$; ***, $p<0.001$; **, $p<0.01$

3.4.3 The GEFs Gef1 and Scd1 differentially regulate Cdc42 to direct branched actin synthesis and dynamics at sites of polarization

Findings that the Cdc42 GEFs Gef1 and Scd1 differentially activate Cdc42 at polarized sites prompted us to define the manner of Cdc42 activation required to direct endocytosis. To investigate this, we tracked the dynamics of Fim1-mEGFP in *gef1Δ* and *scd1Δ* cells compared to *gef1*$^{+}$*scd1*$^{+}$ controls, as previously described (Figure 1). In these experiments, cells also expressed Cdc15-tdTom to corroborate and expand upon our previous findings. As found before (Onwubiku et al., 2019), *gef1Δ* mutants exhibit excessive accumulation and prolonged lifetimes of Cdc15-tdTom at the cell ends compared to *gef1*$^{+}$ control cells (Figure 3.3 A; Supplemental Figure 3.1 A and B). We additionally find that Fim1-mEGFP accumulation within endocytic patches in likewise increased in *gef1Δ* mutants at both the cell ends and the division site compared to controls. (Figure 3.3 A, B, and D). In in *gef1Δ* mutants, Fim1-mEGFP lifetimes are also prolonged at the cell ends; however, we saw no change in patch lifetime at the division site in *gef1Δ* cells (Figure 3.3 H). Notably, the recruitment patterns and lifetimes of Fim1-mEGFP patches are the same at the cell sides of *gef1*$^{+}$ and *gef1Δ* cells (Figure 3.3 F and H), which supports the idea that the dynamics of these patches are not influenced by Cdc42 or its GEFs.

In contrast, in *scd1Δ* mutants, we did not observe any change in the recruitment dynamics of either Cdc15-tdTom or Fim1-mEGFP compared to *scd1*$^{+}$ cells (Supplemental Figure 3.1 C and D; Figure 3.3 A, C, E, and G). We did, however, find that Fim1-mEGFP patches are depolarized rather than concentrated at the cell ends in *scd1Δ* mutants (Supplemental Figure 3.1 E). Fim1-mEGFP patches in *scd1Δ* mutants also display similar lifetimes at all

regions of the cell (Figure 3.3 H), which is consistent with the random, depolarized Cdc42 activation patterns that occur in these cells due to loss of Scd1-mediated restriction of ectopic Gef1 localization (Hercyk et al., 2019b). Together, these results suggest that Gef1 is the primary GEF that regulates Cdc42 activation to direct proper endocytic patch dynamics at polarized regions.

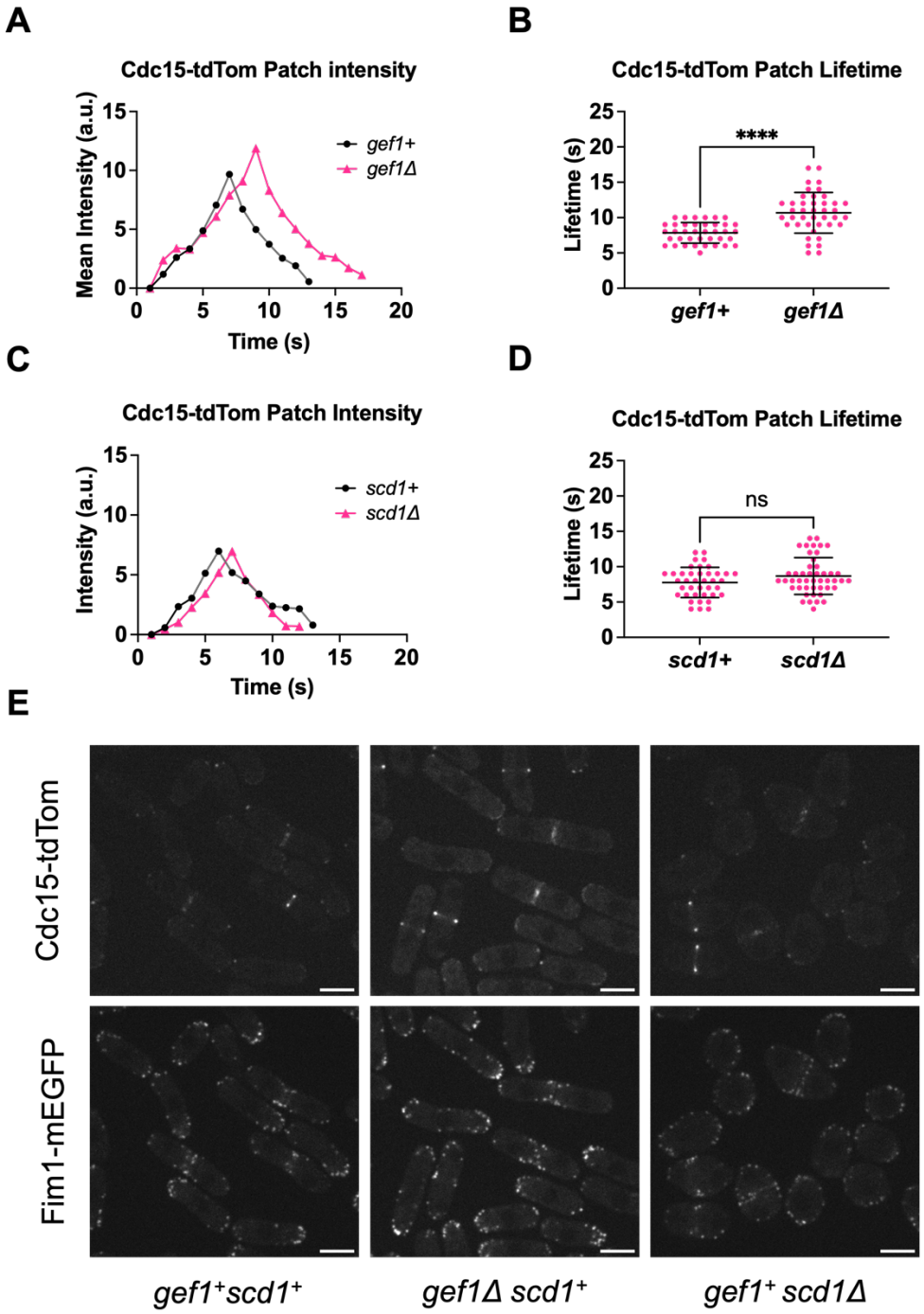

Supplemental Figure 3.1. Loss of *gef1* promotes excessive accumulation of Cdc15 and Fim1 within endocytic patches. (A) and (C) Mean patch intensity of Cdc15-tdTom at the cell ends in the indicated genotypes. (B) and (D) Cdc15-tdTom patch lifetime at the cell ends in the indicated genotypes ($n \geq 32$ patches per genotype. (E) Representative images of Cdc15-tdTom and Fim1-mEGFP in each genotype (scale bar = 5 µm). Unpaired Student's *t*-test. ****, $p<0.0001$; ns, not significant

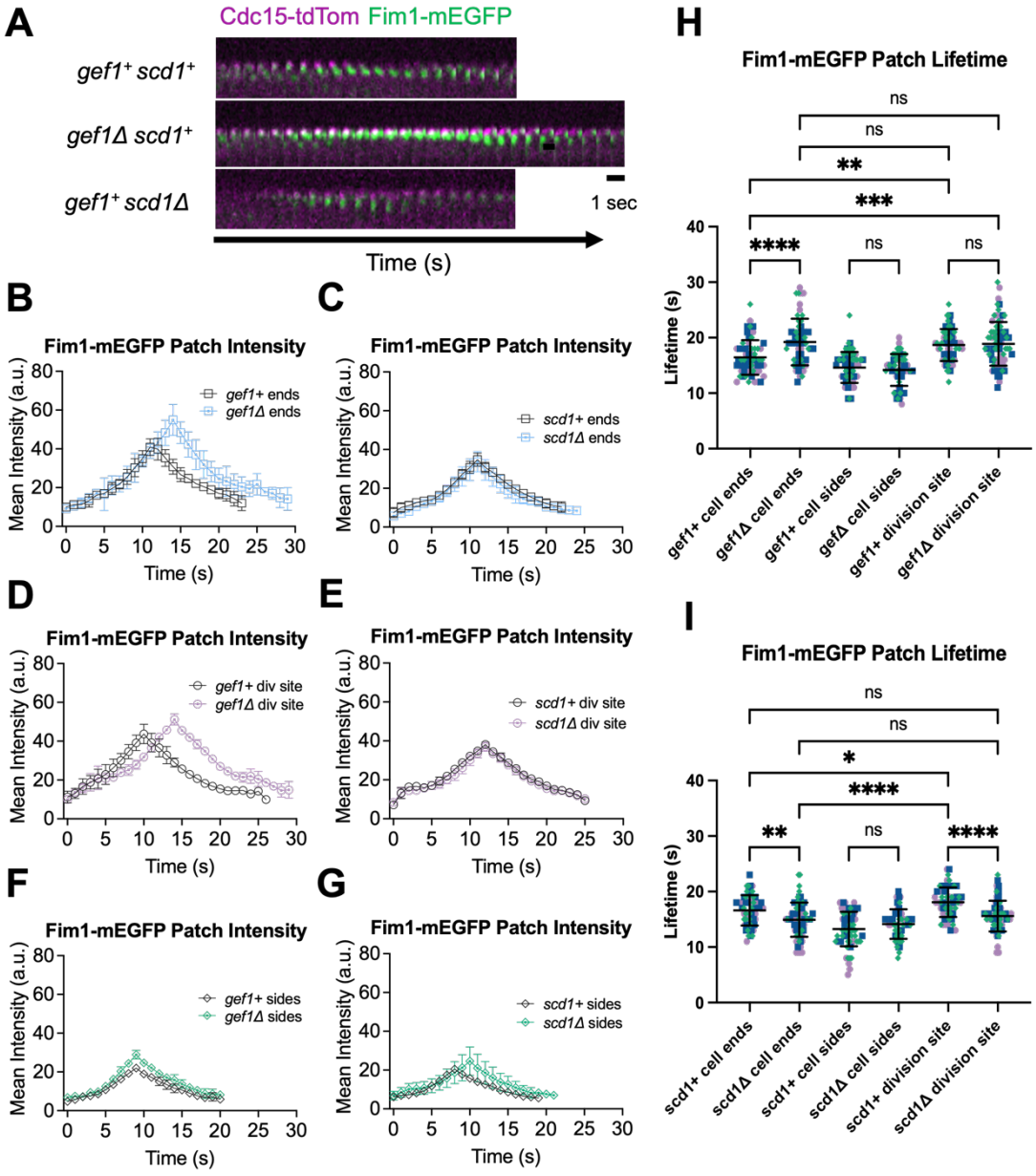

Figure 3.3. The GEFs Gef1 and Scd1 differentially regulate Cdc42 to direct endocytosis at sites of polarization. (A) Representative montages of Cdc15-tdTom and Fim1-mEGFP at growing cell ends in the indicated genotypes. (B) through (G) Mean patch intensities of Fim1-mEGFP at growing cell ends, the division site, and cell sides. (n ≥ 20 endocytic patches per triplicate experiment). (H) and (I) Patch lifetimes of Fim1-mEGFP at each region in the indicated genotypes. (n ≥ 20 endocytic patches per triplicate experiment). Ordinary one-way ANOVA with Tukey's multiple comparisons. ****, p<0.0001; ***, p<0.001; **, p<0.01; *, p< 0.05; ns, not significant

3.4.4 Pak1/Orb2 kinase activity promotes timely formation of endocytic branched actin networks at the division site

As previous reports and our findings show that timely initiation of endocytosis depends on Cdc42 activation, we asked whether timely onset of endocytosis likewise depends on PAK activity. In addition to the cell ends, Pak1 is also present at the division site during cytokinesis where it promotes assembly of the contractile actomyosin ring (Magliozzi et al., 2020). Similar to previously described experiments (Figure 3.2), we measured the time intervals between SPB separation and appearance of Fim1-mEGFP at the division site in *orb2*$^{+}$ cells compared to *orb2-34*, a kinase-dead, temperature-sensitive allele of *pak1* (Verde et al., 1995; Das et al., 2012). Even at permissive temperature, *orb2-34* shows minimal kinase activity compared to wild-type *pak1* (Das et al., 2012). Thus, experiments were performed under permissive 25°C conditions to minimize pleiotropic effects that may arise under temperature restriction, which causes *orb2-34* cells to become rounded and orb-like (Verde et al., 1995). Our experiments show that Fim1-mEGFP appearance (dotted and solid green boxes) is indeed delayed in *orb2-34* mutants to controls, even under permissive conditions (Figure 3.4 A-C). Although this ~2 min delay in Fim1 appearance at the division site is slight at 25°C, our findings suggest that Fim1 would be even further delayed in a true *pak1* null under restrictive conditions. Thus, these data indicate that timely initiation of endocytosis at the division site depends both on Cdc42 and Pak1 activation.

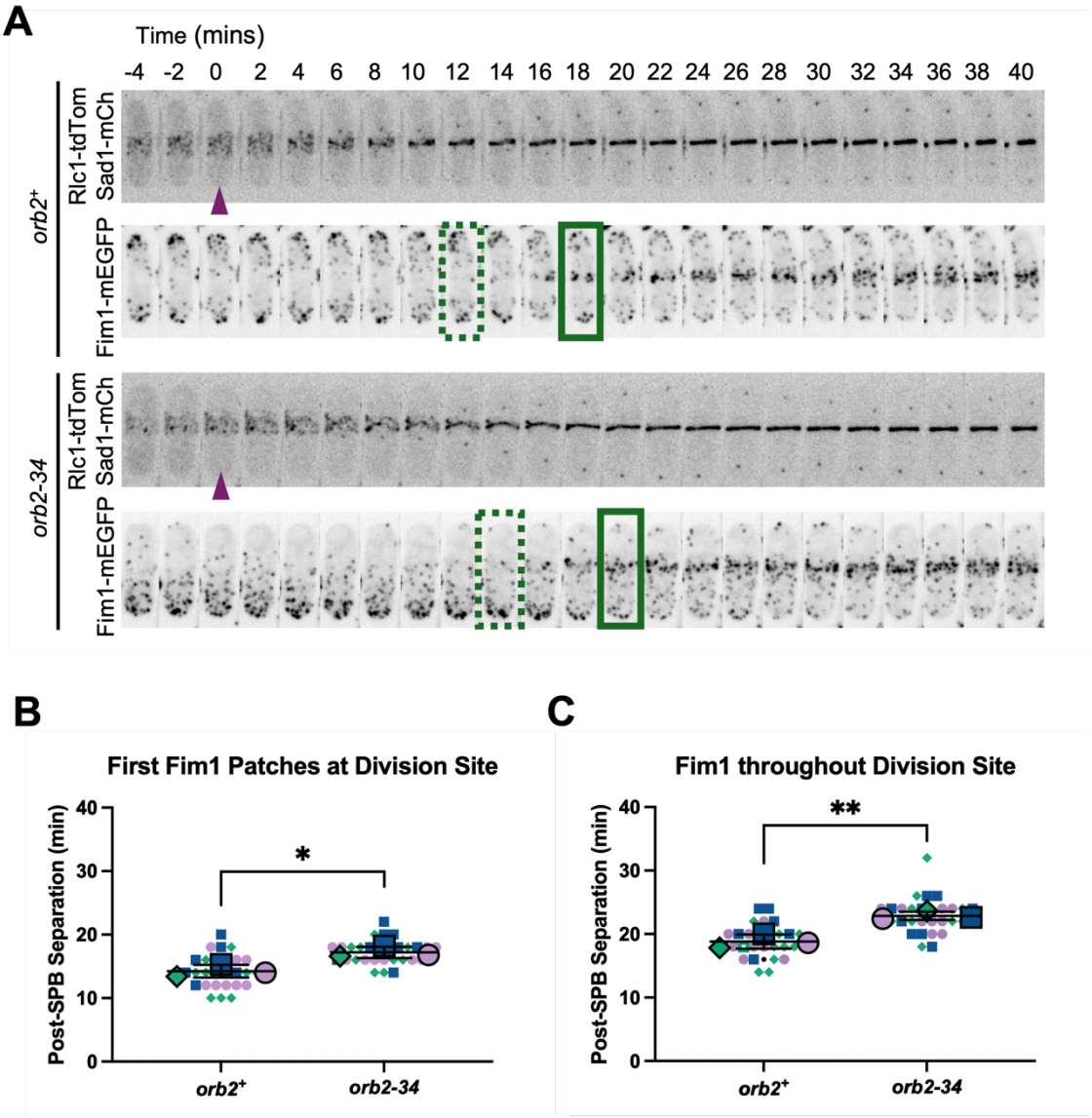

Figure 3.4. Pak1/Orb2 kinase activity is required for timely initiation of endocytosis at the division site. (A) Representative *orb2+* and *orb2-34* cells showing initial (green dotted box) and uniform (solid green box) Fim1-mEGFP appearance at the division site relative to Sad1-mCh to mark spindle pole body separation (purple arrowhead. (B) and (C) Quantification of A, where time 0 = SPB separation. ($n \geq 8$ cells per genotype per experiment). Unpaired Student's *t*-test. **, $p<0.01$; *, $p< 0.05$

3.4.5 Pak1 facilitates proper formation and dynamics of endocytic actin patches at sites of polarization

Given our recent findings that loss of Pak1 kinase function impairs internalization of endocytic patches at polarized cell ends (Harrell et al., 2024), we asked whether similar endocytic defects also occur at the division site and cell sides. To examine this, we tracked Fim1-mEGFP patches in kinase-dead, temperature-sensitive *orb2-34* mutants and compared their dynamics to patches tracked in *orb2*$^{+}$ control cells. As at the cell ends (Harrell et al., 2024), Fim1-mEGP patch internalization at the division site is impaired in *orb2-34* mutants compared to controls, especially at the 35°C restrictive temperature (Figure 3.5 A). Overall, it appears that Fim1 patches largely move within the plane of the plasma membrane in the absence of Pak1 kinase function.

We also observe impaired recruitment of Fim1-mEGFP to endocytic patches in *orb2-34* mutants under permissive conditions. At 25°C, *orb2-34* cells show decreased peak Fim1-mEGFP intensity within endocytic patches at the cell ends and the division site compared to controls (Figure 3.5 B and D). In contrast, at the 35°C restrictive temperature, peak Fim1-mEGFP intensity at the cell ends in *orb2-34* mutants remains the same as observed at 25°C, while *orb2*$^{+}$ controls show decreased Fim1-mEGFP patch intensity at the cell ends at this temperature (Figure 3.5 C). We interestingly observe the opposite effect at the division site. Here at 35°C, Fim1-mEGFP patch intensity dramatically decreases at the division site in *orb2-34* mutants while patch intensity is unchanged in *orb2*$^{+}$ controls (Figure 3.5 E). These observations suggest that Fim1 recruitment to the cell ends of *orb2-34* mutants is insensitive to temperature restriction, while Fim1 recruitment to the division

site of *orb2-34* mutants is impaired under these conditions. Consistent with previous experiments showing that endocytic dynamics are not influenced by changes in polarity regulation, we did not observe changes in Fim1-mEGFP recruitment at the cell sides other than some decrease in peak patch intensity in *orb2*$^{+}$ controls at 35°C (Figure 3.5 F and G).

Across the board at all cell regions, Fim1-mEGFP patch lifetimes decrease at 35°C compared to 25°C (Figure 3.5 H and I), likely due to increased Brownian motion. As previously reported (Harrell et al., 2024), Fim1-mEGFP patch lifetimes do not change at the cell ends of *orb2-34* mutants compared to controls (Figure 3.5 H and I). Conversely, at 25°C, Fim1-mEGFP patch lifetimes are ~5 seconds shorter at the division site in *orb2-34* cells compared to *orb2*$^{+}$ cells (Figure 3.5 H), but this difference is abrogated at 35°C where *orb2*$^{+}$ patch lifetimes decrease (Figure 3.5 I). While loss of Pak1 kinase function impairs endocytic internalization at both the cell ends and the division site, our data suggests that Pak1 may perform additional functions at the division site since we observe changes in Fim1 accumulation and lifetime at this site, but not at the cell ends. Together, these results indicate that Pak1 kinase plays important and differential roles at polarized regions to regulate endocytic patch behavior.

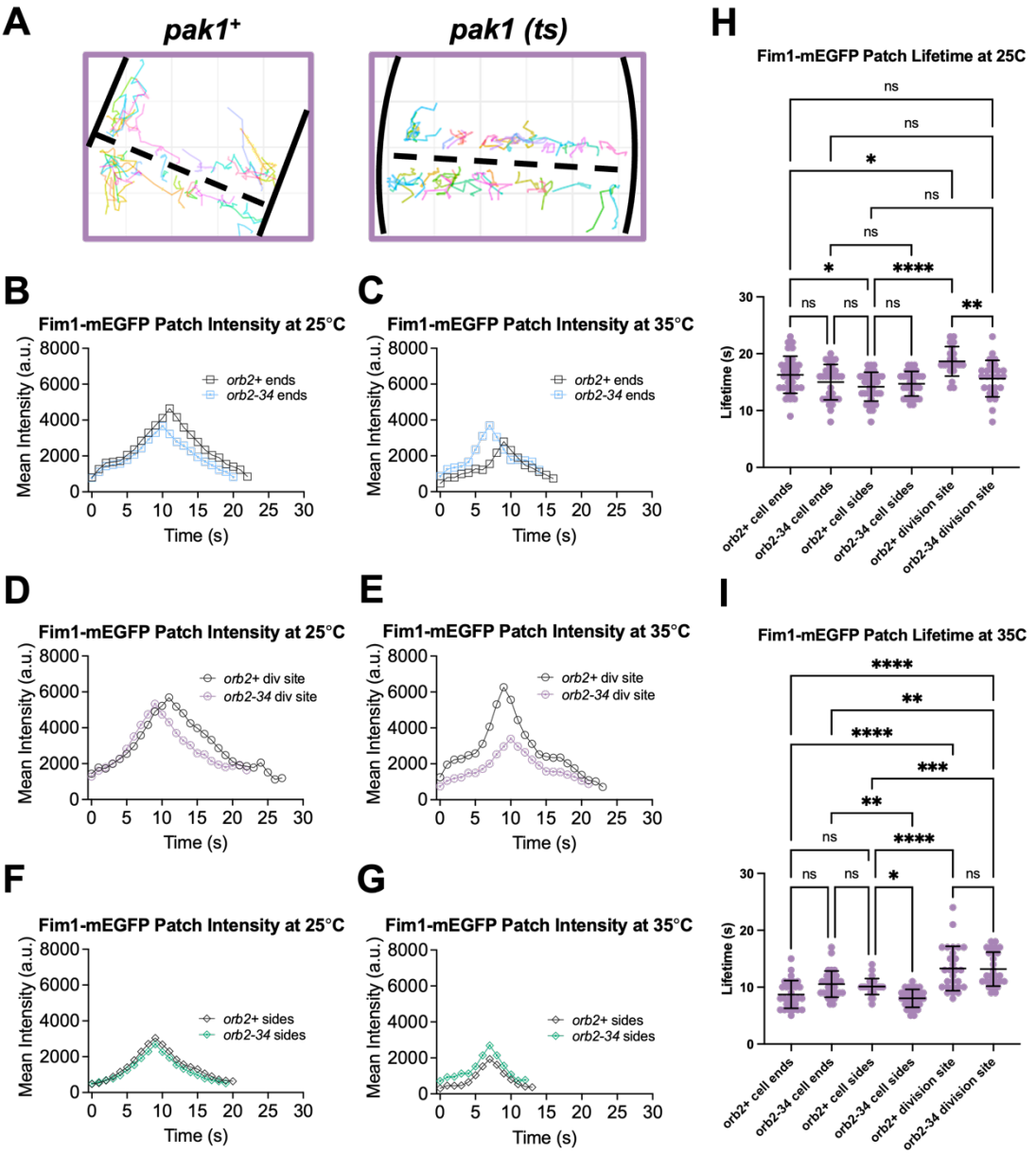

Figure 3.5. Pak1 promotes proper recruitment and dynamics of Fim1 within endocytic patches at sites of polarization. A) Representative cells showing Fim1-mEGFP endocytic events tracked via TrackMate. (B) through (G) Mean patch intensities of Fim1-mEGFP at growing cell ends, the division site, and cell sides in the indicated genotypes and conditions. (n ≥ 20 endocytic patches per experiment). (H) and (I) Patch lifetimes of Fim1-mEGFP at each region in the indicated genotypes and conditions. (n ≥ 20 endocytic patches per triplicate experiment). Ordinary one-way ANOVA with Tukey's multiple comparisons. ****, (p<0.0001; ***, p<0.001; **, p<0.01; *, p< 0.05; ns, not significant

3.4.6 The Type I myosin Myo1 promotes timely internalization of endocytic actin patches via Pak1-mediated phosphorylation of its motor domain

To further define how Pak1-mediated phosphorylation of Myo1 promotes endocytosis, we examined the dynamics of Fim1 in *myo1Δ* cells compared to *myo1*$^{+}$ controls. In the absence of *myo1*, endocytic patches marked with Fim1-mCh display weak internalization and largely slide within the plane of the plasma membrane at both the cell ends and the division site (Figure 3.6 A). Additionally, fewer endocytic patches form in *myo1Δ* mutants, although Fim1-mCh lifetimes are much longer compared to controls at all regions (Figure 3.6 B). Notably, while Fim1-mCh recruitment to endocytic patches reaches higher peak levels in *myo1Δ* cells compared to *myo1*$^{+}$ controls, Fim1 takes longer to accumulate at patches in these mutants (Figure 3.6 D). Indeed, peak Fim1-mCh patch intensity is reached ~8 seconds later at the cell ends (Figure 3.6 E) and ~11 seconds later at the division site in *myo1Δ* mutants compared to *myo1*$^{+}$ controls due to this slower recruitment of Fim1 (Figure 3.6 F). At the cell sides, peak Fim1-mCh patch intensity is slightly increased in *myo1Δ* cells and patches also take longer to reach peak intensity (Figure 3.6 G). Unlike Cdc42 and its regulators, Myo1 can also localize to cell sides in addition to sites of polarization, which may explain these changes in Fim1 behavior at the cell sides in the absence of *myo1*.

While Pak1 phosphorylates Myo1 at the S361 TEDS site located within its N-terminal motor domain (Attanapola et al., 2009), Myo1 also binds and weakly activates the branched actin nucleating Arp2/3 complex via its C-terminal tail (Lee et al., 2000; Sirotkin et al., 2005). Thus, Myo1 may promote endocytic patch internalization via its N-terminal motor function and/or its C-terminal association with Arp2/3. As *myo1Δ* completely abolishes all

Myo1 function, experiments in *myo1Δ* mutants alone cannot distinguish between these mechanistic possibilities. To determine if Pak1-mediated Myo1 phosphorylation is necessary to promote endocytic patch internalization, we examined endocytic patch behavior in the single point TEDS site phospho-null mutant, *myo1-S361A*, which cannot be phosphorylated by Pak1 but retains its C-terminal Arp2/3 binding domain (Attanapola et al., 2009). In the absence of Pak1-mediated phosphorylation of Myo1, we hypothesized that Fim1-mCh patches would show similar weak internalization as observed in *myo1Δ* mutants.

In the TEDS site *myo1-S361A* mutant, we find that Fim1-mCh is adequately recruited to endocytic patches, yet the patches do not properly internalize (Figure 3.6 A and D, Supplemental Figure 3.2 A and B). Additionally, we observe that Myo1-S361A-GFP intensity remains mostly stable at the plasma membrane of polarized cell ends, while WT Myo1-GFP intensity increases as Fim1-mCh is recruited to endocytic patches and is lost as Fim1-mCh patches internalize at the cell ends (Supplemental Figure 3.2), as reported previously (Sirotkin et al., 2005). We also observe increased cytoplasmic intensity of Myo1-S361A-GFP compared to controls (Supplemental Figure 3.2 A and B). In *myo1-S361A* mutants, Fim1-mCh lifetimes are indistinguishable from *myo1*$^{+}$ controls at the cell ends and sides, but patch lifetimes are prolonged at the division site (Figure 3.6 C). Similar to *myo1Δ* mutants, the timing of Fim1 recruitment to endocytic patches is prolonged in *myo1-S361A* mutants (Figure 3.6 D and H; Supplemental Figure 3.2). At the division site, Fim1 recruitment is enhanced in *myo1-S361A* mutants and peak Fim1-mCh intensity is reached slightly later compared to *myo1*$^{+}$ controls (Figure 3.6 I), mimicing *myo1Δ* mutants

(Figure 3.6 F). Similar to *myo1Δ* mutants, peak Fim1-mCh intensity at the cell ends is reached later in *myo1-S361A* mutants compared to controls (Figure 3.6 J). These observations suggest that branched actin formation can occur in the absence of Myo1 function, even though Myo1 is a nucleation promoting factor, albeit weak compared to Wsp1 (Sirotkin et al., 2005).

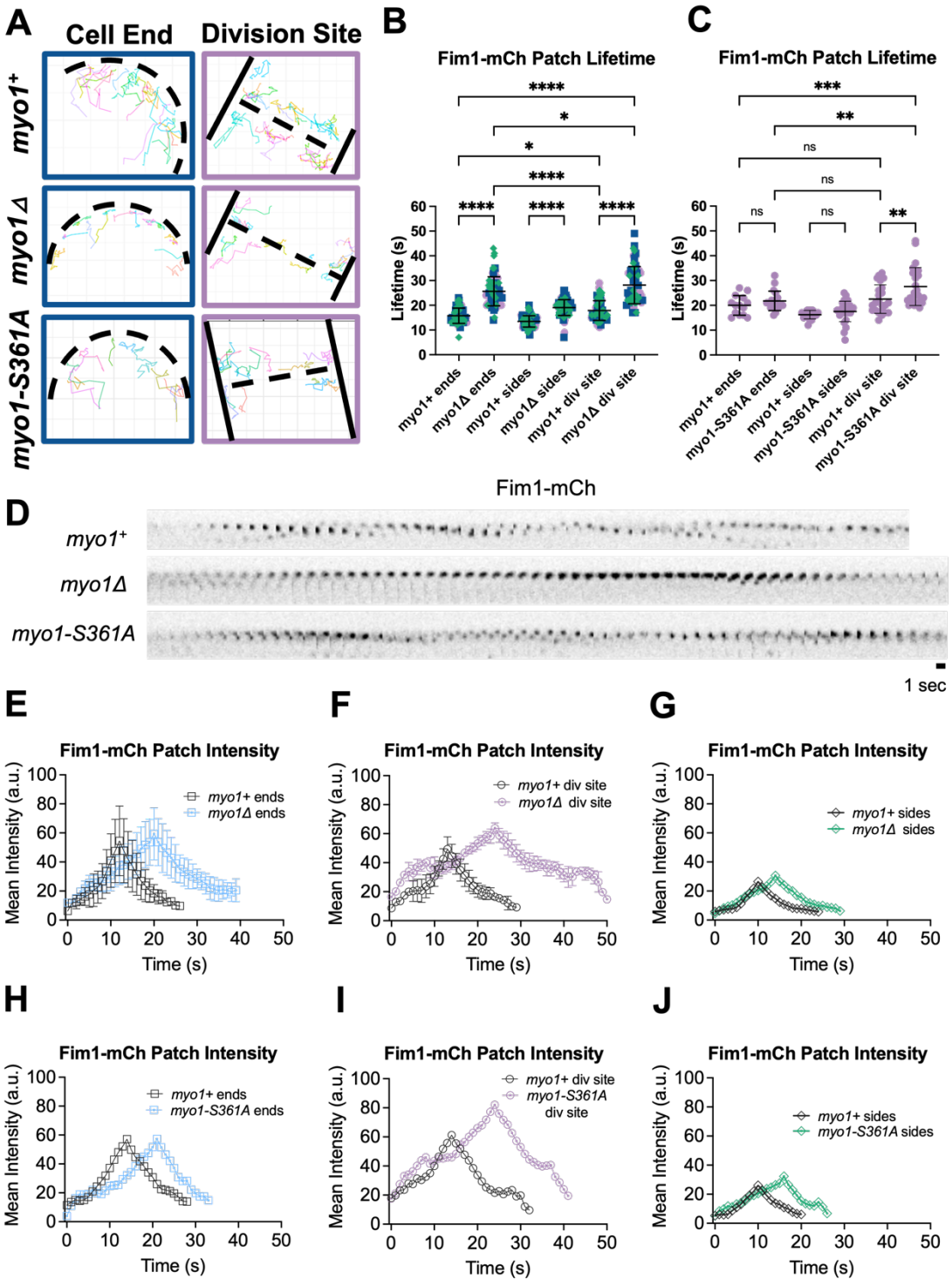

Figure 3.6. The Type I myosin Myo1 promotes timely endocytic patch internalization via Pak1-mediated phosphorylation of its motor domain. (A) Representative cells showing Fim1-mCh endocytic events tracked via TrackMate. (B) and (C) Patch lifetimes of Fim1-mCh at each region in the indicated

genotypes. (D) Montages of Fim1-mCh at the cell ends of the indicated genotypes. (E) through (J) Mean patch intensities of Fim1-mCh at each region in the indicated genotypes. (n ≥ 17 endocytic patches per triplicate experiment). Ordinary one-way ANOVA with Tukey's multiple comparisons. ****, $p<0.0001$; ***, $p<0.001$; **, $p<0.01$; *, $p< 0.05$; ns, not significant

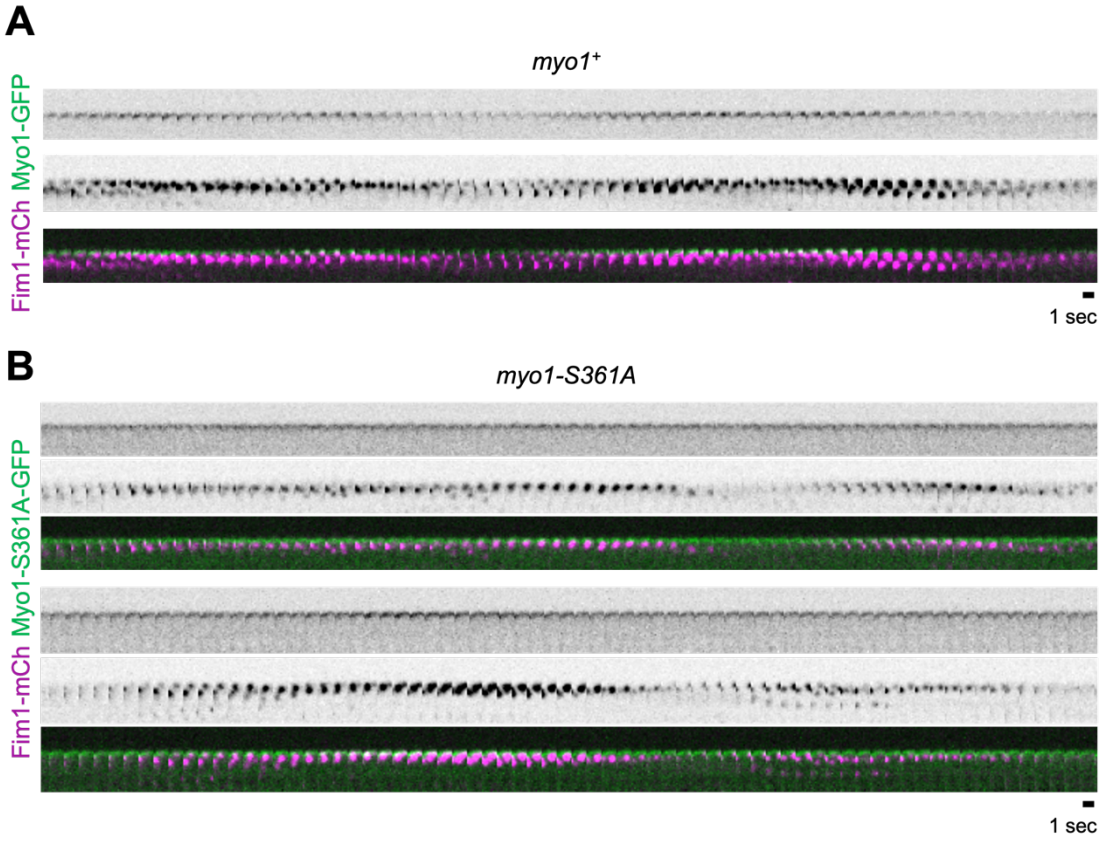

Supplemental Figure 3.2. Fim1-mCh poorly internalizes in *myo1-S361A* mutants and Myo1-S361A-GFP is stable at the plasma membrane rather than dynamic like WT-Myo1-GFP. (A) and (B) Montages of Fim1-mCh and Myo1-GFP at the cell ends of the indicated genotypes (scale bar = 1 sec)

3.4.7 Cdc42 and Pak1 activity regulate the recruitment and dynamics of Myo1 at polarized sites

As our findings indicate that Cdc42 and Pak1 activation promote Myo1 function, we asked whether their activity also promotes timely localization of Myo1 to sites of endocytosis. To test this, we observed whether loss or delay of Cdc42 or Pak1 activation at the division site would delay Myo1 recruitment to this site. Using *gef1Δ* mutants to delay Cdc42 activation at the division site as previously described (Figure 3.2), we saw that Myo1-GFP recruitment to the division site is consequently delayed by ~10 mins compared to *gef1*$^{+}$ control cells (Figure 3.7 A and B). Similarly, in *orb2-34* mutants lacking Pak1 kinase activity, Myo1-GFP recruitment to the division plane is delayed by ~4 mins compared to *orb2*$^{+}$ controls, even under permissive conditions (Figure 3.7 C and D). In summary, these findings indicate that both Cdc42 and Pak1 activation promote timely recruitment of Myo1 to the division site.

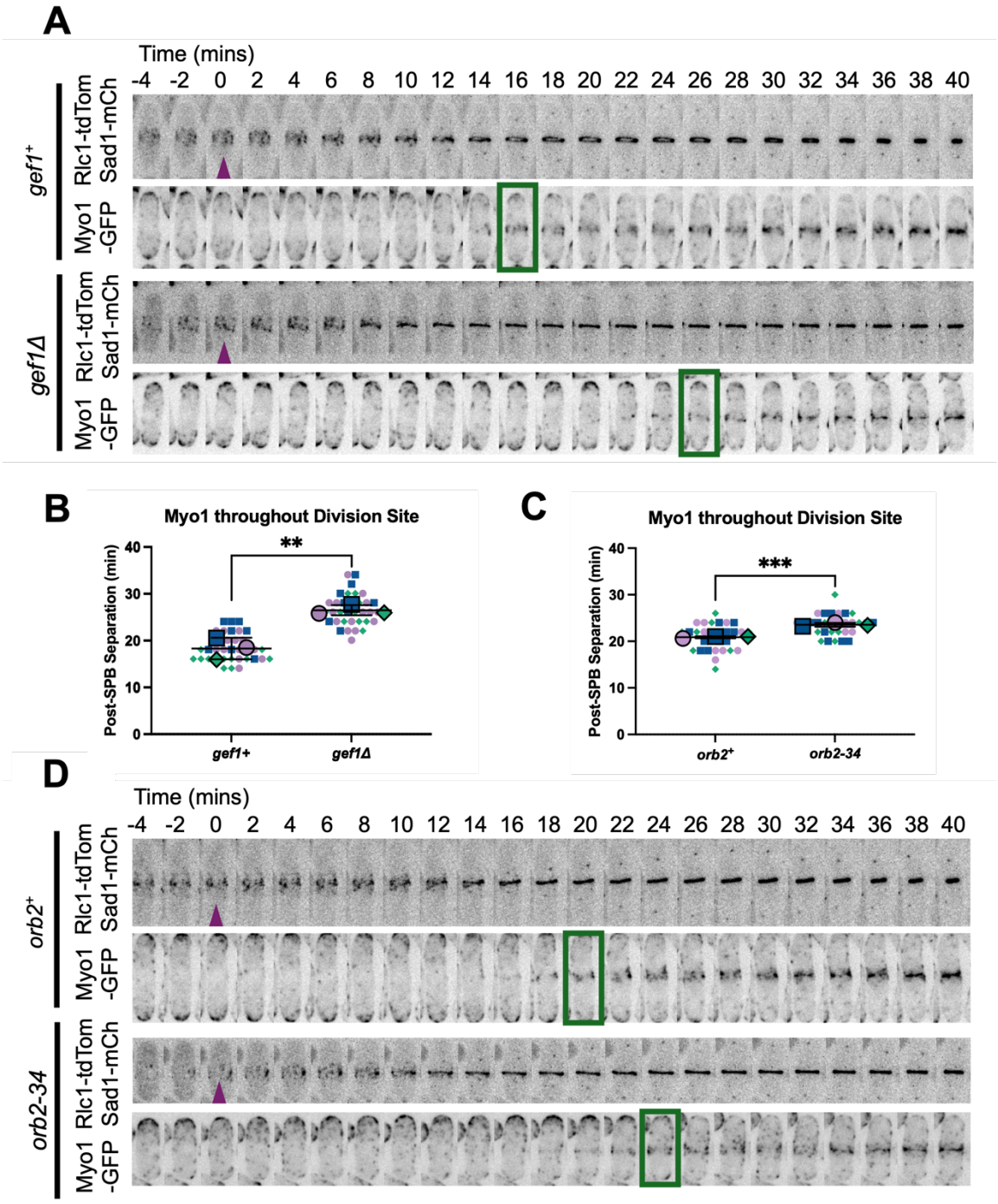

Figure 3.7. Timely Myo1 recruitment to the division site is promoted by both Cdc42 and Pak1 activation. (A) and (D) Representative cells showing Myo1-GFP appearance (green box) at the division site relative to Sad1-mCh to mark spindle pole body (SPB) separation (purple arrowhead). (B) and (C) Quantification of A and D, respectively, where time 0 = SPB separation. (n ≥ 10 cells per genotype per experiment). Unpaired Student's *t*-test. ***, $p<0.001$; **, $p<0.01$

Following our findings at the division site, we then asked if Cdc42 and Pak1 activation similarly regulate Myo1 recruitment to polarized cell ends. To test this, we first measured the mean intensity of Myo1-GFP recruited to the cell ends in genotypes with varying degrees of Cdc42 activity. While loss of *gef1* decreases Cdc42 activity (Wei et al., 2016), loss of the GAPs *rga4* and *rga6* increases Cdc42 activation levels (Campbell et al., 2022). Thus, we measured mean Myo1-GFP intensity at the cell ends of *gef1Δ* and *rga4Δrga6Δ* mutants compared to control cells. Intriguingly, Myo1-GFP recruitment is decreased in *gef1Δ* mutants and conversely enhanced in *rga4Δrga6Δ* mutants compared to controls (Figure 3.8 A and B). To investigate the dynamics of Myo1 at the cell ends, we also performed 1 sec-interval time-lapse imaging and measured the dwell time of Myo1-GFP at the plasma membrane. These analyses reveal that Myo1-GFP dwell time is increased in both *gef1Δ* and *rga4Δ* mutants compared to controls, suggesting that the myosin is less dynamic in both cases (Figure 3.8 C and D).

We then performed similar experiments in *orb2-34* cells to see if decreased Pak1 activation impairs Myo1-GFP recruitment and dynamics at cell ends. Under permissive conditions at 25C°, mean Myo1-GFP intensity is indistinguishable between *orb2-34* and *orb2*$^{+}$ cell ends (Figure 3.8 E and F). In contrast, temperature restriction at 35C° reduces mean Myo1-GFP intensity at the cell ends in both *orb2*$^{+}$ and *orb2-34* cells, although Myo1-GFP recruitment is more severely impacted in *orb2-34* mutants (Figure 3.8 E and F). Finally, loss of Pak1 kinase function likewise impairs Myo1-GFP dynamics at cell ends, as Myo1-GFP dwell times at the plasma membrane are prolonged in *orb2-34* compared to *orb2*$^{+}$ cells under permissive conditions (Figure 3.8 G and H). Together, these data indicate that Cdc42 and

Pak1 activation promote the recruitment of Myo1 to the plasma membrane in a dosage-dependent manner. Additionally, these results suggest that an intermediate range of Cdc42 activation facilitates proper Myo1 dynamics. In summary, our findings suggest that sufficient recruitment of Myo1 to the plasma membrane depends on both Cdc42 and Pak1 activation.

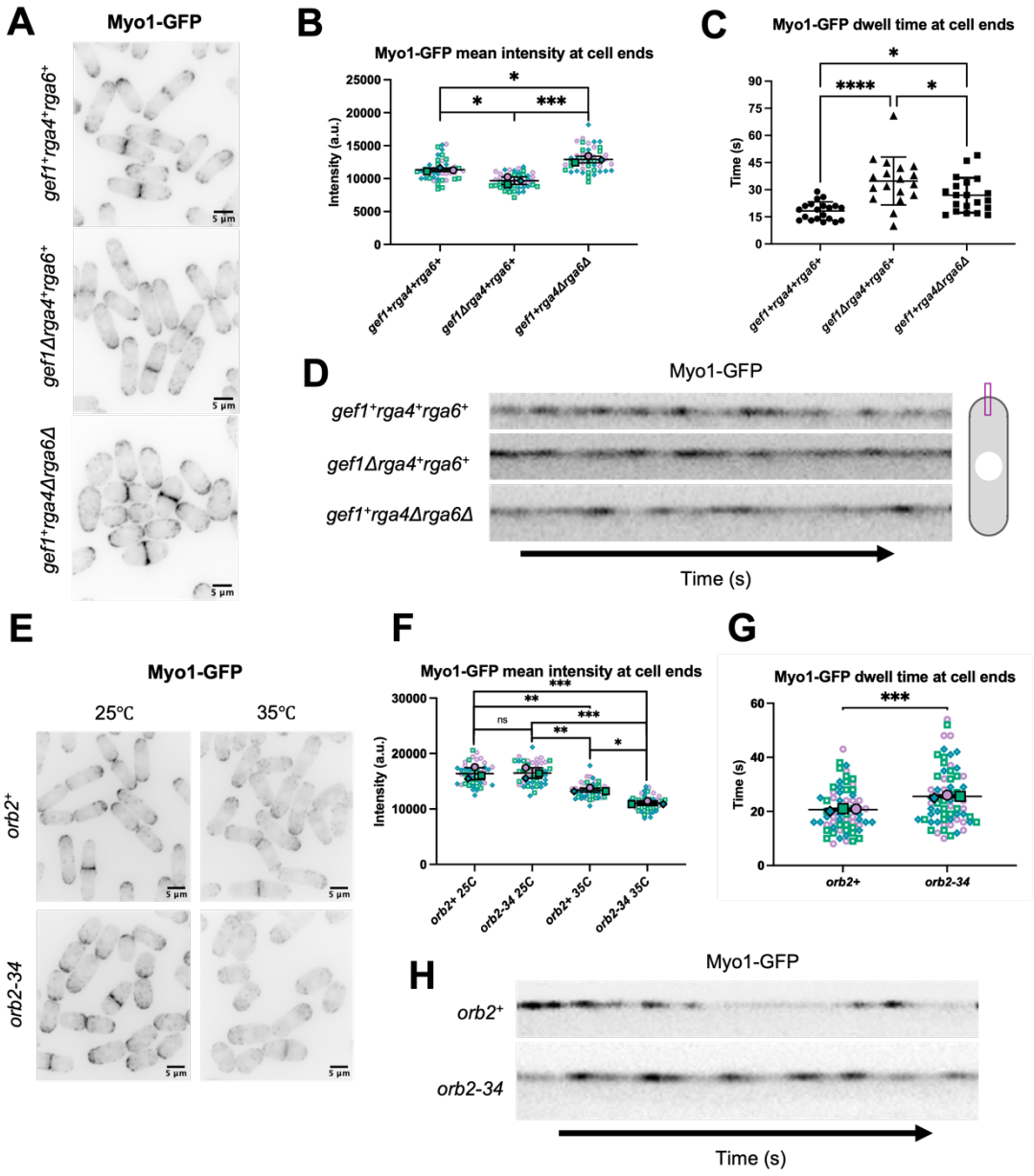

Figure 3.8. Cdc42 and Pak1 activity regulate the recruitment and dynamics of Myo1 at polarized cell ends. (A) and (E) Sum *Z*-projections of Myo1-GFP stills. (B) and (F) Mean Myo1-GFP intensity measured at cell ends in the indicated genotypes (n=15 cells per genotype per triplicate experiment). (C) and (G) Quantification of (D) and (H). (n≥15 dwell time events per genotype. (D) and (H) 3-minute-long kymographs

showing Myo1-GFP dwell time dynamics at individual cell ends. One-way ANOVA with Tukey's multiple comparisons post hoc test. ns, not significant; *, $p<0.05$; **, $p<0.01$; ***, $p<0.001$; ****, $p<0.0001$

3.5 DISCUSSION

3.5.1 The interplay between sites of polarization and clathrin-mediated endocytosis

In many cell-walled organisms, endocytosis is an actin-dependent process since cells must overcome high internal turgor pressure to properly bend and invaginate the plasma membrane (Basu et al., 2014; Lacy et al., 2018). In yeast, branched actin polymerization and crosslinking within actin patches at the plasma membrane provide the force needed to promote successful internalization against high turgor pressure (Basu et al., 2014; Kaksonen and Roux, 2018; Skau et al., 2011). However, it is not known whether the force requirements are the same at all regions of the cell, as endocytic patches can form at the cell ends, sides, and at the division site. For instance, at the division site, patches form in close proximity to the actomyosin ring, the synthesizing septum, as well as other membrane-associated cytoskeletal structures such the septin ring (Wu et al., 2003), which may impact the force required to produce successful internalization. Here, we demonstrate that endocytic patch behavior is intricately linked with cell polarization. We find that endocytic patches at non-growing cell sides weakly recruit the branched actin crosslinker Fim1, have average lifetimes of ~13 seconds, and display diffusive behavior (Figure 3.1). In contrast, endocytic patches within polarized regions recruit twice as much Fim1, have

average lifetimes of ~16-18 seconds, and exhibit directed motion during patch internalization (Figure 3.1). Together, these results suggest that endocytic patches within polarized regions contain more branched actin for Fim1 to bind to provide the force necessary for proper patch internalization (Skau et al., 2011). Furthermore, in polarity mutants, we find that endocytic patches often show aberrant behavior at the cell ends and division site where polarity is disrupted, while patches at the cell sides of these mutants mirror wild-type cell side behavior. These findings suggest that patches that form at the cell sides are not influenced by polarization or under the control of polarity regulators. Given that only patches at polarized sites have access to active Cdc42 and that the Cdc42 GEF Gef1 is present within endocytic patches (Hercyk and Das, 2019), we propose that Cdc42 activity promotes proper actin patch formation and internalization and provide evidence to support this claim.

3.5.2 Cdc42 and Pak1 activity promote initiation of endocytosis at sites of polarization

At polarized cell ends, it has been challenging to determine exactly how Cdc42 activation is established since both GEFs are active at this site, but Gef1 is mostly cytoplasmic and present in small amounts within cortical puncta that are difficult to distinguish, while Scd1 localizes as a cap across the entire cell end (Hercyk and Das, 2019; Hercyk et al., 2019b). Thus, it is difficult to ascertain whether Cdc42 plays a supporting or a necessary role in endocytosis at the cell ends. In contrast, the division site provides a more amenable region to define the mechanisms of Cdc42 activation and polarization establishment. In contrast, the division site provides a more amenable region to define the mechanism of Cdc42

activation and polarization establishment (Hercyk and Das, 2019; Hercyk et al., 2019b; Wei et al., 2016). At the division site, both GEFs can readily be visualized to determine when and how each promotes Cdc42 activation. Gef1 is the first GEF to appear at the division site where it activates Cdc42 during ring formation (Hercyk and Das, 2019; Hercyk et al., 2019b; Wei et al., 2016). Scd1, conversely, does not activate Cdc42 until after onset of ring constriction (Wei et al., 2016) and depends on Gef1 for proper recruitment to the division site (Hercyk et al., 2019b). Thus, using *gef1Δ* mutants to delay Cdc42 activation at the division site, we show that Cdc42 activation is required for initiation of branched actin-mediated endocytosis within this polarized region. Similar to Cdc42 activation patterns, Fim1-mEGFP first appears at the division site of *gef1*$^{+}$ controls during ring maturation well before the onset of ring constriction (Wang et al, 2016). However, in *gef1Δ* mutants, Fim1-mEGFP appearance is delayed to just before the onset of ring constriction (Figure 3.2 A), as reported for Cdc42 activation (Wei et al., 2016). Yet, once Cdc42 is finally activated in *gef1Δ* mutants, Fim1-mEGFP rapidly appears at the division site (Figure 3.2 C and D).

These results suggest that the timing of Cdc42 activation and onset of endocytosis are tightly linked. In a similar manner, we also demonstrate that the Cdc42 downstream effector Pak1 likewise promotes timely onset of endocytosis at the division site (Figure 3.4). Given the previously described challenges, we have not directly shown that Cdc42 activity promotes endocytosis at the cell ends. However, we demonstrate that decreased Cdc42 activation via loss of its GEF *gef1* results in excessive Fim1 recruitment yet delayed

patch internalization at the cell ends. Thus, it is likely that Gef1-mediated Cdc42 activation also facilitates proper patch formation and internalization at the cell ends.

3.5.3 Cdc42 activity promotes endocytic patch formation and internalization in a dose-dependent manner

As we probed the mechanistic details of how Cdc42 activation promotes endocytosis, we found that various polarity mutants exhibit distinct phenotypes of endocytic patch behavior (summarized in Table 3.1, Table 3.2, and Table 3.3). Interestingly, individual loss of each Cdc42 GEF results in disparate phenotypes. Loss of *gef1* severely impacts endocytic patch behavior at polarized sites (Figure 3.3 A, B, D, and H), whereas loss of *scd1* depolarizes the location of endocytic sites across the whole cell cortex (Supplemental Figure 3.1 E) but patches retain mostly normal dynamics (Figure 3.3 A, C, E, and I). These findings suggest that transient, Gef1-mediated Cdc42 activation is required for proper endocytic patch formation and internalization, rather than strong activation via Scd1. While dispensable for proper patch behavior, Scd1 is still required to prevent ectopic Cdc42 activation and thus also regulates where endocytosis occurs. Interestingly, we observe that loss of *gef1* results in some differences between patch dynamics at the cell ends and the division site. In *gef1*$^{+}$ cells, peak Fim1-mEGFP patch intensity is reached ~2 seconds faster at the division site compared to Fim1 recruitment at the cell ends (Figure 3.3 B and D). In contrast, *gef1Δ* mutants appear to recruit Fim1 to endocytic patches at the same rate at both sites (Figure 3.3 B and D). Additionally, Fim1-mEGFP patch lifetimes are increased at the cell ends of *gef1Δ* mutants, lasting as long as Fim1-mEGFP patches at the division site of *gef1*$^{+}$ cells.

Comparatively, patch lifetimes are not longer at the division site of *gef1Δ* mutants compared to controls, even though *gef1Δ* mutants recruit more Fim1 to endocytic patches. These observations indicate that the rate of branched actin synthesis is likely faster in *gef1Δ* mutants, since more branched actin is formed at the patch within the same span of time. As Cdc42 is under strong Scd1-mediated activation in *gef1Δ* mutants, we conclude that Cdc42 is excessively activated in these mutants, which leads to enhanced branched actin synthesis. Our results further show that this excessive branched actin formation is actually deleterious to timely patch internalization in *gef1Δ* mutants, even though branched actin provides the force required to internalize the patch against the cellular turgor pressure. Together, these findings indicate that Cdc42 activation must be tightly regulated at the endocytic patch to form proper amounts of branched actin.

Although loss of *pak1* kinase function impairs endocytic patch internalization at the cell ends (Harrell et al, 2024), it seems that actin patch formation is most greatly impaired at the division site of *orb2-34* mutants. At restrictive temperature, Fim1 recruitment to endocytic patches at the cell ends is not impaired in *orb2-34* mutants, while Fim1 recruitment is greatly decreased to endocytic patches at the division site (Figure 3.5 C and E). We interpret these results to indicate that the cell ends are more robust to loss of *pak1* function than the division site. This may result from functional redundancy with pak2 at the cell ends; however, this cannot be tested since *pak2Δ orb2-34* mutants are inviable. Alternatively, Pak1 could play additional roles at the division site that do not occur at the cell ends. Already some such roles are known since Pak1 phosphorylates several cytokinetic ring proteins (Magliozzi et al., 2020).

Similar to our findings in *gef1Δ* mutants, we observe that the amount of branched actin synthesized at endocytic patches is enhanced at the division site of *myo1Δ* and *myo1-S361A* mutants compared to controls. Strikingly, even though the amount of Fim1 recruited to the division site of *myo1* mutants is enhanced, the timing of endocytic patch internalization is greatly delayed in both *myo1* mutants. As in the *orb2-34* mutant, endocytosis is more impaired at the division site in both *myo1* mutants, since Fim1-mCh lifetime is most prolonged at the division site compared to controls (Figure 3.6 B and C). Even though Fim1 appears to be recruited to endocytic patches at a similar rate in *myo1* mutants compared to controls, it seems that *myo1* mutants cannot initiate patch internalization in a timely manner (Figure 3.6; Supplemental Figure 3.2 A and B). Furthermore, the dynamics of the type I myosin are impaired, as Myo1-S361A-GFP is present nearly continuously on the plasma membrane rather than coinciding with Fim1-mCh patches (Supplemental Figure 3.2 A and B). We posit that this increased stability of Myo1 may contribute to the internalization delays observed in *myo1-S361A* mutants. In line with our findings in *gef1Δ* mutants, these observed delays in endocytic internalization even in the presence of abundant amounts of branched actin indicate that the amount of actin present within the patch is not the sole determining factor for the timing of internalization.

Finally, we also show that Cdc42 promotes Myo1 recruitment to polarized sites in a dose-dependent manner. Our data indicate that both insufficient and excessive Cdc42 activation lead to greater stability of Myo1 at the plasma membrane, as demonstrated by its increased dwell time in mutants of Cdc42 GEFs and GAPs and as well as the Pak1 kinase (Figure 3.8 C-D and G-H). This increased stability is reminiscent of the stable localization

displayed by Myo1-S361A-GFP, which cannot be phosphorylated by Pak1 kinase at its motor domain TEDS site (Supplemental Figure 3.2 A and B). Since endocytic patch internalization defects seem to coincide with increased Myo1 stability, these results suggest that Myo1 requires a certain level of dynamic behavior to properly promote endocytic patch internalization.

Cell ends	Fim1 recruitment rate	Fim1 peak recruitment	Fim1 lifetime	Timing of patch internalization
control	normal	normal	normal	normal
gef1Δ	normal	↑	↑	delayed
scd1Δ	normal	normal	↓	normal
myo1Δ	↓	↑	↑↑	delayed
myo1-S361A	semi-normal	normal	normal	delayed

Table. 3.1. Phenotypes of Fim1-mEGP or Fim1-mCh endocytic patch behaviors at the cell ends in various polarity mutants compared to controls.

Division site	Fim1 recruitment rate	Fim1 peak recruitment	Fim1 lifetime	Timing of patch internalization
control	normal	normal	normal	normal
gef1Δ	↓	↑	normal	delayed
scd1Δ	normal	normal	↓	normal
myo1Δ	↓↓	↑↑	↑↑	very delayed
myo1-S361A	semi-normal	↑	↑	delayed

Table. 3.2. Phenotypes of Fim1-mEGP or Fim1-mCh endocytic patch behaviors at the division site in various polarity mutants compared to controls.

Cell ends	Fim1 recruitment rate	Fim1 peak recruitment	Fim1 lifetime	Timing of patch internalization
25ºC control	normal	normal	normal	normal
25ºC *orb2-34*	normal	↓	normal	normal
35ºC control	↓	↓	↓	early
35ºC *orb2-34*	semi-normal	same as *orb2-34* at 25ºC	↓	early
Division site				
25ºC control	normal	normal	normal	normal
25ºC *orb2-34*	normal	↓	↓	normal
35ºC control	semi-normal	normal	↓	early
35ºC *orb2-34*	↓↓	↓↓	same as control at 35ºC; similar to *orb2-34* at 25ºC	same as control at 35ºC

Table. 3.3. Phenotypes of Fim1-mEGP endocytic patch behaviors in *orb2-34* mutants compared to *orb2*$^{+}$ controls at permissive (25°C) and restrictive (35C°) temperatures.

3.5.4 Cdc42 regulates endocytic patch formation and internalization via two pathways

In summary, our data suggest that Cdc42 and Pak1 may regulate endocytic behavior via two pathways – 1. by promoting proper actin patch formation via sufficient but not excessive Cdc42/Pak1 activation – and 2. by promoting proper Myo1 motor function and association with actin patches via Pak1-mediated phosphorylation of Myo1. Since Myo1 is a direct target of Pak1 (Attanapola et al., 2009; Magliozzi et al., 2020), we initially expected *myo1-S361A* mutants to phenocopy the endocytic defects observed in kinase-dead *orb2-34* mutants. Our results, however, show distinct phenotypes of altered endocytic patch behavior for these mutants, which indicates that Pak1 has additional roles that are yet to be explored.

Furthermore, in line with previous reports, our findings suggest that the Arp2/3 complex can generate branched actin without Pak1 phosphorylation of Myo1's TEDS site (Attanapola et al., 2009) and even without Myo1 altogether. Thus, the internalization defect observed in *myo1-S361A* mutants does not stem from inability to create branched actin. Rather, our data indicate that TEDS site phosphorylation of Myo1 chiefly facilitates proper localization and dynamics of the myosin at the plasma membrane, rather than nucleation of branched actin at the endocytic patch. Given that TEDS site phosphorylation promotes motor function of the Type I myosin in other organisms (Bement & Mooseker, 1995; Fujita-Becker et al., 2005; Pedersen et al., 2023), we suspect that the same likely occurs in *S. pombe*. Indeed, the perturbed localization and increased stability we observe for Myo1-S361A-GFP suggests that its motor function may be impaired. Such findings have been

reported in budding yeast where Type I myosin motor activity is independent of its ability to nucleate actin and loss of motor function cannot be rescued with increased actin nucleation to restore patch internalization (Manenschijn et al., 2019). As the other actin nucleation promoting factor, the WASP homolog Wsp1, activates Arp2/3 independently and more strongly than Myo1 in *S. pombe* (Sirotkin et al., 2005), we suspect that Wsp1 primarily promotes Arp2/3-dependent branched actin formation in *myo1-S361A* mutants. Indeed, it is possible that Myo1 does not bind Arp2/3 in *myo1-S361A* mutants since Myo1-S361A-GFP does not specifically associate with actin patches and is instead localized throughout the plasma membrane (Attanapola et al., 2009, Supplemental Figure 3.2 B), and our data do not preclude this possibility. As such, our data currently only indicate that Pak1-mediated TEDS site phosphorylation is necessary to promote proper localization and dynamics of Myo1 but do not demonstrate whether this phosphorylation is alone sufficient for endocytic patch internalization in the absence of Myo1-Arp2/3 binding. Further experiments eliminating the C-terminal Arp2/3-binding domain in Myo1 are necessary to determine the importance of this interaction. Together, these findings suggest that Pak1-mediated phosphorylation of Myo1 facilitates timely and efficient endocytic patch internalization.

While both the growing cell ends and the division site are sites of polarization, we observe subtle differences in endocytic patch behavior between these sites. Although Fim1 appears to be recruited to the same level within both of these polarized regions (Figure 3.1 C), the lifetime of patches at the division site is ~2 seconds longer than cell end patches (Figure 3.1 B). Additionally, patches at the division site are more stationary during patch formation

and ingress more slowly during internalization (Figure 1.3 D and F). As endocytosis is a force-sensitive and actin-dependent process, these differences in patch dynamics suggest that the forces experienced by patches at the division site are higher than that of the cell ends. If such is the case, patches at the division site would require stronger actin architecture and/or additional assistance from endocytic proteins such as Myo1 to overcome this increased force. This disparate force requirement could arise in several ways. Perhaps the flow of polarized secretion produces some counteractive force that must be overcome for patches to internalize. At the division site, polarized secretion occurs throughout the division plane, while endocytosis is largely confined to the outer rim of the membrane furrow (Wang et al., 2016). At the cell ends, such spatial arrangement has not been detected since both endocytic and exocytic membrane trafficking events occur throughout the plasma membrane at this site. Furthermore, our observations that endocytic patches at the cell sides are weakly formed suggest that the forces they experience are also different than those at polarized regions. It is unclear if the patches at the cell sides internalize, but do not move as far from the plasma membrane since the force produced within the patch is less. It is possible that these patches do not require access to active Cdc42 to internalize. Alternatively, it is possible that they are random assemblies of branched actin that do not represent true sites of endocytosis.

Finally, it seems from our observations in *gef1Δ* mutants that formation of branched actin patches is not sufficient in itself to stimulate timely patch internalization, since patches excessively recruit both Cdc15 and Fim1 yet do not timely internalize. Perhaps the actin architecture within these mutants is improperly organized to internalize the patch. This

hypothesis fits with our observations in *myo1Δ* and *myo1-S361A* mutants, which also assemble branched actin patches with excessive Fim1 yet exhibit severe patch internalization defects. Perhaps proper binding of Myo1 to branched actin is essential for timely initiate internalization. As Cdc42 activation is decreased in *gef1Δ* cells and Myo1 recruitment is also decreased in these mutants, perhaps it takes longer for Myo1 to properly associate with the patch and stimulate patch internalization. Together, our findings indicate a direct role for Cdc42 in regulating endocytic patch formation via the Pak1 kinase and endocytic patch internalization via the Pak1 target, the Type I myosin, in a site-specific manner.

3.6 MATERIALS AND METHODS

3.6.1 Strains and cell culture

The *S. pombe* strains used in this study are listed in Table 1. All strains are isogenic to the original strain PN567. Cells were cultured in yeast extract (YE) medium and grown exponentially at 25°C for 3 rounds of 8 generations before imaging. Standard techniques were used for genetic manipulation and analysis (Moreno et al., 1991).

3.6.2 Microscopy

Imaging was performed at room temperature (23–25°C) for all experiments except for restrictive temperature experiments, which were performed at 35°C (Fig. 5). Images were acquired on a spinning disk confocal system equipped with a Nikon Eclipse inverted microscope with a 100×/1.49 NA lens, a CSU-22 spinning disk system (Yokogawa Electric Corporation), and a Photometrics EM-CCD camera (Photometrics Technology Evolve with excelon Serial No: A13B107000). On this system, images were acquired with MetaMorph (Molecular Devices, Sunnyvale, CA). Imaging was also performed on a 3i spinning disk confocal system using a Zeiss AxioObserver microscope equipped with a 100×/1.49 NA objective, an integrated Yokogawa spinning disk (Yokogawa CSU-X1 A1 spinning disk scanner), and a Teledyne Photometrics Prime 95b back-illuminated sCMOS camera (Serial No: A20D203014). On this system, images were acquired using SlideBook (3i Intelligent Imaging innovations). All images were analyzed with FIJI (National Institutes of Health, Bethesda, MD (Schneider et al., 2012)).

For still imaging, the cells were mounted directly on glass slides with a #1.5 coverslip (Thermo Fisher Scientific, Waltham, MA) and imaged immediately, and with fresh slides prepared every 10 min. *Z*-series images were acquired with a depth interval of 0.4 μm. For time-lapse images, cells were placed in 3.5 mm glass-bottom culture dishes (MatTek, Ashland, MA) and overlaid with YE medium containing 0.6% agarose and 100 μM ascorbic acid as an antioxidant to minimize toxicity to the cell, as reported previously (Frigault et al., 2009; Wei et al., 2017).

3.6.3 Analysis of vesicle tracking

Wild-type and mutant cells expressing Fim1-mEGFP or Fim1-mCh were grown to OD 0.2-0.5 and placed in glass-bottom culture dishes as previously described for time-lapse imaging. Cells were imaged in a single medial plane with a frame rate of 1 sec for ~3-5 minutes using the same laser power and exposure settings for all experiments. To measure patch lifetimes and mean fluorescence intensity of patches throughout their lifetimes, Fim1-mEGFP/Fim1-mCh patches were tracked using the FIJI plugin TrackMate. Background fluorescence was subtracted from the imaging field away from cells to sharpen the signal of patches for ease of tracking. Lifetime was measured as the time from which a patch first displayed distinguishable fluorescence at the cell cortex to when the fluorescence was no longer detectable. Mean speed (μm/sec), MSD (mean squared displacement), and diffusion coefficients (μm^2/sec) were all calculated using TrackMateR, an R package that can analyze data captured and saved by TrackMate as XML files (https://quantixed.org/2022/09/05/tracking-announcing-new-r-package-trackmater/). To ensure that patches were tracked from the beginning of patch formation through patch

disassembly, patches selected for tracking 1. gradually increased in intensity until a peak intensity was reached and 2. decreased in intensity following peak intensity (Berro and Pollard, 2014; Wang et al., 2016). Patches tracked with TrackMate were also manually reviewed to ensure tracking accuracy.

3.6.4 Disruption of Pak1 kinase function via temperature-sensitive allele *orb2-34*

Pak1 kinase was inactivated via the *orb2-34* (*pak1-ts*) temperature-sensitive mutation. Cells were grown for 2 days in YE medium. On the day of the experiment, cells were cultured to an OD of 0.2. A subset of these cells was incubated at the permissive temperature of 25°C, while the other set was incubated at the restrictive temperature of 35°C for 4 h. Cells were imaged after 4 h under temperature-controlled conditions.

3.6.5 Analysis of Myo1-GFP mean fluorescence intensity at cell ends

Wild-type and mutant cells expressing Myo1-GFP were grown to OD 0.2-0.5 and imaged on slides. Still *Z*-images with 21-24 *z*-planes were collected at a *z*-interval of 0.4 μm for the 488 nm channel. The same number of *z*-slices were collected for wild-type and mutant cells for each experiment using the same imaging settings. FIJI was used to generate sum projections from the *z*-series and the polygon selection tool was used to encircle the "cap" of Myo1-GFP signal present at individual cell ends. Mean fluorescence intensity at individual cell ends was then measured within these manually selected Myo1-GFP "caps". The background fluorescence in a cell-free region of the image was subtracted to normalize

intensity measurements. Only cells found within the central 80% of the imaging field were used for analysis. This was done to account for uneven illumination of the imaging field.

3.6.6 Analysis of Myo1-GFP dwell time at cell ends

Wild-type and mutant cells expressing Myo1-GFP were grown to OD 0.2-0.5 and placed in glass-bottom dishes as previously described for time-lapse imaging. Cells were imaged in a single medial plane with a frame rate of 1 sec for 3 minutes using the same imaging settings for all experiments. To visualize Myo1-GFP dwell time throughout the 3-minute time-lapse, kymographs were generated from 1 pixel-wide selection lines drawn across the midline of the cell end, parallel to the cell's long axis. These kymographs were then manually analyzed to measure the dwell time of Myo1-GFP at individual cell ends in the following manner: Using FIJI's rectangle selection tool, individual Myo1-GFP dwell time events were marked on each kymograph and the length of each event was measured in pixels. Since our imaging settings generated kymographs were 1 pixel = 1 sec, the number of pixels measured for an individual event equals Myo1-GFP dwell time in seconds for that event.

3.6.7 Statistical tests

GraphPad Prism was used to determine significance. One-way ANOVA, followed by a Tukey's multiple comparisons post-hoc test, was used to determine individual *p*-values when comparing three or more samples. When comparing two samples, an unpaired Student's *t*-test (two-tailed, unequal variance) was used to determine significance.

4.0 CHAPTER 4 - DISCUSSION

4.1 IMPLICATIONS OF RESEARCH FINDINGS

4.1.1 Cdc42 coordinates distinct membrane trafficking events required for septum formation

Cytokinesis in *S. pombe* is a sequential process of distinct membrane trafficking events. After the actomyosin ring forms and matures, septum synthases are trafficked to the division site to synthesize the septum and aid the constriction of the ring (Cortés et al., 2016; Proctor et al., 2012; Wei et al., 2016). Synthesis of the primary (innermost) septum layer initiates first once the glucan synthase Bgs1 is delivered to the division site (Liu et al., 1999). Shortly thereafter, Bgs4 is trafficked to the division site to synthesize the secondary septum layers which flank the primary septum (Munoz et al., 2013). After septum maturation, glucanases are trafficked to the division site to digest the primary septum and separate the daughter cells (Martin-Cuadrado et al., 2003; Dekker et al., 2004). Thus, these distinct membrane trafficking events require spatiotemporal regulation to ensure sequential synthesis of each septum layer, which is important to prevent cell lysis during primary septum digestion.

Previous work demonstrates that the Rho GTPase Cdc42 participates in the spatiotemporal distinction of these events, as Cdc42 activation is required for Bgs1 trafficking and

glucanase localization to the division site but is not required to deliver Bgs4 (Estravis et al., 2012; Wei et al., 2016; Onwubiko et al., 2021). A recent report from our lab additionally shows that Cdc42 prevents early activation of the Rho GTPase Rho1 at the division site in a Pak1-dependent manner (Onwubiko et al., 2023). Since the glucan synthase function of Bgs1 is activated when Rho1 binds it (Arellano et al., 1996), it is important for Bgs1 to first be delivered to its site of action before binding Rho1. Indeed, in the absence of Pak1 function, Rho1 activity initiates early, leading to early septum deposition which promotes early actomyosin ring constriction (Onwubiko et al., 2023). While it is clear that Cdc42 facilitates the coordination of various membrane trafficking events necessary for septum formation and cytokinesis, it was not known how Cdc42 activity is regulated during cytokinesis to coordinate these processes.

Here, we show that Cdc42 activity is downregulated during actomyosin ring constriction to coordinate the trafficking of distinct septum glucan synthases. Since the primary septum establishes the template upon which the secondary septum layers are synthesized, Cdc42-mediated trafficking of Bgs1 is most required during early cytokinesis for primary septum synthesis. Once ring constriction begins, Bgs4 is needed to synthesize the secondary septum layers flanking the primary septum. As such, Cdc42 activity is downregulated via its GAPs during ring constriction to allow Bgs4 trafficking to the division site. This spatiotemporal coordination of Bgs1 and Bgs4 trafficking via Cdc42 regulation ensures proper septum architecture, in which the primary septum is weak and amenable to glucanase digestion while the secondary septa layers are sturdy enough to remain as cell wall in newly formed daughter cells.

4.1.2 Cdc42 regulates clathrin-mediated endocytosis during membrane furrowing and polarized growth

In the absence of proper regulation of Cdc42, we also find that membrane remodeling is impaired at the cleavage furrow. Specifically, excessive Cdc42 activation during ring constriction leads to excess membrane present along and even within the septum. As endocytosis removes membrane from the membrane furrow and we observe an increase in failed endocytic events at this site compared to controls, we postulate that endocytosis fails to properly remodel and remove membrane along the membrane furrow when Cdc42 is hyperactive. Intriguingly, excessive Cdc42 activation also results in increased rates of endocytic failure at growing cell ends, yet endocytic events at the division site do not behave exactly as those at the cell ends, even among wild-type cells. These observations prompted us to further investigate the connection between Cdc42 activation, polarization, and endocytosis.

4.1.3 Cdc42 and its effector Pak1 regulate endocytic patch formation and behavior at polarized sites

While sites of endocytosis have long been known to mirror sites of polarized growth, we show for the first time that endocytic events display distinct phenotypes at each cellular region. As endocytic patches at the division site and cell ends recruit twice as much branched actin crosslinker as appears at the cell sides, we postulate that patches at these sites contain more actin. Furthermore, while patches at the ends and division site readily internalize, patches at the sides mostly diffuse within the membrane. From these data, we conclude that patches at the ends and division site likely represent true sites of endocytosis, while those at the sides may occur haphazardly without specific regulation.

We also show that initiation of endocytosis at the division site depends on Cdc42 activity and that this likely occurs through its effector, the Pak1 kinase. Interestingly, Cdc42 requires only transient Gef1-mediated activation at endocytic sites to promote proper endocytosis, as strong Scd1-mediated activation prolongs the process of endocytic patch formation and delays internalization. These findings suggest there is a threshold of Cdc42 activation required to initiate branched actin formation within endocytic patches but that there is also an upper limit beyond which Cdc42 activation becomes excessive and hinders the endocytic process. Finally, we demonstrate that changes in cell polarity correlate with changes in endocytic patch behavior at growing cell ends and the division site, yet not at non-growing cell sides. As changes in polarity only affect endocytic behavior at the cell ends and division site where Cdc42 and Pak1 are active, we postulate that Cdc42 and Pak1 only regulate endocytosis at these sites and not at the cell sides.

4.1.4 Cdc42 and Pak1 recruit the Type I myosin in a dose-dependent manner to promote endocytic patch internalization

While the Type I myosin is a well-established target of the PAK kinase in many unicellular eukaryotes, we provide *in vivo* evidence that Cdc42 and Pak1 activity regulate the Type I myosin at endocytic sites. Intriguingly, we find that Cdc42 activity regulates the recruitment and dynamics of the Type I myosin in a dose-dependent manner, since both decreased and excessive Cdc42 activity lead to greater stability of Myo1 at the plasma membrane As Myo1 binds actin and Cdc42 activation promotes branched actin formation in a dose-dependent manner, perhaps these changes in Myo1 recruitment to endocytic patches result from changes in the myosin's ability to properly associate with actin at the endocytic patch. While this hypothesis remains untested, it is possible that sustained Scd1-mediated Cdc42 activation results in excessive yet aberrant branched actin architecture that is not amenable for proper Myo1 binding. This hypothesis could explain why excessive fimbrin is present at endocytic patches in *gef1* mutants, yet less Myo1 is recruited to endocytic sites.

In line with previous reports, we also show that TEDS site phosphorylation of Myo1 is required for proper myosin localization and dynamics, since Myo1-S361A remains stable on the plasma membrane and does not properly localize specifically to endocytic patches. As the TEDS site is a phospho-site target of Pak1 kinase and *pak1* mutants also show enhanced stability of Myo1, we conclude that Pak1 activity also promotes proper Myo1 dynamics. Lastly, we show that increased Myo1 stability on the plasma membrane results in decreased efficiency of endocytic patch internalization, likely due to impaired Myo1

motor function. Together, we conclude that Myo1 must dynamically associate with endocytic patches to promote timely endocytic internalization, since increased stability of Myo1 at the plasma membrane correlates with poor internalization. Together, our results demonstrate that Cdc42 and Pak1 not only promote branched actin formation but also regulate recruitment of Myo1 to branched actin in a dose-dependent manner.

4.2 THE SIGNIFICANCE OF MEMBRANE TRAFFICKING AT THE DIVISION SITE

4.2.1 Trafficking of septum synthases to the division site requires clathrin-mediated endocytosis

Clathrin-mediated endocytosis is essential for actomyosin ring constriction and septum formation in *S. pombe* (Onwubiko et al., 2019). As our findings show that both Bgs1 and Bgs4 trafficking to the division site are blocked upon inhibition of the Arp2/3 complex (Onwubiko et al., 2019; Campbell et al., unpublished data), it appears that endocytosis is particularly required for glucan synthase trafficking to the division site to initiate septum formation. However, the signals that promote polarized secretion of Bgs1 and Bgs4 likely differ since primary septum formation must initiate first to serve as a structural template for secondary septum synthesis. As Cdc42 activity promotes only the trafficking of Bgs1 and not Bgs4 to the division plane (Estravís et al., 2012; Onwubiko et al., 2021), we propose that Cdc42 activity is the signal that ensures the temporal coordination between these pathways. Indeed, our data show that changes in Cdc42 activation lead to an imbalance between Bgs1 and Bgs4 trafficking to the division site (Onwubiko et al., 2019; Campbell et al., 2022) and that this imbalance results in malformed septa (Campbell et al., 2022). Furthermore, recent findings show that the Cdc42 effector Pak1 inhibits Rho1 activation during early anaphase to ensure that Rho1 activates Bgs1 and septum formation only once ring formation has completed (Onwubiko et al., 2023). These findings are significant since proper septum synthesis protects cells from lysing as the primary septum is digested to separate the daughter cells.

4.2.2 Clathrin-mediated endocytosis remodels the membrane furrow to promote cytokinesis in a branched actin dependent manner

Clathrin-mediated endocytosis promotes proper membrane removal along the outer rim of the membrane furrow to facilitate cytokinesis (Feng et al., 2002; Gerald et al., 2001; Wang et al., 2016). In contrast, polarized secretion via exocytosis occurs relatively evenly throughout the division plane (Wang et al., 2016). As clathrin-mediated endocytosis is an actin-dependent process in yeast (Basu et al., 2014; Lacy et al., 2018), our data in *S. pombe* suggest that endocytosis at the cleavage furrow requires significant amounts of force since endocytic patch lifetimes are longest at the division site and an increased percentage of endocytic patches fail to internalize at this region compared to the cell ends (Campbell et al., 2024 – in preparation (this dissertation – Chapter 3); Campbell et al., 2022). Polarity mutants also show greater defects at this site than at the cell ends (Campbell et al., 2024 – in preparation), which further suggests that the division site is particularly sensitive. While the molecular details remain unclear, perhaps more robust actin patch formation is required at the division site to counteract the additional force produced by the dense trafficking of exocytic vesicles which occurs throughout the membrane furrow (Wang et al., 2016). As the membrane at the division site is also closely associated with the actomyosin ring and the septin cytoskeleton (Wu et al., 2003), it is possible that the presence of these cytoskeletal elements provides additional challenges to the endocytosis machinery.

4.2.3 Cdc42 promotes endocytic branched actin formation via disparate mechanisms in yeast and animals

The Arp2/3 complex relies on nucleation promoting factors to enhance its activity to synthesize branched actin needed for clathrin-mediated endocytosis (Machesky et al., 1999; Rohatgi et al., 1999; Winter et al., 1999; Yarar et al., 1999). In animals, one group of nucleation promoting factors, members of the WASP family, are direct effectors of Cdc42 (Higgs and Pollard, 1999). Specifically, binding of Cdc42 relieves the autoinhibition of WASP proteins, enabling them to bind the Arp2/3 complex and stimulate branched actin synthesis (Higgs and Pollard, 2000; Kim et al., 2000). In contrast, yeast WASP proteins do not directly interact with Cdc42 since they lack Cdc42/Rac Interactive Binding (CRIB) domains (Lechler et al., 2001). Furthermore, while experiments in budding yeast show that the WASP-related protein Bee1 is recruited to bud sites in a Cdc42-dependent manner, a significant fraction of *cdc42-1* mutants can still properly recruit Bee1 (Lechler et al., 2001), yet these mutants do not properly polarize branched actin to establish the bud site (Adams et al., 1990). Intriguingly, constitutively active expression of another nucleation promoting factor, the Type I myosin, in *cdc42-1* mutants restores actin polarization *in vivo* as well as actin polymerization activity *in vitro* (Lechler et al., 2001). In contrast, actin polymerization is equally defective in TEDS site phospho-null *myo3* mutants as in *cdc42-1* mutants (Lechler et al., 2001). Together with our findings that Cdc42 and its effector Pak1 regulate branched actin formation in *S. pombe*, these findings illustrate that Cdc42 also promotes clathrin-mediated endocytosis in yeast, albeit not through direct

activation of the WASP. Rather, Cdc42 activity appears to promote branched actin formation via PAK-mediated phosphorylation of the Type I myosin.

4.2.4 The endocytic Type I myosin regulates branched actin formation via divergent mechanisms in yeast and animals

In animals, Type I myosins regulate many essential cellular processes beyond endocytosis, including migration, cell adhesion, membrane fusion, maintenance of membrane tension, microvilli formation, and exocytic trafficking of post-Golgi vesicles (McIntosh and Ostap, 2016). In contrast, the only known function of Type I myosins in yeast is to promote endocytosis. In yeast and animals, endocytic Type I myosins bind both actin and the plasma membrane and generate force within the endocytic patch via their motor domains (Pedersen et al., 2023). A recent report shows that Type I myosins regulate branched actin formation by breaking dense actin networks and limiting Arp2/3 association with actin, perhaps promoting debranching of actin networks (Xu et al., 2024). Thus, while Type I myosins can function as nucleation promoting factors to activate the Arp2/3 complex (Sirotkin et al., 2005), perhaps their main role in clathrin-mediated endocytosis is to remodel the branched actin network rather than promote its synthesis. This hypothesis aligns with our observations that the *S. pombe* Type I myosin appears to promote timely internalization of endocytic patches but not synthesis of branched actin itself. Together, these data suggest that the Type I myosin uses the force generated by its motor domain to remodel branched actin networks into architecture that is favorable for endocytic internalization by limiting excessive branching to prevent the actin meshwork from becoming too rigid. As we show

that Cdc42 activity regulates Myo1 in a dose-dependent manner, these observations further illustrate that Cdc42 activation requires tight control to regulate Myo1 function and promote proper formation of branched actin networks. As Type I myosins in animals contain charged residues that do not require phosphorylation rather than TEDS sites, Cdc42 likely does not regulate Type I myosins via the PAK as we describe here for yeast, although this remains an area of open investigation.

4.2.5 Clathrin-mediated endocytosis and polarized growth reciprocally regulate each other via crosstalk

While we show here that Cdc42 activity regulates the formation of branched actin networks required for endocytosis, other recent work from our lab indicates that Arp2/3-mediated endocytosis at the cell ends is required for oscillations of active Cdc42 between these polarized sites (Harrell et al., 2024). These findings suggest that crosstalk occurs between endocytosis and polarized growth. Upon Arp2/3 inhibition, Pak1 stability at the cell ends increases, which completely breaks the Scd1-mediated positive feedback required to sustain Cdc42 activation at the cell ends (Harrell et al., 2024; Das et al., 2012). Thus, while Cdc42 activity promotes clathrin-mediated endocytosis at polarized sites (Campbell et al., 2024 – in preparation – Chapter 3), endocytosis is reciprocally required to promote Cdc42 activation to sustain polarization (Harrell et al., 2024). These observations suggest that polarization requires tight coupling of Cdc42 signaling and endocytosis.

4.3 CONCLUSION & FUTURE DIRECTIONS

The findings of this dissertation shed light on the intricate connections between polarized secretion, endocytosis, and the role of Cdc42 in each of these processes. Future work may further define how Bgs1 and Bgs4 trafficking are spatiotemporally coordinated to synthesize the septum. If Cdc42 activity is the signal required to traffic Bgs1 to the division site, what is the signal for Bgs4? Could it be one of the other Rho GTPases found in *S. pombe*? One such candidate could be Rho3, as *rho3* mutants exhibit severe septum defects, including improper positioning of the septum that sometimes results in anucleate cells (Nakano et al., 2002). Furthermore, For3 is an effector of Rho3, which suggests that Rho3 activity promotes trafficking of membrane-bound cargo (Nakano et al., 2002).

Future work will also examine the importance of Gef1-mediated Cdc42 activation in regulating endocytosis. Why does transient Cdc42 activity via Gef1 promote proper endocytic patch formation and internalization rather than sustained Cdc42 activation via Scd1? One possible interpretation is that Cdc42 activity promotes endocytosis in a dose-dependent manner, where strong Cdc42 activity via Scd1 results in excessive and disorganized branched actin formation that is not conducive for proper endocytosis. While our data in *gef1Δ* mutants indeed shows that enhanced Cdc42 activation via Scd1 results in excessive accumulation of branched actin at endocytic patches, we do not know whether this branched actin is organized properly. The structure of the actin architecture formed in *gef1Δ* cells and other polarity mutants could be investigated in the future to better understand the molecular details of how Cdc42 activity regulates the formation of endocytic patches.

Another future direction is to determine exactly how the Type I myosin promotes endocytic patch internalization. Is Myo1's primary function in anchoring the actin patch to the plasma membrane so that Wsp1 can stimulate Arp2/3 activation, or does Myo1 play a more direct role in branched actin formation? Additionally, it is not known how its motor functions to promote endocytosis. Does Myo1 use its motor to shift the position of actin filaments to facilitate better polymerization or crosslinking within the endocytic patch? Our data certainly indicate that the dynamics of Myo1 are important to promote patch internalization, since enhanced stability of the myosin at the membrane seems to result in decreased efficiency of patch internalization.

Finally, it would be interesting to determine if endocytic patches at different regions of the cortex require disparate amounts of force to internalize. Does the geometry of the plasma membrane regulate the timing and force required for internalization? What is the influence of the septum and the actomyosin ring on the formation and internalization rates of patches at the division site? Does the rate of endocytosis change during different stages of ring constriction and septum formation? Truly, the future directions that can be taken from this dissertation are endless.

4.4 REFERENCES

Adams, A.E., D.I. Johnson, R.M. Longnecker, B.F. Sloat, and J.R. Pringle. 1990. CDC42 and CDC43, two additional genes involved in budding and the establishment of cell polarity in the yeast Saccharomyces cerevisiae. *J Cell Biol*. 111:131-142.

Aghamohammadzadeh, S., and K.R. Ayscough. 2009. Differential requirements for actin during yeast and mammalian endocytosis. *Nat Cell Biol*. 11:1039-1042.

Arasada, R., and T.D. Pollard. 2011. Distinct roles for F-BAR proteins Cdc15p and Bzz1p in actin polymerization at sites of endocytosis in fission yeast. *Curr Biol*. 21:1450-1459.

Arasada, R., and T.D. Pollard. 2014. Contractile ring stability in S. pombe depends on F-BAR protein Cdc15p and Bgs1p transport from the Golgi complex. *Cell Rep*. 8:1533-1544.

Arasada, R., and T.D. Pollard. 2015. A role for F-BAR protein Rga7p during cytokinesis in S. pombe. *J Cell Sci*. 128:2259-2268.

Arellano, M., P.M. Coll, and P. Pérez. 1999. RHO GTPases in the control of cell morphology, cell polarity, and actin localization in fission yeast. *Microsc Res Tech*. 47:51-60.

Arellano, M., A. Durán, and P. Pérez. 1996. Rho 1 GTPase activates the (1-3)beta-D-glucan synthase and is involved in Schizosaccharomyces pombe morphogenesis. *Embo j*. 15:4584-4591.

Atkins, B.D., S. Yoshida, K. Saito, C.F. Wu, D.J. Lew, and D. Pellman. 2013. Inhibition of Cdc42 during mitotic exit is required for cytokinesis. *J Cell Biol*. 202:231-240.

Attanapola, S.L., C.J. Alexander, and D.P. Mulvihill. 2009. Ste20-kinase-dependent TEDS-site phosphorylation modulates the dynamic localisation and endocytic function of the fission yeast class I myosin, Myo1. *J Cell Sci*. 122:3856-3861.

Bähler, J., and J.R. Pringle. 1998. Pom1p, a fission yeast protein kinase that provides positional information for both polarized growth and cytokinesis. *Genes Dev*. 12:1356-1370.

Basu, R., E.L. Munteanu, and F. Chang. 2014. Role of turgor pressure in endocytosis in fission yeast. *Mol Biol Cell*. 25:679-687.

Bement, W.M., and M.S. Mooseker. 1995. TEDS rule: a molecular rationale for differential regulation of myosins by phosphorylation of the heavy chain head. *Cell Motil Cytoskeleton*. 31:87-92.

Bendezú, F.O., and S.G. Martin. 2011. Actin cables and the exocyst form two independent morphogenesis pathways in the fission yeast. *Mol Biol Cell*. 22:44-53.

Bendezú, F.O., V. Vincenzetti, and S.G. Martin. 2012. Fission yeast Sec3 and Exo70 are transported on actin cables and localize the exocyst complex to cell poles. *PLoS One*. 7:e40248.

Berro, J., and T.D. Pollard. 2014. Local and global analysis of endocytic patch dynamics in fission yeast using a new "temporal superresolution" realignment method. *Mol Biol Cell*. 25:3501-3514.

Bishop, A.L., and A. Hall. 2000. Rho GTPases and their effector proteins. *Biochem J*. 348 Pt 2:241-255.

Bokoch, G.M. 2003. Biology of the p21-activated kinases. *Annu Rev Biochem*. 72:743-781.

Bose, I., J.E. Irazoqui, J.J. Moskow, E.S. Bardes, T.R. Zyla, and D.J. Lew. 2001. Assembly of scaffold-mediated complexes containing Cdc42p, the exchange factor Cdc24p, and the effector Cla4p required for cell cycle-regulated phosphorylation of Cdc24p. *J Biol Chem*. 276:7176-7186.

Boyd, C., T. Hughes, M. Pypaert, and P. Novick. 2004. Vesicles carry most exocyst subunits to exocytic sites marked by the remaining two subunits, Sec3p and Exo70p. *J Cell Biol*. 167:889-901.

Brzeska, H., U.G. Knaus, Z.Y. Wang, G.M. Bokoch, and E.D. Korn. 1997. p21-activated kinase has substrate specificity similar to Acanthamoeba myosin I heavy chain kinase and activates Acanthamoeba myosin I. *Proc Natl Acad Sci U S A*. 94:1092-1095.

Campbell, B.F., B.S. Hercyk, A.R. Williams, E. San Miguel, H.G. Young, and M.E. Das. 2022. Cdc42 GTPase activating proteins Rga4 and Rga6 coordinate septum synthesis and membrane trafficking at the division plane during cytokinesis. *Traffic*. 23:478-495.

Carnahan, R.H., and K.L. Gould. 2003. The PCH family protein, Cdc15p, recruits two F-actin nucleation pathways to coordinate cytokinetic actin ring formation in Schizosaccharomyces pombe. *J Cell Biol*. 162:851-862.

Chang, E., G. Bartholomeusz, R. Pimental, J. Chen, H. Lai, L. Wang, P. Yang, and S. Marcus. 1999. Direct binding and In vivo regulation of the fission yeast p21-activated kinase shk1 by the SH3 domain protein scd2. *Mol Cell Biol*. 19:8066-8074.

Chappell, T.G., and G. Warren. 1989. A galactosyltransferase from the fission yeast Schizosaccharomyces pombe. *J Cell Biol*. 109:2693-2702.

Cheffings, T.H., N.J. Burroughs, and M.K. Balasubramanian. 2016. Actomyosin Ring Formation and Tension Generation in Eukaryotic Cytokinesis. *Curr Biol*. 26:R719-r737.

Coll, P.M., Y. Trillo, A. Ametzazurra, and P. Perez. 2003. Gef1p, a new guanine nucleotide exchange factor for Cdc42p, regulates polarity in Schizosaccharomyces pombe. *Mol Biol Cell*. 14:313-323.

Cortés, J.C., E. Carnero, J. Ishiguro, Y. Sánchez, A. Durán, and J.C. Ribas. 2005. The novel fission yeast (1,3)beta-D-glucan synthase catalytic subunit Bgs4p is essential during both cytokinesis and polarized growth. *J Cell Sci*. 118:157-174.

Cortés, J.C., J. Ishiguro, A. Durán, and J.C. Ribas. 2002. Localization of the (1,3)beta-D-glucan synthase catalytic subunit homologue Bgs1p/Cps1p from fission yeast suggests that it is involved in septation, polarized growth, mating, spore wall formation and spore germination. *J Cell Sci*. 115:4081-4096.

Cortés, J.C., M. Konomi, I.M. Martins, J. Muñoz, M.B. Moreno, M. Osumi, A. Durán, and J.C. Ribas. 2007. The (1,3)beta-D-glucan synthase subunit Bgs1p is responsible for the fission yeast primary septum formation. *Mol Microbiol*. 65:201-217.

Cortés, J.C., M. Ramos, M. Osumi, P. Pérez, and J.C. Ribas. 2016. Fission yeast septation. *Commun Integr Biol*. 9:e1189045.

Das, M., T. Drake, D.J. Wiley, P. Buchwald, D. Vavylonis, and F. Verde. 2012. Oscillatory dynamics of Cdc42 GTPase in the control of polarized growth. *Science*. 337:239-243.

Das, M., I. Nuñez, M. Rodriguez, D.J. Wiley, J. Rodriguez, A. Sarkeshik, J.R. Yates, 3rd, P. Buchwald, and F. Verde. 2015. Phosphorylation-dependent inhibition of Cdc42 GEF Gef1 by 14-3-3 protein Rad24 spatially regulates Cdc42 GTPase activity and oscillatory dynamics during cell morphogenesis. *Mol Biol Cell*. 26:3520-3534.

Das, M., and F. Verde. 2013. Role of Cdc42 dynamics in the control of fission yeast cell polarization. *Biochem Soc Trans*. 41:1745-1749.

Das, M., D.J. Wiley, S. Medina, H.A. Vincent, M. Larrea, A. Oriolo, and F. Verde. 2007. Regulation of cell diameter, For3p localization, and cell symmetry by fission yeast Rho-GAP Rga4p. *Mol Biol Cell*. 18:2090-2101.

Davidson, R., J.A. Pontasch, and J.Q. Wu. 2016. Sbg1 Is a Novel Regulator for the Localization of the β-Glucan Synthase Bgs1 in Fission Yeast. *PLoS One*. 11:e0167043.

Dekker, N., D. Speijer, C.H. Grün, M. van den Berg, A. de Haan, and F. Hochstenbach. 2004. Role of the alpha-glucanase Agn1p in fission-yeast cell separation. *Mol Biol Cell*. 15:3903-3914.

Drechsel, D.N., A.A. Hyman, A. Hall, and M. Glotzer. 1997. A requirement for Rho and Cdc42 during cytokinesis in Xenopus embryos. *Curr Biol*. 7:12-23.

Estravis, M., S. Rincon, and P. Pérez. 2012. Cdc42 regulation of polarized traffic in fission yeast. *Commun Integr Biol*. 5:370-373.

Estravís, M., S.A. Rincón, B. Santos, and P. Pérez. 2011. Cdc42 regulates multiple membrane traffic events in fission yeast. *Traffic*. 12:1744-1758.

Etienne-Manneville, S. 2004. Cdc42--the centre of polarity. *J Cell Sci*. 117:1291-1300.

Faix, J., and R. Grosse. 2006. Staying in shape with formins. *Dev Cell*. 10:693-706.

Feng, B., H. Schwarz, and S. Jesuthasan. 2002. Furrow-specific endocytosis during cytokinesis of zebrafish blastomeres. *Exp Cell Res*. 279:14-20.

Finger, F.P., T.E. Hughes, and P. Novick. 1998. Sec3p is a spatial landmark for polarized secretion in budding yeast. *Cell*. 92:559-571.

Frigault, M.M., J. Lacoste, J.L. Swift, and C.M. Brown. 2009. Live-cell microscopy - tips and tools. *J Cell Sci*. 122:753-767.

Fujita-Becker, S., U. Dürrwang, M. Erent, R.J. Clark, M.A. Geeves, and D.J. Manstein. 2005. Changes in Mg2+ ion concentration and heavy chain phosphorylation regulate the motor activity of a class I myosin. *J Biol Chem*. 280:6064-6071.

Fukui, Y., and M. Yamamoto. 1988. Isolation and characterization of Schizosaccharomyces pombe mutants phenotypically similar to ras1. *Mol Gen Genet*. 215:26-31.

Gachet, Y., and J.S. Hyams. 2005. Endocytosis in fission yeast is spatially associated with the actin cytoskeleton during polarised cell growth and cytokinesis. *J Cell Sci*. 118:4231-4242.

Gallo Castro, D., and S.G. Martin. 2018. Differential GAP requirement for Cdc42-GTP polarization during proliferation and sexual reproduction. *J Cell Biol*. 217:4215-4229.

Gerald, N.J., C.K. Damer, T.J. O'Halloran, and A. De Lozanne. 2001. Cytokinesis failure in clathrin-minus cells is caused by cleavage furrow instability. *Cell Motil Cytoskeleton*. 48:213-223.

Gulli, M.P., M. Jaquenoud, Y. Shimada, G. Niederhäuser, P. Wiget, and M. Peter. 2000. Phosphorylation of the Cdc42 exchange factor Cdc24 by the PAK-like kinase Cla4 may regulate polarized growth in yeast. *Mol Cell*. 6:1155-1167.

Hachet, O., F.O. Bendezú, and S.G. Martin. 2012. Fission yeast: in shape to divide. *Curr Opin Cell Biol*. 24:858-864.

Harrell, M.A., Z. Liu, B.F. Campbell, O. Chinsen, T. Hong, and M. Das. 2024. Arp2/3-dependent endocytosis ensures Cdc42 oscillations by removing Pak1-mediated negative feedback. *J Cell Biol*. 223.

He, B., F. Xi, X. Zhang, J. Zhang, and W. Guo. 2007. Exo70 interacts with phospholipids and mediates the targeting of the exocyst to the plasma membrane. *Embo j*. 26:4053-4065.

Hercyk, B.S., and M.E. Das. 2019. F-BAR Cdc15 Promotes Cdc42 Activation During Cytokinesis and Cell Polarization in Schizosaccharomyces pombe. *Genetics*. 213:1341-1356.

Hercyk, B.S., U.N. Onwubiko, and M.E. Das. 2019a. Coordinating septum formation and the actomyosin ring during cytokinesis in Schizosaccharomyces pombe. *Mol Microbiol*. 112:1645-1657.

Hercyk, B.S., J. Rich-Robinson, A.S. Mitoubsi, M.A. Harrell, and M.E. Das. 2019b. A novel interplay between GEFs orchestrates Cdc42 activity during cell polarity and cytokinesis in fission yeast. *J Cell Sci*. 132.

Higgs, H.N., and T.D. Pollard. 1999. Regulation of actin polymerization by Arp2/3 complex and WASp/Scar proteins. *J Biol Chem*. 274:32531-32534.

Higgs, H.N., and T.D. Pollard. 2000. Activation by Cdc42 and PIP(2) of Wiskott-Aldrich syndrome protein (WASp) stimulates actin nucleation by Arp2/3 complex. *J Cell Biol*. 150:1311-1320.

Hirota, K., K. Tanaka, K. Ohta, and M. Yamamoto. 2003. Gef1p and Scd1p, the Two GDP-GTP exchange factors for Cdc42p, form a ring structure that shrinks during cytokinesis in Schizosaccharomyces pombe. *Mol Biol Cell*. 14:3617-3627.

Jena, B.P. 2011. Role of SNAREs in membrane fusion. *Adv Exp Med Biol*. 713:13-32.

Johnson, D.I. 1999. Cdc42: An essential Rho-type GTPase controlling eukaryotic cell polarity. *Microbiol Mol Biol Rev*. 63:54-105.

Jones, L., K. Tedrick, A. Baier, M.R. Logan, and G. Eitzen. 2010. Cdc42p is activated during vacuole membrane fusion in a sterol-dependent subreaction of priming. *J Biol Chem*. 285:4298-4306.

Jordan, S.N., T. Davies, Y. Zhuravlev, J. Dumont, M. Shirasu-Hiza, and J.C. Canman. 2016. Cortical PAR polarity proteins promote robust cytokinesis during asymmetric cell division. *J Cell Biol*. 212:39-49.

Kaksonen, M., and A. Roux. 2018. Mechanisms of clathrin-mediated endocytosis. *Nat Rev Mol Cell Biol*. 19:313-326.

Kim, A.S., L.T. Kakalis, N. Abdul-Manan, G.A. Liu, and M.K. Rosen. 2000. Autoinhibition and activation mechanisms of the Wiskott-Aldrich syndrome protein. *Nature*. 404:151-158.

Kroschewski, R., A. Hall, and I. Mellman. 1999. Cdc42 controls secretory and endocytic transport to the basolateral plasma membrane of MDCK cells. *Nat Cell Biol*. 1:8-13.

Lacy, M.M., R. Ma, N.G. Ravindra, and J. Berro. 2018. Molecular mechanisms of force production in clathrin-mediated endocytosis. *FEBS Lett*. 592:3586-3605.

Lamas, I., L. Merlini, A. Vještica, V. Vincenzetti, and S.G. Martin. 2020. Optogenetics reveals Cdc42 local activation by scaffold-mediated positive feedback and Ras GTPase. *PLoS Biol*. 18:e3000600.

Lechler, T., G.A. Jonsdottir, S.K. Klee, D. Pellman, and R. Li. 2001. A two-tiered mechanism by which Cdc42 controls the localization and activation of an Arp2/3-activating motor complex in yeast. *J Cell Biol*. 155:261-270.

Lechler, T., A. Shevchenko, and R. Li. 2000. Direct involvement of yeast type I myosins in Cdc42-dependent actin polymerization. *J Cell Biol*. 148:363-373.

Lee, W.L., M. Bezanilla, and T.D. Pollard. 2000. Fission yeast myosin-I, Myo1p, stimulates actin assembly by Arp2/3 complex and shares functions with WASp. *J Cell Biol*. 151:789-800.

Liu, J., H. Wang, D. McCollum, and M.K. Balasubramanian. 1999. Drc1p/Cps1p, a 1,3-beta-glucan synthase subunit, is essential for division septum assembly in Schizosaccharomyces pombe. *Genetics*. 153:1193-1203.

Longo, L.V.G., E.G. Goodyear, S. Zhang, E. Kudryashova, and J.Q. Wu. 2022. Involvement of Smi1 in cell wall integrity and glucan synthase Bgs4 localization during fission yeast cytokinesis. *Mol Biol Cell*. 33:ar17.

Machesky, L.M., R.D. Mullins, H.N. Higgs, D.A. Kaiser, L. Blanchoin, R.C. May, M.E. Hall, and T.D. Pollard. 1999. Scar, a WASp-related protein, activates nucleation of actin filaments by the Arp2/3 complex. *Proc Natl Acad Sci U S A*. 96:3739-3744.

Magliozzi, J.O., J. Sears, L. Cressey, M. Brady, H.E. Opalko, A.N. Kettenbach, and J.B. Moseley. 2020. Fission yeast Pak1 phosphorylates anillin-like Mid1 for spatial control of cytokinesis. *J Cell Biol*. 219.

Manenschijn, H.E., A. Picco, M. Mund, A.S. Rivier-Cordey, J. Ries, and M. Kaksonen. 2019. Type-I myosins promote actin polymerization to drive membrane bending in endocytosis. *Elife*. 8.

Manser, E., T. Leung, H. Salihuddin, Z.S. Zhao, and L. Lim. 1994. A brain serine/threonine protein kinase activated by Cdc42 and Rac1. *Nature*. 367:40-46.

Marcus, S., A. Polverino, E. Chang, D. Robbins, M.H. Cobb, and M.H. Wigler. 1995. Shk1, a homolog of the Saccharomyces cerevisiae Ste20 and mammalian p65PAK protein kinases, is a component of a Ras/Cdc42 signaling module in the fission yeast Schizosaccharomyces pombe. *Proc Natl Acad Sci U S A*. 92:6180-6184.

Martin, S.G., and R.A. Arkowitz. 2014. Cell polarization in budding and fission yeasts. *FEMS Microbiol Rev*. 38:228-253.

Martin, S.G., S.A. Rincón, R. Basu, P. Pérez, and F. Chang. 2007. Regulation of the formin for3p by cdc42p and bud6p. *Mol Biol Cell*. 18:4155-4167.

Martín-Cuadrado, A.B., E. Dueñas, M. Sipiczki, C.R. Vázquez de Aldana, and F. del Rey. 2003. The endo-beta-1,3-glucanase eng1p is required for dissolution of the primary septum during cell separation in Schizosaccharomyces pombe. *J Cell Sci*. 116:1689-1698.

Martín-Cuadrado, A.B., J.L. Morrell, M. Konomi, H. An, C. Petit, M. Osumi, M. Balasubramanian, K.L. Gould, F. Del Rey, and C.R. de Aldana. 2005. Role of septins and the exocyst complex in the function of hydrolytic enzymes responsible for fission yeast cell separation. *Mol Biol Cell*. 16:4867-4881.

McIntosh, B.B., and E.M. Ostap. 2016. Myosin-I molecular motors at a glance. *J Cell Sci*. 129:2689-2695.

Melendez, J., M. Grogg, and Y. Zheng. 2011. Signaling role of Cdc42 in regulating mammalian physiology. *J Biol Chem*. 286:2375-2381.

Miki, H., T. Sasaki, Y. Takai, and T. Takenawa. 1998. Induction of filopodium formation by a WASP-related actin-depolymerizing protein N-WASP. *Nature*. 391:93-96.

Miller, P.J., and D.I. Johnson. 1994. Cdc42p GTPase is involved in controlling polarized cell growth in Schizosaccharomyces pombe. *Mol Cell Biol*. 14:1075-1083.

Mitchison, J.M., and P. Nurse. 1985. Growth in cell length in the fission yeast Schizosaccharomyces pombe. *J Cell Sci*. 75:357-376.

Moreno, S., A. Klar, and P. Nurse. 1991. Molecular genetic analysis of fission yeast Schizosaccharomyces pombe. *Methods Enzymol*. 194:795-823.

Motegi, F., R. Arai, and I. Mabuchi. 2001. Identification of two type V myosins in fission yeast, one of which functions in polarized cell growth and moves rapidly in the cell. *Mol Biol Cell*. 12:1367-1380.

Mulvihill, D.P., S.R. Edwards, and J.S. Hyams. 2006. A critical role for the type V myosin, Myo52, in septum deposition and cell fission during cytokinesis in Schizosaccharomyces pombe. *Cell Motil Cytoskeleton*. 63:149-161.

Muñoz, J., J.C. Cortés, M. Sipiczki, M. Ramos, J.A. Clemente-Ramos, M.B. Moreno, I.M. Martins, P. Pérez, and J.C. Ribas. 2013. Extracellular cell wall β(1,3)glucan is required to couple septation to actomyosin ring contraction. *J Cell Biol*. 203:265-282.

Murray, J.M., and D.I. Johnson. 2001. The Cdc42p GTPase and its regulators Nrf1p and Scd1p are involved in endocytic trafficking in the fission yeast Schizosaccharomyces pombe. *J Biol Chem*. 276:3004-3009.

Nakano, K., J. Imai, R. Arai, E.A. Toh, Y. Matsui, and I. Mabuchi. 2002. The small GTPase Rho3 and the diaphanous/formin For3 function in polarized cell growth in fission yeast. *J Cell Sci*. 115:4629-4639.

Nakano, K., K. Satoh, A. Morimatsu, M. Ohnuma, and I. Mabuchi. 2001. Interactions among a fimbrin, a capping protein, and an actin-depolymerizing factor in organization of the fission yeast actin cytoskeleton. *Mol Biol Cell*. 12:3515-3526.

Nance, J., and J.A. Zallen. 2011. Elaborating polarity: PAR proteins and the cytoskeleton. *Development*. 138:799-809.

Nickaeen, M., J. Berro, T.D. Pollard, and B.M. Slepchenko. 2022. A model of actin-driven endocytosis explains differences of endocytic motility in budding and fission yeast. *Mol Biol Cell*. 33:ar16.

Onishi, M., N. Ko, R. Nishihama, and J.R. Pringle. 2013. Distinct roles of Rho1, Cdc42, and Cyk3 in septum formation and abscission during yeast cytokinesis. *J Cell Biol*. 202:311-329.

Onwubiko, U.N., D. Kalathil, E. Koory, S. Pokharel, H. Roberts, A. Mitoubsi, and M. Das. 2023. Cdc42 prevents precocious Rho1 activation during cytokinesis in a Pak1-dependent manner. *J Cell Sci*. 136.

Onwubiko, U.N., P.J. Mlynarczyk, B. Wei, J. Habiyaremye, A. Clack, S.M. Abel, and M.E. Das. 2019. A Cdc42 GEF, Gef1, through endocytosis organizes F-BAR Cdc15 along the actomyosin ring and promotes concentric furrowing. *J Cell Sci*. 132.

Onwubiko, U.N., J. Rich-Robinson, R.A. Mustaf, and M.E. Das. 2021. Cdc42 promotes Bgs1 recruitment for septum synthesis and glucanase localization for cell separation during cytokinesis in fission yeast. *Small GTPases*. 12:257-264.

Ottilie, S., P.J. Miller, D.I. Johnson, C.L. Creasy, M.A. Sells, S. Bagrodia, S.L. Forsburg, and J. Chernoff. 1995. Fission yeast pak1+ encodes a protein kinase that interacts with Cdc42p and is involved in the control of cell polarity and mating. *Embo j*. 14:5908-5919.

Pedersen, R.T.A., A. Snoberger, S. Pyrpassopoulos, D. Safer, D.G. Drubin, and E.M. Ostap. 2023. Endocytic myosin-1 is a force-insensitive, power-generating motor. *J Cell Biol*. 222.

Pérez, P., E. Portales, and B. Santos. 2015. Rho4 interaction with exocyst and septins regulates cell separation in fission yeast. *Microbiology (Reading)*. 161:948-959.

Pinar, M., H.N. Arst, Jr., A. Pantazopoulou, V.G. Tagua, V. de los Ríos, J. Rodríguez-Salarichs, J.F. Díaz, and M.A. Peñalva. 2015. TRAPPII regulates exocytic Golgi exit by mediating nucleotide exchange on the Ypt31 ortholog RabERAB11. *Proc Natl Acad Sci U S A*. 112:4346-4351.

Pollard, T.D. 2010. Mechanics of cytokinesis in eukaryotes. *Curr Opin Cell Biol*. 22:50-56.

Pollard, T.D. 2014. The value of mechanistic biophysical information for systems-level understanding of complex biological processes such as cytokinesis. *Biophys J*. 107:2499-2507.

Proctor, S.A., N. Minc, A. Boudaoud, and F. Chang. 2012. Contributions of turgor pressure, the contractile ring, and septum assembly to forces in cytokinesis in fission yeast. *Curr Biol*. 22:1601-1608.

Revilla-Guarinos, M.T., R. Martín-García, M.A. Villar-Tajadura, M. Estravís, P.M. Coll, and P. Pérez. 2016. Rga6 is a Fission Yeast Rho GAP Involved in Cdc42 Regulation of Polarized Growth. *Mol Biol Cell*. 27:1524-1535.

Rich-Robinson, J., A. Russell, E. Mancini, and M. Das. 2021. Cdc42 reactivation at growth sites is regulated by local cell-cycle-dependent loss of its GTPase-activating protein Rga4 in fission yeast. *J Cell Sci*. 134.

Ridley, A.J. 2006. Rho GTPases and actin dynamics in membrane protrusions and vesicle trafficking. *Trends Cell Biol*. 16:522-529.

Rincón, S.A., M. Estravís, and P. Pérez. 2014. Cdc42 regulates polarized growth and cell integrity in fission yeast. *Biochem Soc Trans*. 42:201-205.

Rincón, S.A., Y. Ye, M.A. Villar-Tajadura, B. Santos, S.G. Martin, and P. Pérez. 2009. Pob1 participates in the Cdc42 regulation of fission yeast actin cytoskeleton. *Mol Biol Cell*. 20:4390-4399.

Rohatgi, R., L. Ma, H. Miki, M. Lopez, T. Kirchhausen, T. Takenawa, and M.W. Kirschner. 1999. The interaction between N-WASP and the Arp2/3 complex links Cdc42-dependent signals to actin assembly. *Cell*. 97:221-231.

Roumanie, O., H. Wu, J.N. Molk, G. Rossi, K. Bloom, and P. Brennwald. 2005. Rho GTPase regulation of exocytosis in yeast is independent of GTP hydrolysis and polarization of the exocyst complex. *J Cell Biol*. 170:583-594.

Saito, K., K. Fujimura-Kamada, H. Hanamatsu, U. Kato, M. Umeda, K.G. Kozminski, and K. Tanaka. 2007. Transbilayer phospholipid flipping regulates Cdc42p signaling during polarized cell growth via Rga GTPase-activating proteins. *Dev Cell*. 13:743-751.

Santos, B., A.B. Martín-Cuadrado, C.R. Vázquez de Aldana, F. del Rey, and P. Pérez. 2005. Rho4 GTPase is involved in secretion of glucanases during fission yeast cytokinesis. *Eukaryot Cell*. 4:1639-1645.

Schneider, C.A., W.S. Rasband, and K.W. Eliceiri. 2012. NIH Image to ImageJ: 25 years of image analysis. *Nat Methods*. 9:671-675.

Sells, M.A., J.T. Barratt, J. Caviston, S. Ottilie, E. Leberer, and J. Chernoff. 1998. Characterization of Pak2p, a pleckstrin homology domain-containing, p21-activated protein kinase from fission yeast. *J Biol Chem*. 273:18490-18498.

Sethi, K., S. Palani, J.C. Cortés, M. Sato, M. Sevugan, M. Ramos, S. Vijaykumar, M. Osumi, N.I. Naqvi, J.C. Ribas, and M. Balasubramanian. 2016. A New Membrane Protein Sbg1 Links the Contractile Ring Apparatus and Septum Synthesis Machinery in Fission Yeast. *PLoS Genet*. 12:e1006383.

Sipiczki, M. 2007. Splitting of the fission yeast septum. *FEMS Yeast Res*. 7:761-770.

Sirotkin, V., C.C. Beltzner, J.B. Marchand, and T.D. Pollard. 2005. Interactions of WASp, myosin-I, and verprolin with Arp2/3 complex during actin patch assembly in fission yeast. *J Cell Biol*. 170:637-648.

Sirotkin, V., J. Berro, K. Macmillan, L. Zhao, and T.D. Pollard. 2010. Quantitative analysis of the mechanism of endocytic actin patch assembly and disassembly in fission yeast. *Mol Biol Cell*. 21:2894-2904.

Skau, C.T., D.S. Courson, A.J. Bestul, J.D. Winkelman, R.S. Rock, V. Sirotkin, and D.R. Kovar. 2011. Actin filament bundling by fimbrin is important for endocytosis, cytokinesis, and polarization in fission yeast. *J Biol Chem*. 286:26964-26977.

Takenawa, T., and S. Suetsugu. 2007. The WASP-WAVE protein network: connecting the membrane to the cytoskeleton. *Nat Rev Mol Cell Biol*. 8:37-48.

Tatebe, H., K. Nakano, R. Maximo, and K. Shiozaki. 2008. Pom1 DYRK regulates localization of the Rga4 GAP to ensure bipolar activation of Cdc42 in fission yeast. *Curr Biol*. 18:322-330.

Toya, M., Y. Iino, and M. Yamamoto. 1999. Fission yeast Pob1p, which is homologous to budding yeast Boi proteins and exhibits subcellular localization close to actin patches, is essential for cell elongation and separation. *Mol Biol Cell*. 10:2745-2757.

Verde, F., J. Mata, and P. Nurse. 1995. Fission yeast cell morphogenesis: identification of new genes and analysis of their role during the cell cycle. *J Cell Biol*. 131:1529-1538.

Vicente-Manzanares, M., and F. Sánchez-Madrid. 2000. Cell polarization: a comparative cell biology and immunological view. *Dev Immunol*. 7:51-65.

Wang, H., X. Tang, J. Liu, S. Trautmann, D. Balasundaram, D. McCollum, and M.K. Balasubramanian. 2002. The multiprotein exocyst complex is essential for cell separation in Schizosaccharomyces pombe. *Mol Biol Cell*. 13:515-529.

Wang, N., I.J. Lee, G. Rask, and J.Q. Wu. 2016. Roles of the TRAPP-II Complex and the Exocyst in Membrane Deposition during Fission Yeast Cytokinesis. *PLoS Biol*. 14:e1002437.

Wang, N., M. Wang, Y.H. Zhu, T.W. Grosel, D. Sun, D.S. Kudryashov, and J.Q. Wu. 2015. The Rho-GEF Gef3 interacts with the septin complex and activates the GTPase Rho4 during fission yeast cytokinesis. *Mol Biol Cell*. 26:238-255.

Wei, B., B.S. Hercyk, J. Habiyaremye, and M. Das. 2017. Spatiotemporal Analysis of Cytokinetic Events in Fission Yeast. *J Vis Exp*.

Wei, B., B.S. Hercyk, N. Mattson, A. Mohammadi, J. Rich, E. DeBruyne, M.M. Clark, and M. Das. 2016. Unique spatiotemporal activation pattern of Cdc42 by Gef1 and Scd1 promotes different events during cytokinesis. *Mol Biol Cell*. 27:1235-1245.

Winter, D., T. Lechler, and R. Li. 1999. Activation of the yeast Arp2/3 complex by Bee1p, a WASP-family protein. *Curr Biol*. 9:501-504.

Wodarz, A., and I. Näthke. 2007. Cell polarity in development and cancer. *Nat Cell Biol*. 9:1016-1024.

Wu, C., V. Lytvyn, D.Y. Thomas, and E. Leberer. 1997. The phosphorylation site for Ste20p-like protein kinases is essential for the function of myosin-I in yeast. *J Biol Chem*. 272:30623-30626.

Wu, J.Q., J.R. Kuhn, D.R. Kovar, and T.D. Pollard. 2003. Spatial and temporal pathway for assembly and constriction of the contractile ring in fission yeast cytokinesis. *Dev Cell*. 5:723-734.

Xu, M., D.M. Rutkowski, G. Rebowski, M. Boczkowska, L.W. Pollard, R. Dominguez, D. Vavylonis, and E.M. Ostap. 2024. Myosin-I synergizes with Arp2/3 complex to enhance the pushing forces of branched actin networks. *Sci Adv*. 10:eado5788.

Yarar, D., W. To, A. Abo, and M.D. Welch. 1999. The Wiskott-Aldrich syndrome protein directs actin-based motility by stimulating actin nucleation with the Arp2/3 complex. *Curr Biol*. 9:555-558.

Zhang, Y., R. Sugiura, Y. Lu, M. Asami, T. Maeda, T. Itoh, T. Takenawa, H. Shuntoh, and T. Kuno. 2000. Phosphatidylinositol 4-phosphate 5-kinase Its3 and calcineurin Ppb1 coordinately regulate cytokinesis in fission yeast. *J Biol Chem*. 275:35600-35606.